LIQUID CRYSTAL - TEMPLATED SYNTHESIS OF POLYMERIC MICROPARTICLES WITH COMPLEX NANOSTRUCTURES

A THESIS SUBMITTED TO
THE GRADUATE SCHOOL OF NATURAL AND APPLIED SCIENCES
OF
MIDDLE EAST TECHNICAL UNIVERSITY

BY

BURAK AKDENIZ

IN PARTIAL FULFILLMENT OF THE REQUIREMENTS
FOR
THE DEGREE OF MASTER OF SCIENCE
IN
CHEMICAL ENGINEERING

AUGUST 2019

Approval of the thesis:

LIQUID CRYSTAL - TEMPLATED SYNTHESIS OF POLYMERIC MICROPARTICLES WITH COMPLEX NANOSTRUCTURES

submitted by **BURAK AKDENIZ** in partial fulfillment of the requirements for the degree of **Master of Science in Chemical Engineering Department, Middle East Technical University** by,

Prof. Dr. Halil Kalıpçılar
Dean, Graduate School of **Natural and Applied Sciences** _____

Prof. Dr. Pınar Çalık
Head of Department, **Chemical Engineering** _____

Assist. Prof. Dr. Emre Büküşoğlu
Supervisor, **Chemical Engineering, METU** _____

Examining Committee Members:

Prof. Dr. Nihal Aydoğan
Chemical Engineering Dept., Hacettepe University _____

Assist. Prof. Dr. Emre Büküşoğlu
Chemical Engineering, METU _____

Assoc. Prof. Dr. Erhan Bat
Chemical Engineering Dept., METU _____

Assist. Prof. Dr. Simge Çınar
Metallurgical and Materials Engineering Dept., METU _____

Assist. Prof. Dr. İnci Ayrancı Tansık
Chemical Engineering Dept., METU _____

Date: 08.08.2019

I hereby declare that all information in this document has been obtained and presented in accordance with academic rules and ethical conduct. I also declare that, as required by these rules and conduct, I have fully cited and referenced all material and results that are not original to this work.

Name, Surname: Burak Akdeniz

Signature:

ABSTRACT

LIQUID CRYSTAL - TEMPLATED SYNTHESIS OF POLYMERIC MICROPARTICLES WITH COMPLEX NANOSTRUCTURES

Akdeniz, Burak
Master of Science, Chemical Engineering
Supervisor: Assist. Prof. Dr. Emre Büküşoğlu

August 2019, 92 pages

Liquid crystals (LC), when combined with photolithography, enable synthesis of microparticles with two- and three-dimensional shapes and internal complexities. We prepared films of nematic LCs using mixtures of reactive (RM257) and non-reactive mesogens (E7) with controlled alignment of LCs at the confining surfaces, photo-polymerized the RM257 using a photomask, and then extracted the unreacted mesogens to yield polymeric microparticles. The extraction resulted in a controlled anisotropic shrinkage with an amount dependent on the RM257 content and the direction dependent the on LC alignment. Moreover, control over the aspect ratio, size and thickness of the microparticles were obtained with a coefficient of variance less than 2%. In addition, non-parallel LC anchoring at the two surfaces resulted in a controllable right- or left-handed twisting of microparticles (Chapter 4). Besides these results, we used circular, triangular, rectangular, square, star and heart shaped lithography masks to provide initial shapes to the microparticles (Chapter 5). The configuration of the reactive and non-reactive mesogen mixtures maintained initially played a critical role in determining the chiral twisting and bending of the microparticles. We found that the pitch size of the bulk chiral twisting of the polymeric microparticles to depend linearly on the angle of chiral twist of the LCs, whereas it is independent of the length and thickness of the objects ranging from 1.5 μm to 160 μm

in thickness and 100 μm to 2.45 cm in length. The shapes of the polymeric microparticles synthesized from LC films with bent in the ordering of LC molecular templates, however, were critically dependent on the thickness of the microparticles. We found that this was due to the interplay between the elastic energy and surface anchoring of the LCs. The critical role of LC elasticity was observed for thicknesses below 20 μm, whereas surface ordering played critical role on the thickness of the films above 20 μm (Chapter 5). Overall, the proposed method was shown to provide a precise control over the three-dimensional architectures of the objects ranging sizes covering the microscopic and macroscopic scales.

The library of the microparticles demonstrated in this study may find substantial use in applications including drug delivery, emulsions, separations and sensors, besides their potential in revealing new fundamental concepts in self-assembly and colloidal interactions.

Keywords: microparticles, liquid crystals, templated synthesis, photolithography, chirality

ÖZ

SIVI KRİSTAL ŞABLONUNDA KOMPLEKS NANOYAPILARA SAHİP POLİMERİK MİKRO PARÇACIKLARIN SENTEZLENMESİ

Akdeniz, Burak
Yüksek Lisans, Kimya Mühendisliği
Tez Danışmanı: Dr. Öğr. Üyesi Emre Büküşoğlu

Ağustos 2019, 92 sayfa

Sıvı kristaller, fotolitografi yöntemi ile birleştirildiğinde, iki ve üç boyutlu şekiller ve iç yapısı değiştirilebilen mikro parçacıkların sentezini sağlar. Yüzeyde istenilen yönelimde duran reaktif (RM257) ve reaktif olmayan mezojenlerin karışımları kullanılarak, nematik sıvı kristal filmleri hazırlandı, film içeriğindeki RM257 bir fotomaske kullanarak ultraviyole ışık yardımı ile polimerleşmesi sağlandı ve reaksiyona girmemiş mezojenlerin ekstraksiyonu ile polimer bazlı mikro parçacıkları elde edildi. Reaksiyona girmemiş mezojenlerin ekstraksiyonu sonrasında, RM257 içeriğine ve sıvı kristal yönelimine bağlı olarak kontrollü anizotrop büzülme gözlemlendi. Bunlara ek olarak, mikroparçacıkların en boy oranı, büyüklükleri ve kalınlıkları kontrol edildi ve %2'den daha az varyasyon katsayısına sahip parçacıklar elde edildi. Ek olarak, iki yüzeyde birbirine belli açılarla yerleştirilmiş sıvı kristal yönelimi kullanıldığında, sağa ya da sola doğru bükülmüş mikroparçacıkların oluşumu ile sonuçlandı (Bölüm 4). Bu sonuçların yanı sıra, mikroparçacıkların ilk şekillerini verebilmek için dairesel, üçgen, dikdörtgen, kare, yıldız ve kalp şekline sahip litografi maskeleri kullanıldı (Bölüm 5). Polimerleştirme öncesi sahip olunan reaktif ve reaktif olmayan mezojen karışımının konfigürasyonu, mikroparçacıkların kiral döngüde yapılar oluşturması veya istenilen yöne doğru bükülmesinin belirlenmesinde kritik bir rol oynadı. Polimer yapılı mikroparçacıkların kiral adım

sayısının, sıvı kristallerin arasında belirlenen açı ile doğrusal bir ilişki olduğu, ama 1.5 µm ile 160 µm arasında değişen kalınlıktan ya da 100 µm ila 2,45 cm arasında değişen uzunluktan bağımsız olduğu gözlemlendi. Bununla birlikte, sıvı kristal moleküler şablonunun bükülmüş olduğu ortamda sentezlenen polimer bazlı mikroparçacıkları şekilleri, kritik olarak mikroparçacıkların kalınlığına bağlı olduğu gözlemlendi. Bunun, elastik enerji ile sıvı kristallerin yüzey yönelimi arasındaki karşılıklı etkileşimden kaynaklandığını gördük. Sıvı kristal elastisitesinin kritik rolü, 20 µm altındaki kalınlıklar için gözlenirken, 20 µm üzerindeki filmlerin kalınlığında ise sıvı kristallerin yüzey bağlantısının baskın olduğu gözlenmiştir (Bölüm 5). Sonuç olarak, önerilen yöntemin, mikroskobik ve makroskobik ölçeklerde değişen nesnelerin üç boyutlu mimarileri üzerinde hassas bir kontrol sağladığı gösterilmiştir.

Bu çalışma içeriğinde sentezlenen parçacık şekilleri mimarileri ilaç salınımı, emülsiyonlar, ayırma prosesleri ve sensör gibi önemli uygulama alanlarında, bunun haricinde ise kendiliğinden düzenlenme ve koloidal etkileşimlerde üzerinde yeni temel kavramları ortaya çıkarılmasına üzerinde kullanılabilir.

Anahtar Kelimeler: mikroparçacıklar, sıvı kristaller, şablonla sentezlenme, fotolitografi, kiralite

To my lovely family,

ACKNOWLEDGEMENTS

First and foremost, I would like to express my sincere gratitude to my advisor and my mentor Asst. Prof. Dr. Emre Bukusoglu. I acquired valuable experience during my study under his supervision. I want to thank Dr. Emre Bukusoglu for his guidance, endless help, support, and patience. I must also express my gratitude to our cluster; Assoc. Prof. Dr. P. Zeynep Çulfaz Emecen, Assoc. Prof. Dr. Erhan Bat, and Asst. Prof. Dr. Simge Çınar.

I wish to express my great appreciations to soft and functional materials laboratory members; Asli Karausta, Özge Batır, Deniz Işınsu Avşar, Selin Şengül, Elif Kurt and Ceren Kocaman for beautiful and peaceful environment. It was a very valuable experience for me to work with them. I am happy for being met with you all and having spent all that time together. I would like to thank my gratitude to my colleagues' friends; Canan Aksoy, Toprak Çağlar, Ecem Volkan, Neslin Güler, Öznur Doğan, Merve Sarıyer, Soner Yaşar, Selin Şahin, Nisa Erişen, Begüm Yılmaz, Zeynep İmir, Seda Sivri, Ezgi Yavuzyilmaz, Fatma Şahin, Zeynep Karakaş, Merve Özkutlu. In particular, I would like to thank Berkan Atman for enthusiastic and inspiring discussions about science. I wish I had more time to spend together with you. I am well aware that words just too simple to describe my gratitude to you; Berrak Erkmen, Özge Batir, Cihan Ateş and Ceren Ateş. I also would like to thank Karden Ant, Ceren Fırat, İrem Gözübüyük, Erkin Erdoğan for endless support. My special thanks go to Can Atılgan, Nilsu Parlakyıldız and Berkin Nergis for their friendship, endless support and help. For the good times past, and better ones to come! Last but never the least, I would like to thank my parents Nazmiye and Uğur Akdeniz and my 'big' brother Barış Akdeniz for supporting me. For financial supports, I would like to thank Middle East Technical University scientific research fund (bap) through the grant number BAP-YLT-304-2018-3741 and the Scientific and Technological Research Council of Turkey (TÜBİTAK) through the grant number 217M268.

TABLE OF CONTENTS

ABSTRACT v

ÖZ… vii

ACKNOWLEDGEMENTS x

TABLE OF CONTENTS xi

LIST OF TABLES xiii

LIST OF FIGURES xiv

LIST OF ABBREVIATIONS xxiv

1. INTRODUCTION 1

2. LITERATURE SURVEY 5

3. MATERIALS AND EXPERIMENTAL SECTION 25

3.1. Materials 25

3.2. Preparation of the LC-Reactive Mesogen Mixtures 26

3.3. Preparation of the Glass Substrates 26

3.4. Polymerization of LC-Monomer Mixtures 27

3.5. Extraction of Polymeric Particles 28

3.6. Optical Characterization and Brightfield (BF) and Polarized Light (PL) Microscopy 28

3.7. Measurement of the LC-Twist Angles 28

3.8. Toluene Vapor Experiment 28

4. LIQUID CRYSTAL TEMPLATED POLYMERIC MICROPARTICLES SYNTHESIS COMBINED WITH PHOTOLITHOGRAPHY 31

4.1. Liquid Crystal Templated Microparticle Synthesis Method 31
4.2. Effect of Reactive Mesogen Concentration and Thickness of the Film on Microparticle Shape 37
4.3. Changing Aspect Ratios of Microparticles with UV Light 43
4.4. Synthesis of Three-dimensional Microstructure 46
4.5. Synthesis of Chiral Microparticles 49
5. DESIGN PARAMETERS AND PRINCIPLES OF LIQUID CRYSTAL TEMPLATED SYNTHESIS OF POLYMERIC MICROPARTICLES VIA PHOTOLITHOGRAPHY 55
5.1. Synthesis Method and Design Parameters 55
5.2. Effect of Photomask Feature and LC Alignment 56
5.3. Design Parameters of Bulk Chiral Twisted Polymeric Materials 63
5.4. Design Parameters of Bent Microparticles 70
5.5. Microparticle Size Reduction Strategies 73
6. CONCLUSIONS 75
6.1. Future Outlook 76
6.1.1. Microparticle Sensors 76
6.1.2. Alignment of LC-templated Microparticles in LC medium 77
REFERENCES 79
A. Representative Micrograph Images 89
B. Theoretical Aspect Ratio and Top Angle Calculation of Rectangular and Triangle Shaped Microparticles 91

LIST OF TABLES

TABLES

Table 4.1 Diameter and coefficient of variable of the synthesized microparticles with 10 wt. %, 15 wt. %, 20 wt. %, 25 wt. %, and 30 wt. % RM257 concentrations after polymerization.....38
Table 4.2 Dimensions of the synthesized microparticles with 10 wt. %, 15 wt. %, 20 wt. %, 25 wt. %, and 30 wt. % RM257 concentrations after extraction. 39
Table 4.3 Diameter and coefficient of variance of the synthesized microparticles with 1.5 μm, 6 μm, 20 μm, 40 μm, 80 μm, and 160 μm film thicknesses after polymerization.....41
Table 4.4 Dimensions of the synthesized microparticles with 1.5 μm, 6 μm, 20 μm, 40 μm, 80 μm, and 160 μm film thicknesses after extraction. 41
Table 5.1 UV exposure times required to synthesize microparticle from mixtures of 20 wt. % RM257 in E7. Collimated light source energy was adjusted to 0.7A or 1.2A. Red boxes indicates the UV exposure times used in the synthesis of the corresponding microparticles. 60

LIST OF FIGURES

FIGURES

Figure 1.1 (A) The graph shows microparticle synthesis methods with chemical anisotropy versus shape complexity. (B) Size limits of the synthesized microparticles with varied methods.[9] 2
Figure 2.1 (A) Four main steps of the photolithography synthesis method. (B) Fluorescent polymeric 'LithoParticles' were synthesized via photopolymerization. Scale bar is 5 μm. (C) Three dimensional micro particles were synthesized from multilayer approach.[14] 6
Figure 2.2 (A) Schematic illustration of the CFL procedure with top and side view. (B) Synthesized microparticles via CFL technique. Scale bars are 10 μm. (C) Janus synthesis method and synthesized microparticles. Scale bar is 100 μm.[18] 7
Figure 2.3 Two general approach for the synthesis of diverge range of PS particles. (A) Top image is the scheme representation of the method A. The bottom images are the synthesized (a) spherical, (b) rectangular disc, (c) rods, (d) worms, (e) oblate ellipses, (f) elliptical discs, (g) UFOs, and (h) circular disks shape particles. Scale bars: 2 μm. (B) Top image is the scheme representation of the method B. The bottom images are the synthesized (a) barrels, (b) bullets, (c) pills, and (d) pulleys shape particles. Scale bars: 2 μm.[34] 9
Figure 2.4 Key parameters of the liquid crystalline materials. (A) Surface ordering, (B) elasticity of the LCs, and (C) topological defect in LC medium. 11
Figure 2.5 Various types of liquid crystalline monomers. Reactive groups are at the both end (end-on) (A), one end (C), or at the side (side-on) (B, D) of their rigid structure. 13
Figure 2.6 Molecular structure of the liquid crystalline monomers M3 and M4 used for this study. Microscopy images of the colloidal microparticles synthesized from (B) pure ethanol, (C) 8:1 ethanol to 2-methoxy ethanol ratio, (D) 4:1 ethanol to 2-methoxy

ethanol ratio with M3. Top images show broader size distributions, whereas bottom images show narrower size distributions with 10:1 ethanol to 2-methoxy ethanol ratio (E), 9:1 ethanol to 2-methoxy ethanol ratio with M3 (F) and pure ethanol with M4 (G). [53] 14
Figure 2.7 (a-d) LCE pillars were heated up systematically to isotropic temperature (around 170°C), (e) then cooled back to the room temperature. Scale bar: 100 μm.[58] 16
Figure 2.8 Schematic illustration of core shell microparticle synthesis method by double emulsion microfluidic device (A) and temperature response experiment setup (B). (C and D) Temperature response of the core-shell microparticles. [50] 17
Figure 2.9 Schematic illustration of the top view of elastomeric film is on the left panel of the figure. Cutting direction changed the final structure of the elastomer as form almost flat (Ribbon A), left and right handed ribbons (Ribbon B and D, respectively), and open ring (Ribbon C) structure.[32] 18
Figure 2.10 Synthesis of (A) spindle-shaped, (B) spherical, (C) spherocylindrical or (D) tear-shaped polymeric microparticles templated from LC droplets in (A) bipolar, (B) radial, (C) axial or (D) preradial configurations, respectively. Bright field and polarized light images of each configurations can be seen below the schematic illustration of the configuration. Scale bars: 5 μm. (E) (o) Ratio of the final and initial volume of the bipolar microparticles, and (X) mass density of the same particles with varied RM257 concentrations. [24].....20
Figure 2.11 Schematic illustration of the bipolar microparticle (left side of A) and spindle shape microparticle (right side of A). (B) Images of the polymeric microparticles corresponding to fraction of ethanol = 0, 0.4, 0.6, and 0.8. [63].....22
Figure 2.12 Optical images of LCE films synthesized from 20 wt.% RM257 and their extracted states. LC director is indicated with 'n'. n is planar in (A), homeotropic in (B), and hybrid in (C). (D) The result of shrinkage percentage versus RM257 concentration graph. (E) Ratio of final volume to initial volume versus RM 257 concentration graph.[23] 23

Figure 3.1 Micrograph images of the lithography masks. (A and B) Circular, (C) heart shape, (D) star shape, (E) square, (F) rectangular, (G) equiangular triangle. 26
Figure 4.1 Schematic illustration of the method used for the synthesis of the microparticles. (A) the molecular structures of the reactive, nonreactive mesogens, and photo initiator used in this study, (B) The sketch of the four-step microparticle synthesis method. 32
Figure 4.2 Representative optical micrographs collected during the synthesis of polymeric microparticles from a mixture of 20% by weight RM257 in E7. The top two images of each set are the brightfield and polarized light micrographs at the same orientation where the rubbing direction (indicated as R) was parallel to the polarizer. The bottom two images of each set are the brightfield and polarized light micrographs of the films when rotated 45 degrees. A 6 μm-thick film was confined between two rubbed-PVA coated glass surfaces. Micrographs shown (A) before polymerization, (B) after polymerization with UV light and a photomask (inset showing a magnified part shown in dashed lines), and (C) after detachment of the two glass surfaces after polymerization. The red arrow in (B) indicates the polymerized regions of the film. The arrows with A and P show the orientation of the two polarizers and R shows the rubbing direction of the glass slides to maintain planar anchoring. Scale bars: 500 μm, inset in B, 100 μm. 34
Figure 4.3 (A) A representative image of a microparticle synthesized from 20 wt.% RM257 in E7 where the nematic director was along the long axis of the microparticle. Scale bars: 100 μm. (B) The size distribution of the microparticles synthesized from a mixture of 20% RM257 in E7 before and after extraction of the unreacted mesogens, dashed line in the sketch shows the nematic director profile. 35
Figure 4.4 Microparticles synthesized under isotropic condition. Micrographs were collected (A) after detachment, and (B) after extraction. Images on the left panel of each figure set are brightfield (top) and 45° rotated brightfield (bottom) images whereas images on the right side of each panel are polarized light and 45° rotated polarized light images. The arrows with A and P show the orientation of the two polarizers. Scale bars in A: 500 μm, scale bars in B, 100 μm. 37

Figure 4.5 Shrinkage percentage change with respect to the monomer percentage. (A) A representative image of a microparticle synthesized from 10 wt. %, 15 wt. %, 20 wt. %, 25 wt. %, and 30 wt. % RM257 in E7 where the nematic director was along the long axis of the microparticle. (B) The plot of shrinkage percent parallel and perpendicular to the nematic director and aspect ratio of the microparticles after extraction as a function of the monomer concentration. 40
Figure 4.6 Bright field and polarized light microscope images of the microparticles were synthesized from 20 wt. % RM257 in E7 with 1.5 μm, 6 μm, 20 μm, 40 μm, 80 μm, and 160 μm film thicknesses. Thickness of the films are indicated at the top of the Figure. 42
Figure 4.7 (A) Sketch showing the labeling used to define dimensions of a single microparticle. (B) Amounts of the shrinkage of the microparticles measured after extraction of the unreacted mesogens from the microparticles. The particles were synthesized from 20 wt. % RM257 in E7. 43
Figure 4.8 Experimental results showing the effect of the UV exposed area on the initial and final shapes and aspect ratios of the microparticles where the nematic director was along their long axis. 20 wt.% RM257 in E7 with 6 μm thickness were used in the synthesis. (A) sketch showing the UV light-exposed area (top) and corresponding brightfield (middle) and polarized light (bottom) micrographs of the microparticles synthesized. Scale bars: 100 μm. (B) The aspect ratio of the microparticles maintained after polymerization. (C) The aspect ratio of the microparticles maintained after extraction. 44
Figure 4.9 Experimental results showing the effect of the UV exposed area on the initial and final shapes and aspect ratios of the microparticles where the nematic director was along their short axis. 6 μm-thick films of 20 wt.% RM257 in E7 were used in the synthesis. (A) Sketch showing the UV light-exposed area (top) and corresponding brightfield (middle) and polarized light (bottom) micrographs of the microparticles synthesized. Scale bars: 100 μm. (B) The aspect ratio of the microparticles maintained after polymerization. (C) The aspect ratio of the microparticles maintained after extraction. 45

Figure 4.10 Representative optical micrographs collected from the synthesis of polymeric microparticles with homeotropic anchoring from a mixture of 20% by weight RM257 in E7. A 6 μm-thick film was confined between two PFDTS coated glass surfaces. Micrographs were collected (A) before polymerization, (B) after polymerization with UV light and a photomask (inset showing a magnified part shown in dashed lines. Images on the left panel of each figure set are brightfield (top) whereas images on the right side of each panel are polarized light images. Insets showing the conoscopic images indicative of homeotropic anchoring. Scale bars: A and B 500 μm; inset in B, 100 μm. 47
Figure 4.11 Representative sketches of the LC anchoring maintained at the confining surfaces before polymerization (left panel) and optical micrographs collected from the polymeric microparticles (brightfield, middle; polarized light, right panel) synthesized from a mixture of 20% by weight RM257 in E7 with different anchoring conditions. The film thicknesses were 6 μm and films were (A) confined between two PFDTS-coated glass surfaces mediating homeotropic alignment (inset image shows conoscopic image indicative of homeotropic anchoring), (B) confined between a PFDTS surface mediating homeotropic alignment and a rubbed PVA surface mediating uniform planar alignment along the long axis, and (C) confined between a PFDTS surface mediating homeotropic alignment and a rubbed PVA surface mediating uniform planar alignment along the short axis. n indicates the nematic director of the surface mediating planar anchoring. Scale bars: 100 μm. 48
Figure 4.12 Image processing results that show LC mixture align in the direction of rubbed PVA. (A-E) The maps of the measured angles within a piece of a film is shown, the rubbing of the surfaces was done at angles of (A) 0°, (B) 30°, (C) 45°, (D) 60° and (E) 90°. (F)The plot of the measured LC-twist and rubbing angle. 49
Figure 4.13 Micrographs of the microparticles synthesized between rubbed PVA glass slides mediating left-hand and right-hand twisted nematic ordering. (A) Scanning electron micrographs, scale bars: 20 μm. (B) brightfield (middle) and polarized light (right) micrographs of the microparticles synthesized between two glass slides of indicated twist angle shown in the left panel of each figure set, scale bars: 100 μm.

The particles were synthesized from 20 wt.% RM257 in E7 with a film thickness of 6 μm. 51
Figure 4.14 SEM images of chiral microparticles which was synthesized from a mixture of 20% by weight RM257 in E7, 6 μm spacer thickness, and adjusted LC twist angles. Circler photolithography mask with (A) 100 μm and (B) 260 μm features were used. (A-i) and (B-i) represents L-LC twist, whereas (A-ii) and (B-ii) shows R-LC twist conformation. Scale bars in A: 20 μm, Scale bars in B: 50 μm. 52
Figure 4.15 Additional micrographs of the chiral microparticles synthesized from mixtures of 20% by weight RM257 in E7, 6 μm spacer thickness, and 30° LC twist angles. Circle photolithography mask with (A and B) 260 μm and (C) 100 μm features sizes was used. (A) and (B) are the representative micrographs of the microparticles synthesized from left-handed and right-handed twist conformation, respectively. (C) SEM image of the microparticles that demonstrates the homogenous distribution of the microparticles. Scale bars in A and B: 100 μm, SEM images scale bars in A and B: 50 μm, and Scale bar in C: 200 μm. 53
Figure 5.1 Schematic representation of the LC-templated microparticle synthesis procedure followed in the study. The left column shows the schematic representation of the procedure. The right column shows representative micrographs collected during the synthesis of star shaped microparticles following the procedure on the left. Scale bars = 300 μm for the top two micrographs, 50 μm for the inset in the middle micrograph and the bottom figure. 56
Figure 5.2 Optical micrographs of the microparticles synthesized from mixtures of 20 wt. % RM257 in E7. The top row indicates the representative features of the photomasks used in each column and the sketches on the left column indicates the LC configuration initially maintained within the film. 6 μm spacers were used to separate two functionalized surfaces. Micrographs shows the microparticles synthesized from films with an LC alignment (A) horizontal, (B) vertical, (C) in plane and (D) with 45° angle with respect to brightfield images shown. Two insets corresponding to each image were taken under polarized light. The left insets are taken at the same direction whereas the right insets were taken after the image was rotated 45° with respect to the

brightfield images. Rubbed PVA surfaces were used for planar, and DMOAP functionalized surfaces were used for homeotropic anchoring. Scale bars: 50 μm... 57
Figure 5.3 SEM images of microparticles synthesized from the mixture of 20 wt.% RM257 in E7 and 6 μm thickness. (A) The images of a heart shaped microparticle synthesized from a mixture maintained at homeotropic alignment between two DMOAP surfaces. (B) The images of a rectangular shaped microparticle synthesized from a mixture maintained at planar alignment between two rubbed PVA surfaces. The inset figures show the FFT patterns of the corresponding SEM images. 59
Figure 5.4 Features of the triangular shapes with varied current and UV exposure time. The images in column 1-A show the polymerized regions after exposure with current setting of 0.7A whereas the images in column 1-B show the polymerized regions after exposure with current setting of 1.2A. UV exposure times were changed from (i) 1 second, (ii) 2 seconds, (iii) 3 seconds, (iv) 4 seconds, and (v) 5 seconds. The films in column 1 were prepared between two glass surfaces with thickness of 1 mm. In the films shown in columns 2-A and 2-B were maintained between glass cover slides with 0.13 to 0.16 mm thicknesses. Microparticles were synthesized at 0.7A current in 3 seconds in 2-A, whereas in 2-B it was synthesized at 1.2A in 2 seconds. 61
Figure 5.5 Schematic representation of (A) rectangle and (D) triangle shaped particles before and after extraction. The arrow ‘n’ represents the rubbing direction of the PVA functionalized surfaces. Micrograph images of rectangular (B) and triangular (E) particles. Scale bars: 50 μm. Theoretical and experimental aspect ratio of the rectangular shape particles can be found in (C). Theoretical and experimental top angle data of the triangular shape particles can be seen in (F). 63
Figure 5.6 Micrographs of the microparticles synthesized between rubbed PVA glass slides mediating left-hand and right-hand twisted nematic ordering. (A) Scanning electron micrographs, scale bars: 20 μm. (B) transmission (middle) and reflection (right) mode micrographs of the microparticles synthesized between two glass slides of indicated twist angle shown in the left panel. (C) Pitch size of the chiral particles characterized with respect to angle between two PVA coated glasses. The particles were synthesized from 20 wt.% RM257 in E7 with a film thickness of 6 μm. 65

Figure 5.7 (A-F) The maps of the measured twist angles within a piece of a film with various thicknesses are shown. The thicknesses of the films were (A) 1.5 μm, (B) 6 μm, (C) 20 μm, (D) 40 μm, (E) 80 μm and (F) 160 μm, and a right-handed LC twist of 30° were maintained within the films. The plot in (G) shows the average twist angle measured with respect to thickness. 66
Figure 5.8 Left-hand microparticles synthesized between rubbed PVA glass slides right-hand twisted nematic ordering. (A) Configuration of the zenithal angles representing angle variation inside the particles. Twist angle of the LC adjusted as (A-i) 0°, (A-ii) 30°, (A-iii) 45°, (A-iv) 60°, and (A-v) 90°. (B) The graph of the particle zenithal angles with respect to LC twist angle. 67
Figure 5.9 (A) Optical micrographs of particles obtained from mixtures of 20 wt. % RM257 in E7 with left handed 30° degrees twist. The thickness of the functionalized surfaces with PVA varied between 1.5 μm to 160 μm indicated at the below of each figure. Scale bars: 50 μm. (B) The graph that show the pitch of the synthesized microparticles with respect to thickness. 68
Figure 5.10 Micrographs of the spiral ribbons synthesized between rubbed PVA glass slides mediating left-hand and right-hand twisted nematic ordering. LC twist angle was adjusted (A) 0°, (B) 20°, (C) 25°, (E) 30°, and (F) 60°. Helicoid shape observed in B. Spiral ribbons can be seen in C, E, and F. Scale bars: 300 μm. (D) Scanning electron micrographs of E, scale bars: 100 μm. The chiral films were synthesized from 20 wt.% RM257 in E7 with a film thickness of 6 μm. 70
Figure 5.11 (A) Micrographs of microparticles synthesized from mixtures of 20 wt.% RM 257 in E7 between two surfaces mediating homeotropic anchoring at one side and planar anchoring at the opposite side. Thicknesses of the particles were varied from 1.5 μm to 320 μm. Scale bars: 25 μm. (B) SEM images of a microparticle synthesized from a 6 μm thick film. (C) A plot of the radius of curvature of the microparticles measured as a function of the thickness of the microparticles. 72
Figure 5.12 Size reduction of the microparticles which were synthesized from mixtures of 20 wt.% RM257 in E7 with 6 μm thickness. (A) Schematic representation of the experimental setup for size reduction. Micrograph of the microparticles with

(B) 2 sec., (C) 3 sec., (D) 4 sec., and (E) 5 sec. exposure times. (F) A plot of the microparticle diameter as a function of UV exposure time. 74
Figure 6.1 Toluene vapor exposure test was performed microparticles that were synthesized hybrid condition. The thickness of the microparticles were (A) 1.5 μm, (B) 40 μm, and (C) 160 μm. The top micrographs show initial state (0 ppm). The bottom images of the Figure represent the maximum toluene vapor limit (30000 ppm). 77
Figure 6.2 Behavior of the microparticles under LCs medium. The microparticles were synthesized mixtures of 20 wt. % RM257 in E7, 6 μm spacer thickness, and (A) two rubbed PVA surfaces or (B) two DMOAP coated surfaces. Anchoring of LC molecules were planer (A-i and B-i) or homeotropic (A-ii and B-ii). Top images show schematic representation of the system. Middle images are the brightfield micrograph images. 'n' indicates LC alignment. Bottom images are the polarized light images. Scale bars: 50 μm. 78
Figure A. 1. Representative brightfield micrograph image after polymerization with UV light (inset showing a magnified part shown in dashed lines). The red arrows indicate the polymerized regions, whereas the blue arrow indicate the unpolymerized regions of the film. The figure is same as Figure 1B with the adjusted as +30% brightness. Scale bar: 500 μm, inset, 100 μm. ……89
Figure A. 2. Representative (A) brightfield and (B) polarized light micrographs of the microparticles synthesized from a mixture of 20% by weight RM257 in E7 with uniform planar anchoring. The photomask circular features used in the synthesis was 100 μm. Scale bars: 300 μm. ……90
Figure A. 3. Representative brightfield micrograph image after polymerization with UV light (inset showing a magnified part shown in dashed lines). The red arrows indicate the polymerized regions, whereas the blue arrow indicate the unpolymerized regions of the film. The figure is same as Figure 1B with the adjusted as +30% brightness. Scale bar: 500 μm, inset, 100 μm. ……..90

Figure B. 1. Schematic representation of rectangular shaped microparticles. Rubbing direction (indicated as n) is (*i*) parallel to long axis, or (*ii*) short axis. The equation for each case can be seen below. ……..91

Figure B. 2. Schematic representation of triangular shaped microparticles. Rubbing direction (indicated as n) is (*i*) parallel to b, or (*ii*) a. ……92

LIST OF ABBREVIATIONS

ABBREVIATIONS

LC	Liquid Crystal
LCE	Liquid Crystal Elastomer
COV	Coefficient of Variance
CFL	Continuous Flow Lithography

CHAPTER 1

INTRODUCTION

In recent years, there is a demand for miniaturization of three dimensional objects for certain applications including medical diagnostics[1], drug delivery[2], emulsion stabilization[3], and catalysis[4]. Within these applications, there are evidences that highlight the significance of the shapes of the micrometer sized objects in the applications, for instance, shape of the microparticles affects the targeting efficiency of the drugs[5,6], or emulsion type[7]. In other words, shape complexity is an important parameter in stabilizing the Pickering emulsions[3] or designing drug delivery[8] agents and it plays an important role in the Brownian motion and colloidal interactions between particles, which underlie important physical phenomena. For this reason, there are wide range of materials of construction, shapes, and internal morphology of the microparticles.[9–11] Therefore, more recent application areas and scientific advancements require to broaden the size, shape and chemical complexity, and internal structures of the micrometer sized objects.

There are various available methods that can fulfill the requirements of shaping microparticles. These well-established methods include traditional top down methods[12,13], soft lithography[10], photolithography[14], spray drying[15], mold stretching[16], microfluidic[9,17–19], and emulsion-based polymerization[20]. To observe the effect of the synthesis method on the microparticles shape complexity and chemical anisotropy, Dedunkuri prepared Figure 1.1[9]. Figure 1.1-A summarizes microparticle synthesis methods which have significant effect on chemical anisotropy and shape complexity due to employed method. Figure 1.1-B shows the particle size coverage of the synthesis methods. Although given methods have their own advantages such as scalability, reproducibility and precise control over the shape, most of them suffer from control over the morphology and the internal structure of the particles. For

example, flow lithography provides high-throughput synthesis of morphologically or chemically unique particles (Figure 1.1-A), the size of the microparticles are limited to micrometer scale (Figure 1.1-B). Or while it is possible the synthesize nanoscale microparticles via emulsion polymerization, their shapes are limited to spheres. To solve the limitations of such methods and improve the library of the microparticle shape, templated synthesis of polymeric materials has been shown to architect the polymeric materials. Recently, it has been shown that low molecular weight non-reactive LCs are good candidate for the templated synthesis of polymeric materials.[21–24]

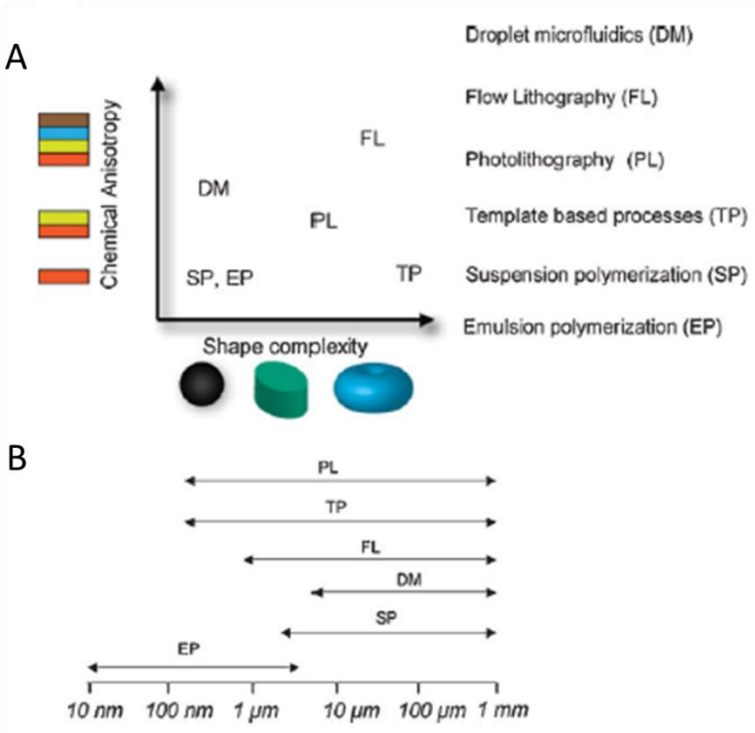

Figure 1.1 (A) The graph shows microparticle synthesis methods with chemical anisotropy versus shape complexity. (B) Size limits of the synthesized microparticles with varied methods.[9]

Here, we underline the fundamentals of liquid crystals (LCs) which we significantly employ in this study because our main approach is combining photolithography process and LC molecular templates. LCs are a phase between crystalline solids and isotropic liquids. These phases of matters are classified as thermotropic LCs when temperature is critical to form LC phase. These thermodynamically stable phases are generally seen in rod like molecules (anisotropic behavior) such as pentyl cyanobiphenyl (5CB) and the mesoscale ordering is represented as director (average orientation). The simplest and best studied phase is the nematic LCs. In nematic LCs, molecules are aligned in almost at the same direction but exhibit no position order. Moreover, addition of chiral dopant to the nematic LCs lead to form cholesteric LCs. In cholesteric LCs, LC molecules show helical twist perpendicular to the director. Addition of the chiral dopant, and closeness to nematic to isotropic transition temperature cause blue phases. In blue phase, LC molecules have two directions which are perpendicular to the director (three-dimensional periodic lattice).

In this study, our main aim is to improve microparticle shape complexity and morphology by employing LCs as templating molecules. Photolithography method was employed for the synthesis of microparticles and the combination of the photolithography process with LC template method provide improvement in microparticle shape complexity and morphologically tunable microparticle synthesis. In this thesis, specifically, chapter 2 provides information regarding to microparticle synthesis methods, LCs, LC elastomers, and the combined methods (synthesis method and LC) will be discussed. Chapter 3 will give information related to the materials used, and experimental methods followed in this study. Chapter 4 will underline the development of the method which we combine the lithography process with LCs and define a generalized boundary of the accessible microparticle shapes. Chapter 5 will explain the key parameters and principles for the synthesis of microparticles, their precision and define future possibilities. Conclusions of the thesis can be found in Chapter 6.

CHAPTER 2

LITERATURE SURVEY

Polymeric microparticles are used in diverse range of applications such as drug delivery[25], emulsion stabilization[3], catalysis[26], separation process[27,28] and sensors[29]. The shape complexity, size and internal morphology of the particles are critical for uses in these fields ranging from fundamental sciences to specific applications. Beyond the currently available microparticle architectures, there is an interest in the synthesis of custom design particles, therefore, there is a need of methods to broaden the range of the microparticle types that enable new scientific and technological advancements. For instance, macroscopic chiral twisting of polymeric materials is often required for emerging technologies that require response against external stimuli resulting from their chiral twist, such as artificial muscles or micro swimmers, however, the synthesis of such polymeric materials often requires labor intensive procedures.[30–33] Therefore, our aim for this study is to describe a method that combine liquid crystal (LC) molecular templates with photolithography for the synthesis of monodisperse polymeric microparticles. The method provides control over the size, complex internal structure, and shape including a micrometer-scale chiral twisting and bending via the use of liquid crystals, which would not be possible with their isotropic molecular counterparts.

Here, we would like to underline some polymeric microparticle synthesis methods which are linked with this study. Photolithography method is well established in circuit technology and is adapted to synthesis of polymeric microparticle by Hernandez and Mason.[14] In their study, four main steps were the same with ordinary photolithography procedure; spin coating, UV exposure, development and lift-off. The details of the synthesis steps can be seen in Figure 2.1-A. By employing these methods, they have synthesized exotic colloids, or “LithoParticles” in mass scale

(around billions of copies). To show the shape broadness of the fluorescent polymeric microparticles, alphabet soup (26 letters of the Latin alphabet) were synthesized through photolithography method. On the other hand, hybrid and three-dimensional shapes of particles are synthesized through multilayer approach in photolithography (Figure 2.1-C). These show the full potential of the photolithography process in terms of microparticle synthesis. However, the synthesis of chiral shape microparticles or ribbons is almost impossible through this procedure.

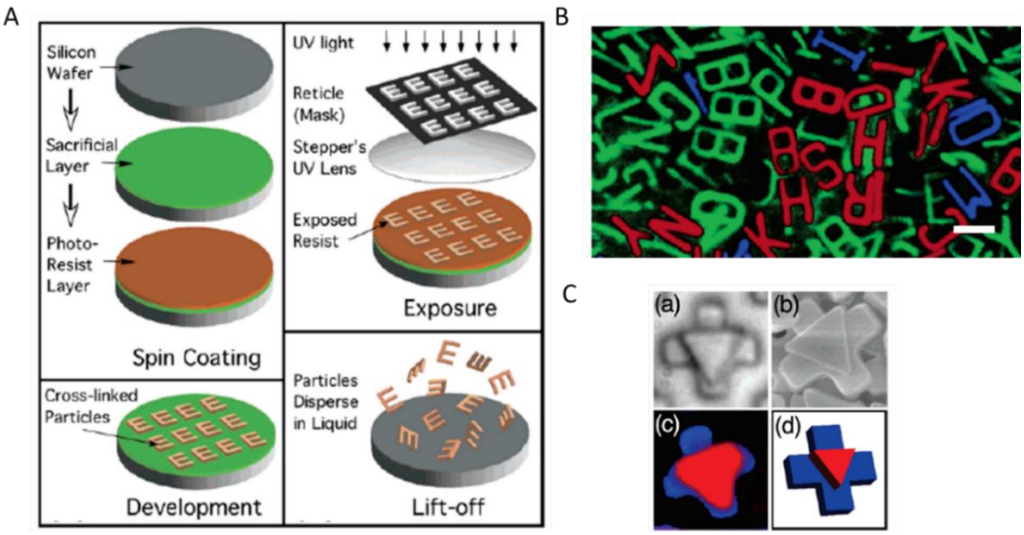

Figure 2.1 (A) Four main steps of the photolithography synthesis method. (B) Fluorescent polymeric 'LithoParticles' were synthesized via photopolymerization. Scale bar is 5 μm. (C) Three dimensional micro particles were synthesized from multilayer approach.[14]

One of the favorable methods is microfluidic devices which contain microchannel and deal with the low Reynold numbers within the channels. These microchannel architectures result in the improvement of the microparticle synthesis in terms of time, rate and sensitivity (monodispersity)[18]. To illustrate, Dendukuri *et al.* have developed new perspective by coupling photolithography approach with the microfluidic perspective in order to synthesize much complex shapes[18]. In continuous flow lithography (CFL), monomer flowed in the polydimethylsiloxane (PDMS) based

microchannel and exposed to UV light where shape of microparticles was defined with photomasks. Figure 2.2-A shows the schematic illustration of the CFL synthesis setup. Photopolymerization of the microparticles were almost instantaneous and did not show any plugging inside the channels due to oxygen mediated inhibition of PDMS surface. Synthesized microparticles through this method can be seen in Figure 2.2-B. Moreover, combining several microchannels with CFL procedure increases the chemically distinct regions like Janus type particles. (Figure 2.2-C). Although suggested method has significantly improved microparticle shape, speed of the microchannels might lead to decrease the resolution and form blurring and smearing of the shape of the particles, and the accessible particle shapes were limited to those that can only be extended from a two-dimensional drawing on the mask.

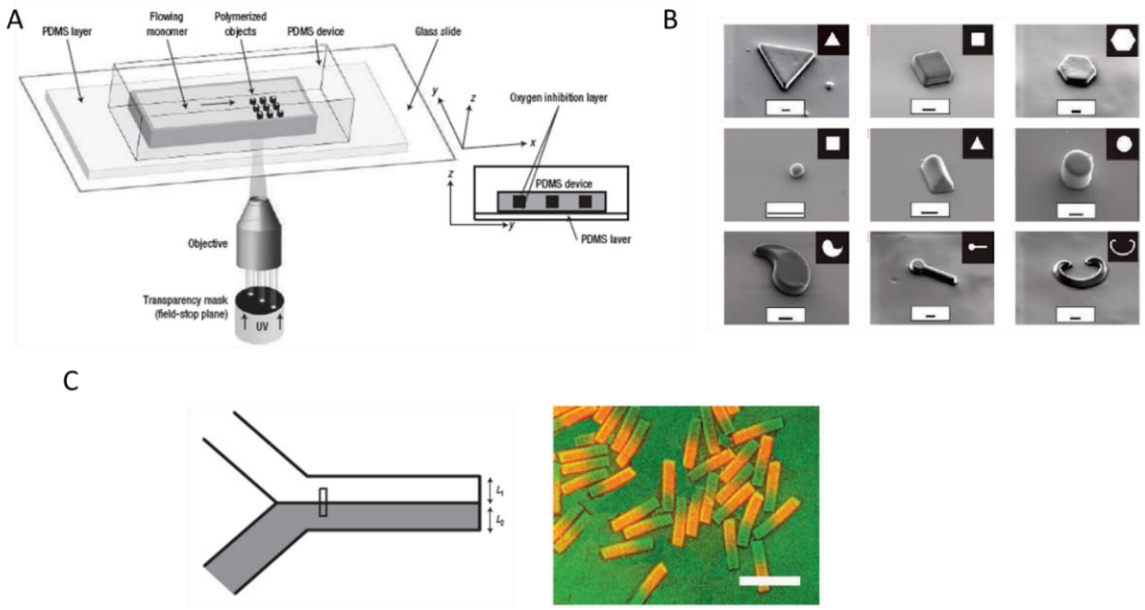

Figure 2.2 (A) Schematic illustration of the CFL procedure with top and side view. (B) Synthesized microparticles via CFL technique. Scale bars are 10 μm. (C) Janus synthesis method and synthesized microparticles. Scale bar is 100 μm.[18]

Mold stretching provides diverse range of particle shapes that could broaden the shape symmetry of the particles that can be synthesized by photolithography methods. Champion *et al.* used two general approaches for the synthesis of 60 nm to 30 μm polystyrene (PS) particles.[34] In the first approach (Figure 2.3-A), PS particles were liquefied on PVA based mold and then stretched in one or two dimensions to synthesize spherical, rectangular disc, rods, worms, oblate ellipses, elliptical discs, UFOs, and circular disks shape particles. In the second approach (Figure 2.3-B), PVA films were stretched to create voids around PS particles. Then, PS particles were liquefied and solidified again. This approach leads to synthesis of barrels, bullets, pills, and pulleys shape particles. Design parameters of the diverse range of particles were identified as Tg and thickness of film, Tg and viscosity of particle, adhesion strength between particle and film, and stretch parameters. These parameters were adjusted to obtaine desired particle shape and size. Unfortunately, internal structuring of particles is not possible through this method, in addition, the accessible shapes were limited to the shapes that can be formed by complete or partial filling of the elongated cavities defined by the molds.

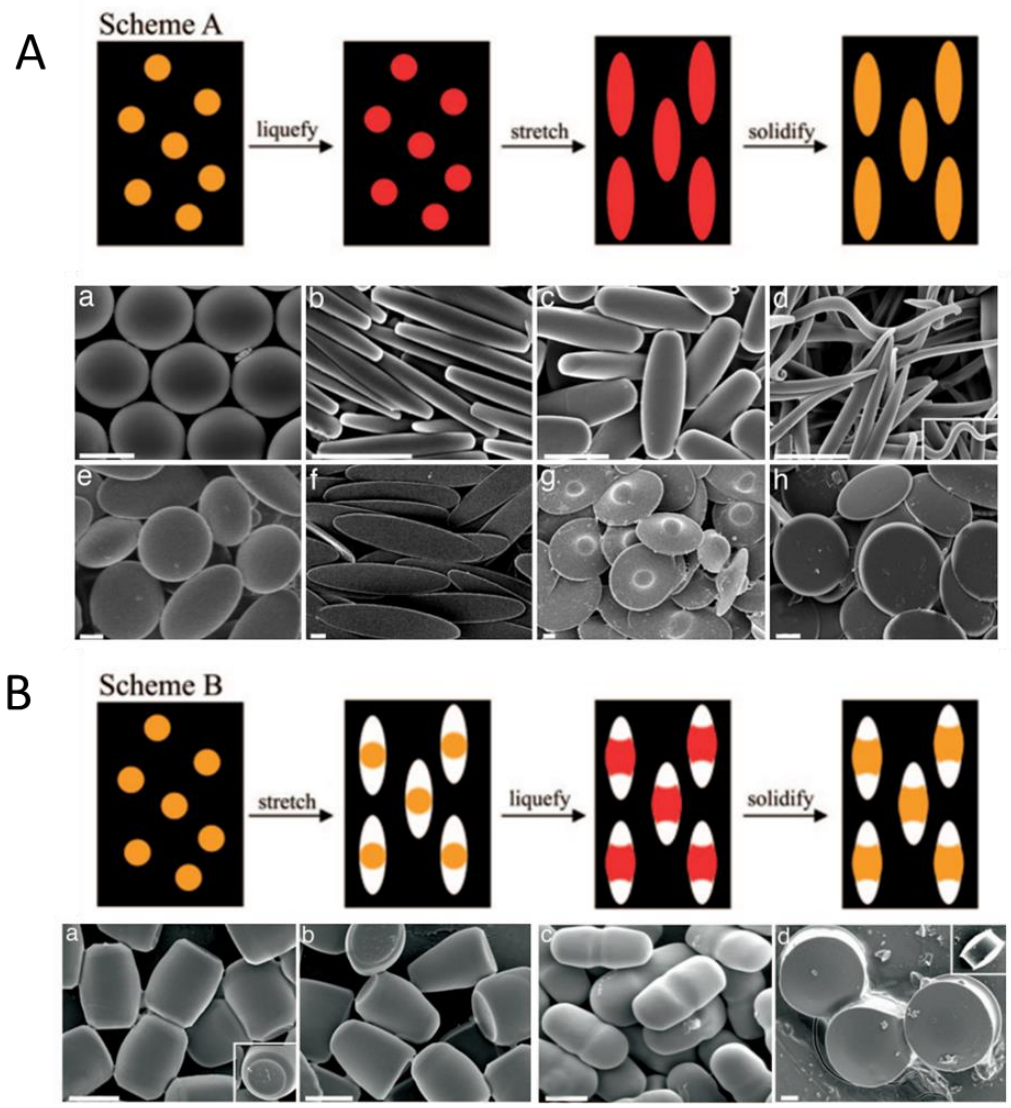

Figure 2.3 Two general approach for the synthesis of diverge range of PS particles. (A) Top image is the scheme representation of the method A. The bottom images are the synthesized (a) spherical, (b) rectangular disc, (c) rods, (d) worms, (e) oblate ellipses, (f) elliptical discs, (g) UFOs, and (h) circular disks shape particles. Scale bars: 2 μm. (B) Top image is the scheme representation of the method B. The bottom images are the synthesized (a) barrels, (b) bullets, (c) pills, and (d) pulleys shape particles. Scale bars: 2 μm.[34]

All listed methods for the synthesis of polymeric microparticles have their own advantages and disadvantages as discussed previously. To give one more example, hydrodynamic effects (Peclet number) and drying conditions in spray drying to modify microparticles morphology[15], or chemical and structural complexity can be incorporated to the microparticles through combination of several methods, for example through combination of microfluidics with photolithography[35], they still provide limited solutions especially for three dimensional architectures. For instance, the shapes and their symmetries are limited to those that can be given by the confinement symmetry of the micro-environment surrounding the synthesis media, such as spherical compartments or channels with cylindrical or rectangular cross section[36]. In addition, the introduction of complexity in the three-dimensional shapes (such as chirality) of the particles is challenging, and usually impossible, through these methods. Moreover, since the chirality, within a size range that spans from molecular sizes to meso- and macroscopic scales, is an important phenomenon that plays a significant role in determining the behavior [37–39], application[31,40,41], and performance[42,43] of the nanoscopic to microscopic objects; control over the synthesis of objects with such symmetries provides significant contribution to their use in certain applications. Thus, further control over the shapes and structures of the micrometer sized objects requires additional methods to be established.

In this study, LCs were selected as templating molecule to control the shape and internal structure of the particle because LCs can be reorganized under stimulus and they can change their director depending on the chemical and physical properties of the surrounding environment.[44] In addition, their orientation can easily be determined using polarized optical microscopy.

Surface ordering of LCs, elasticity of LCs, and the formation of the topological defects in LCs are the three key parameters that strongly affect orientation and behavior of the LCs. Therefore, here we outline the design parameters of the LC templated microparticle synthesis methods.

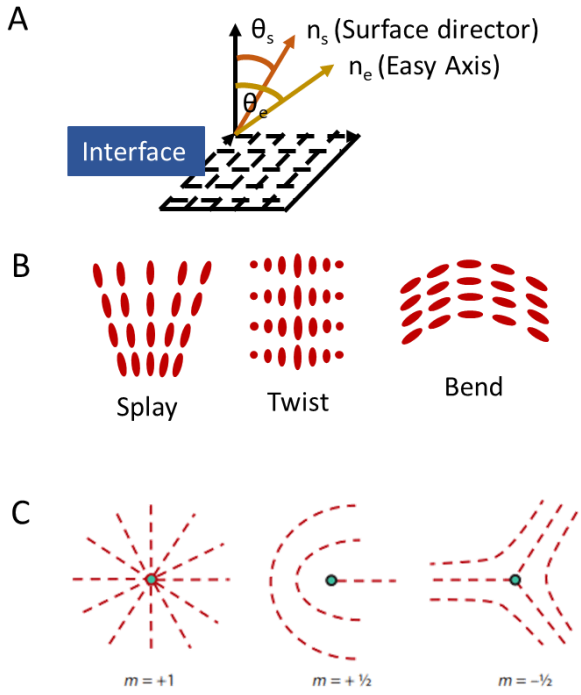

Figure 2.4 Key parameters of the liquid crystalline materials. (A) Surface ordering, (B) elasticity of the LCs, and (C) topological defect in LC medium.

Surface ordering of the LC molecules are connected with intermolecular interactions between LCs and a confining medium. LCs has the minimum energy in easy direction without any external field. Application of external field may redefine the orientation of the LCs and the direction of the LCs at the surfaces is called surface director. (Figure 2.4-A) This causes a deviation from easy axis and increases the free energy. Interfacial free energy (F_s) is often described by following formula,[44,45]

$$F_S = F_0 + \frac{1}{2} \cdot W_a \cdot \sin^2(\theta_s - \theta_e) \qquad \text{Equation 1}$$

where W_a is anchoring energy and has the value 10^{-3}-10^{-2} mJ/m^2. Surface ordering of LCs can be changed by functionalization of the surfaces with different chemicals. For example, rubbed polyvinyl alcohol (PVA) or polyamide (PA) show planar anchoring at the surface of the glass substrate, while functionalizing with the

octadecyltrichlorosilane (OTS), dimethyloctadecyl [3-(trimethoxysilyl) propyl] ammonium chloride (DMOAP), or perfluorodecyltrichlorosilane (PFDTS) show homeotropic anchoring (perpendicular to the surface of the glass substrate).

Elasticity of the LCs behavior is related to long-range orientation of the LCs. Twist, bend and splay are the three main strain modes of the LCs (Figure 2.4-B). There are many different representations of free energy density considering elastic property of LCs. One of the best-known representations of the free energy density is the Frank – Oseen equation as follows;[46,47]

$$F_e = \frac{1}{2} \cdot K_1 \cdot \left(\nabla \cdot \underline{n}\right)^2 + \frac{1}{2} \cdot K_2 \cdot \left(\underline{n} \cdot \nabla \times \underline{n}\right)^2 + \frac{1}{2} \cdot K_3 \cdot \left[\underline{\mathrm{n}} \times \left(\nabla \times \underline{n}\right)\right]^2 \quad \text{Equation 2}$$

where K_1, K_2, and K_3 are the strain constants for twist, bend and splay modes, respectively in the order of 10^{-11} N.

The phenomena of topological defect underline the discontinuity regions of the LC molecules under different geometries (Figure 2.4-C). LCs molecules are forced to form defect points or lines under some geometric constrains. For example, LC molecules align perpendicular to the wall of spherical geometry. LCs alignment is not continuous at the center of the spherical geometry. Therefore, it forms point defect at the center of the sphere. Examples of topological defects are illustrated in Figure 2.4-C.

The route for the synthesis of liquid crystal elastomer (LCE) microparticles involve the polymerization of single- or multicomponent mixtures of reactive mesogens with mono- or diacrylate or epoxy end groups.[23,48–50] Moreover, reactive groups can be at the both end (end-on), one end, or at the side (side-on) of the mesogenic unit. In addition to symmetry of the reactive groups, they can be attached side chains of the monomer units to form side chain polymers (Figure 2.5-B and -D) or directly linked to each other to form main chain polymers (Figure 2.5-A and -C). Since acrylate groups are used for starting materials, free radical polymerization takes place. The

reactive mesogenic architecture of the polymer network directly affects response to the external stimulus or application area.

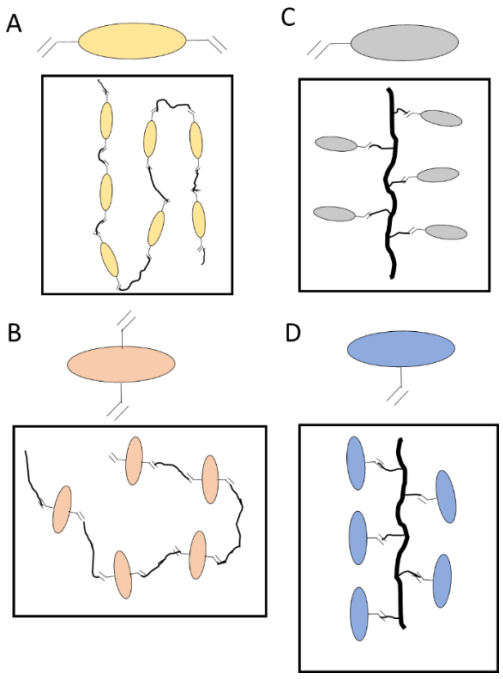

Figure 2.5 Various types of liquid crystalline monomers. Reactive groups are at the both end (end-on) (A), one end (C), or at the side (side-on) (B, D) of their rigid structure.

Polymeric microparticles which have liquid crystalline network are attractive since they have interesting behavior to broaden their functional properties. In order to synthesize liquid crystalline network inside microparticles, replica molding[51], emulsion polymerization[52], dispersion polymerization[53], 3D printing[54,55], inkjet printing[56] and microfluidic[22] methods can be used. Here are some examples of the LCE material synthesis methods and their functional properties.

Vennes and Zentel synthesized colloidal microparticles from nematic and smectic phases via dispersion polymerization[53]. Characterizations of the microparticles were done by DSC and polarizing microscopy. In order to synthesize microparticles, a

solvent was selected considering its solubility of monomer and polymer network. Ethanol and 2-methoxyethanol were selected as solvent which can dissolve in monomer and non-solvent for the polymer. For the initiation of the polymerization step, dibenzoyl peroxide was employed and hydroxypropyl cellulose was added for dispersion polymerization. The amount of dibenzoyl peroxide and hydroxypropyl cellulose did not affect the result, whereas solvent mixture ratio had a significant effect on the size and distribution of the microparticles. Increasing methoxy to ethanol ratio provided larger particles. (Figure 2.6). However, dispersion polymerization was limited to the synthesis of spherical particles.

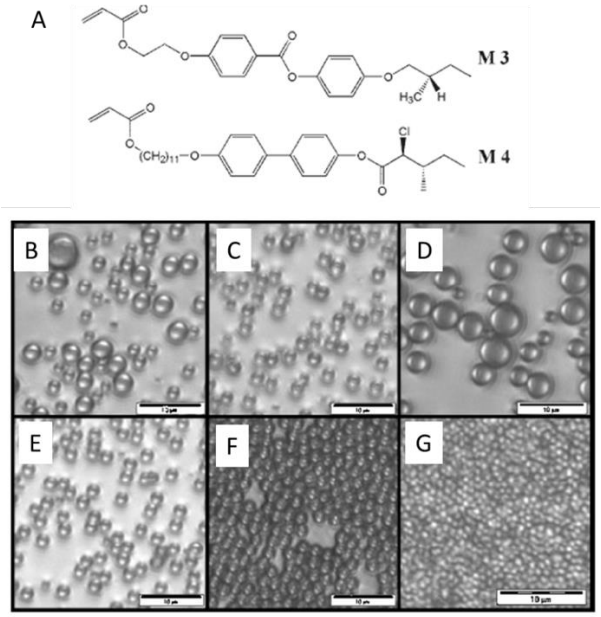

Figure 2.6 Molecular structure of the liquid crystalline monomers M3 and M4 used for this study. Microscopy images of the colloidal microparticles synthesized from (B) pure ethanol, (C) 8:1 ethanol to 2-methoxy ethanol ratio, (D) 4:1 ethanol to 2-methoxy ethanol ratio with M3. Top images show broader size distributions, whereas bottom images show narrower size distributions with 10:1 ethanol to 2-methoxy ethanol ratio (E), 9:1 ethanol to 2-methoxy ethanol ratio with M3 (F) and pure ethanol with M4 (G).[53]

Yang *et al.* successfully prepared non-spherical particles via mini-emulsion technique[57]. They mixed three different polymers, which show liquid crystalline phase, with chloroform, water and surfactant (SDS). After 5 minutes sonication, mini-emulsions of the polymer networks were formed. Size and shape (aspect ratio) of the nanoparticles were different as outlined below. Small particles (below 30 nm) tend to be spherical (aspect ratio is 1.0). However, intermediate size particles (major axis is 138 nm and minor axis is 90 nm) show ellipsoid shape (aspect ratio is 1.5). Larger particles (above 1000 nm) again tend to be spherical (aspect ratio is 1.0). This result indicates that interfacial tension distorts the equilibrium ellipsoids elastically back to spheres when the particles size is decrease. Moreover, ellipsoid shaped particles were heated to their isotropic phase temperature and particles showed spherical shape (around 100°C). Cooling down to the room temperature resulted in the formation ellipsoid shape again. They observed that change in the shape is a reversible process and dependent on the temperature. Although manipulation of the particle shape is hard to achieve through mini-emulsion technique, the described method provides limited solution to synthesize internally complex shapes.

As a different method, Yang *et al.* used replica molding technique to synthesize micrometer sized liquid crystalline elastomer actuators.[58] To synthesize polymeric microparticles, PDMS mold pressed down to isotropic mixture, which consists of nematic thiol-ene monomer (94.5 mol%), crosslinker (5 mol%), and initiator (0.5 mol%), with applied magnetic field to maintain the alignment of the nematic director parallel to the long axis of the pillars. Then, the system cooled down to nematic temperature in above position. UV was exposed (30 minutes) to nematic mesophase mixture and rectangular array covered by a thin glassy polymer film was synthesized. Then, LCE pillars were cut off by a razor blade from the surface of glassy polymer film. The temperature of LCE pillars was increased to isotropic temperature (around 170°C) to show actuating behavior of pillars. Pillars maintain a ‘coin’ shape. After cooling down to the room temperature, original shape and size of pillars was maintained. (Figure 2.7). They predicted that this actuating behavior can be used to

fabricate active surfaces or small elementary muscles or as a micro-pumps and micro-robots[51,58]. However, it is hard to manipulate microparticle's internal structure or complexity through replica molding method.

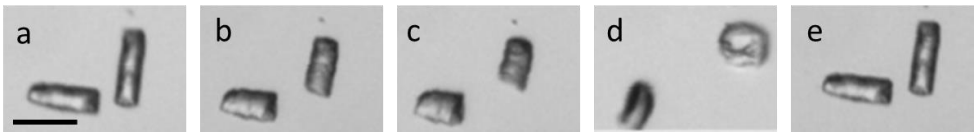

Figure 2.7 (a-d) LCE pillars were heated up systematically to isotropic temperature (around 170°C), (e) then cooled back to the room temperature. Scale bar: 100 μm.[58]

Fleischmann et al. synthesized core-shell liquid crystalline microparticles by employing microfluidic double emulsion process (Figure 2.8-A)[50]. The core of the microparticle consist of glycerol, which has relatively low viscosity at elevated temperature, while shell contains liquid crystalline monomer. As a continuous phase of co-flow microfluidic device, silicone oil, which is immiscible with monomer mixture, was selected. Surfactants or shell stabilizers were not introduced to the system since they can affect and change the liquid crystalline orientation. Then, UV light was exposed to the core-shell microparticles at nematic liquid crystalline phase (65°C). The main axis of the ellipsoidal shaped microparticles (aspect ratio is 1.3-1.5) were 545 μm and exhibited mono-dispersity. To show actuation behavior of the microparticles, the temperature of the system was increased to 130°C (above the nematic to isotropic transition temperature). They observed that aspect ratio of the microparticles were changed significantly (1.5 to 0.73) to use them as a micropump and maintained initial shape after cooling to the room temperature. To verify the concept of micropump, glass capillary (orifice diameter is 40 μm and capillary tip has 3° angle), which was hydrophobized with trichloro(3,3,3-trifluoropropyl) silane to solve wetting problem, pierced into the core shell microparticles at 90°C. Then, hot plate was set to 130°C to change the aspect ratio of the microparticles. Setup of the experimental system can be seen in Figure 2.8-B. Glycerol inside the microparticle

was raised due to the change in the aspect ratio of the particles. Once the system lifted away from the hot plate, glycerol is returned to the core of the microparticles as seen Figure 2.8-C, D. This actuator behavior illustrates that core shell particles can be used as micropump which then incorporated in lab-on-chip systems. This example shows that the microfluidic devices can be integrated for the synthesis of LCE particles and their potential application area as a responsive material.

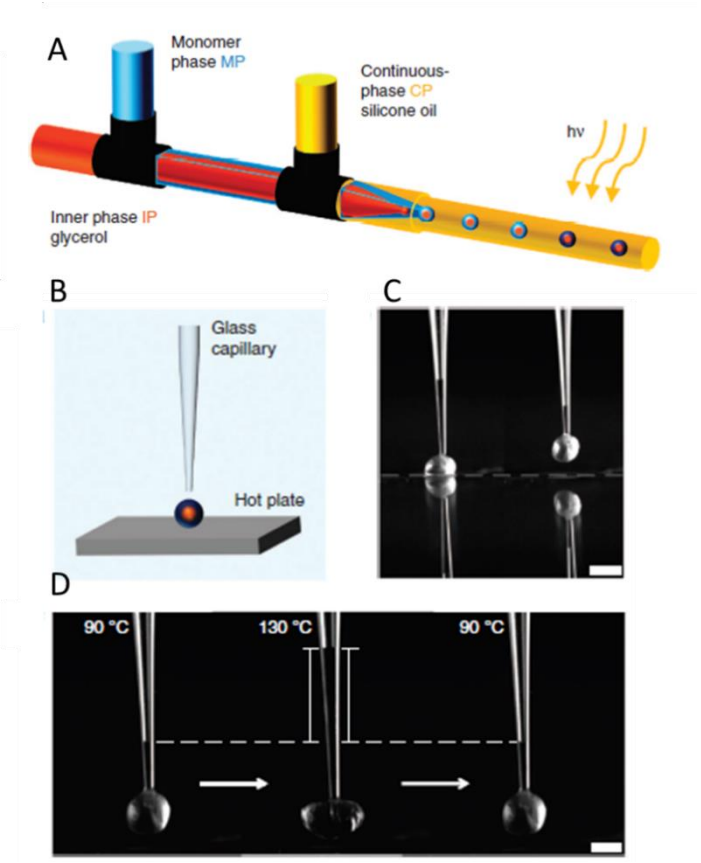

Figure 2.8 Schematic illustration of core shell microparticle synthesis method by double emulsion microfluidic device (A) and temperature response experiment setup (B). (C and D) Temperature response of the core-shell microparticles. [50]

Iamsaard *et al*. converted molecular movement of helical materials into macroscopic work by using LCEs with azobenzene containing units.[32] They synthesized chiral

liquid crystalline networks by combining 4 different liquid crystalline monomers (one of the monomers contain azobenzene group in its structure) with chiral dopant (0.04 wt. %) and non-reactive mesogen mixture E7 (ratio of 1 to 2.5 monomer mixture). The reason for chiral dopant usage was to obtain twist behavior of LC materials between two glasses with 200 μm pitch size. Since the gap between the two glasses was selected as 50 μm, LCs were able to twist 90° with respect to bottom glass and twist direction was dependent on the chiral dopant type. After polymerization by UV exposure, polymeric film was cut 0.8 – 1.3 cm in length and 0.7 - 0.9 mm in width in the direction of ϕ (mid-plane of the twisted LCs mixture). The direction of cutting specified the final pitch size, handedness of the structure and therefore their photoresponsive behavior. Right side of Figure 2.9 shows the formation of flat, open ring, left or right handed twisted ribbon synthesized with different φ values. Then, they were exposed UV light to the demonstrate their shape change.

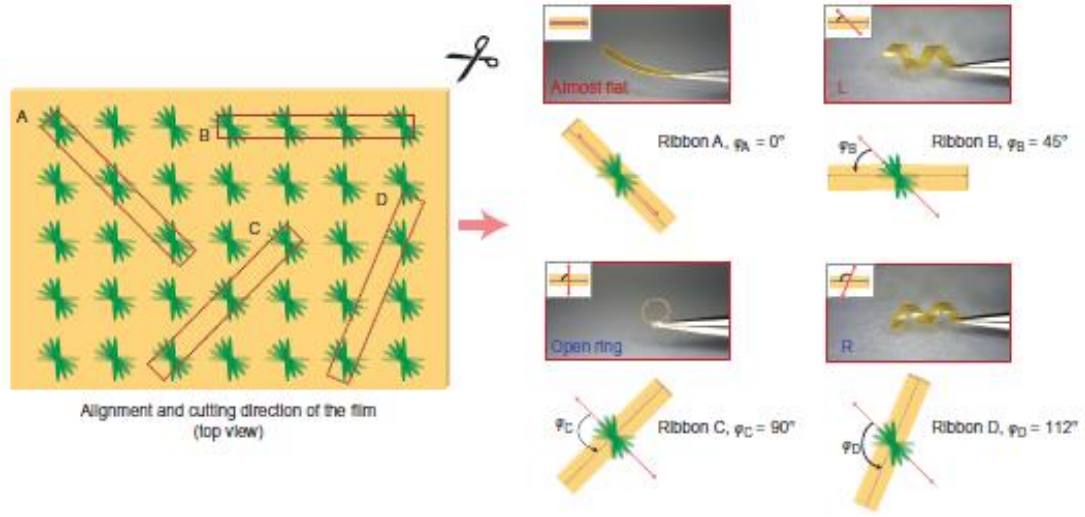

Figure 2.9 Schematic illustration of the top view of elastomeric film is on the left panel of the figure. Cutting direction changed the final structure of the elastomer as form almost flat (Ribbon A), left and right handed ribbons (Ribbon B and D, respectively), and open ring (Ribbon C) structure.[32]

Liquid crystals (LCs) as molecular templates[23,24] has been shown to provide practical solutions to overcome some of the limitations of the currently available methods described above. Key properties of the LCs such as molecular alignment and elasticity (while maintaining fluidic properties) were used to modify the internal structure, morphology and response of the micrometer sized objects.[30,32,44,59,60] With LC templated route, additional control over the shapes, internal structuring, and porosity of the microparticles have been shown to be provided to the microparticles during anisotropic shrinking following the extraction of the unreacted part.[59,61,62] In other words, opportunities to extent the library of the microparticles do exist through combination of the methods that involve non-reactive LCs as templates. Below, we demonstrate some methods using LC templated route for the synthesis of particles.

To illustrate, synthesis methods involving LC-in-water emulsions showed that initially spherical shapes of the particles would shrink anisotropically (after removal of the unreacted part) to maintain various shapes that depend on the initial LC director configurations maintained within the droplets.[24,61,63] Specifically, Wang *et al.* capsulated reactive (RM257) and non-reactive mesogens (5CB) by continuous phase (glycerol) to form liquid crystal droplets.[24] LC droplets initially (top image of the Figure 2.10) had the spherical shaped with different topological defects (internal structure). Position of the topological defects directly changed the internal structure of the droplet and was directly linked with the sodium dodecyl sulfate (SDS) concentration on the surface of the droplets. After polymerization and extraction of the non-reactive mesogens 5CB, microparticles shrank depending on LCs alignment. Droplets which have bipolar, radial, axial, or pre-radial configurations before extraction, became spindle-shaped, spherical, spherocylindrical, or tear-shape particles after the removal of non-reactive units, respectively and bright field and polarized light images can be seen in Figure 2.10-A, B, C, and D. In addition, they showed that final to initial volume ratio had linear dependency on the concentration of the RM257. Therefore, bipolar shape particles are linearly decreased by lowering RM257 concentration. On the other hand, mass density of the microparticles is

constant as a function of RM257 concentration. These results show that spherical droplets can be formed exotic shapes by using LCs as a templating molecule. However, initial shape of the microparticles is limited to spherical shapes since the emulsion leads to form spherical droplet formation due to lowering interfacial energy, therefore limiting the microparticle shapes that can be formed from spheres.

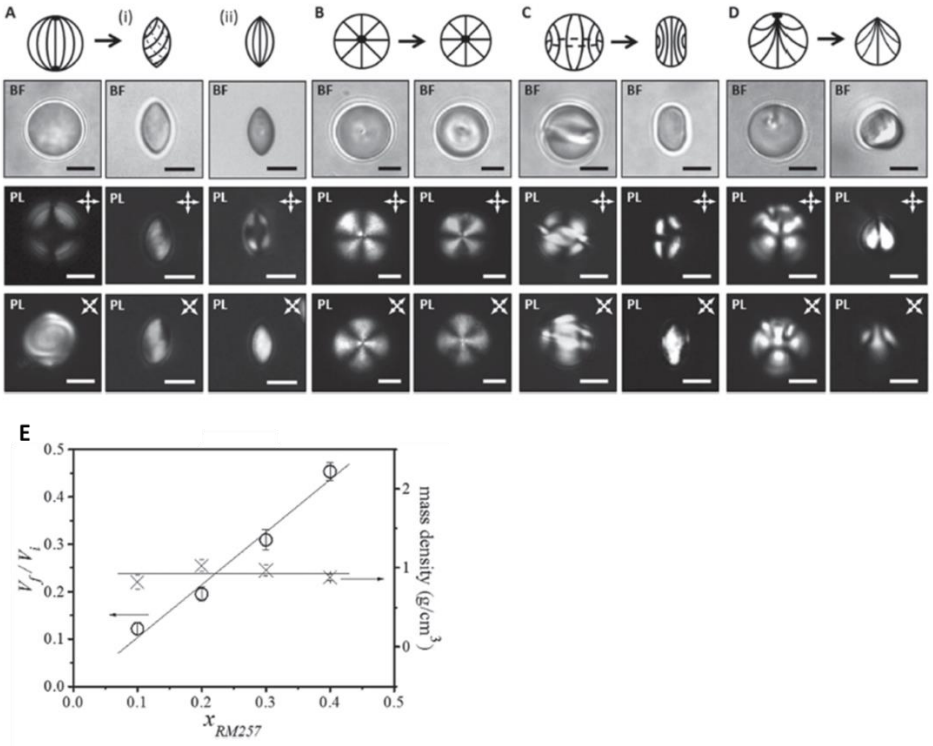

Figure 2.10 Synthesis of (A) spindle-shaped, (B) spherical, (C) spherocylindrical or (D) tear-shaped polymeric microparticles templated from LC droplets in (A) bipolar, (B) radial, (C) axial or (D) preradial configurations, respectively. Bright field and polarized light images of each configurations can be seen below the schematic illustration of the configuration. Scale bars: 5 μm. (E) (o) Ratio of the final and initial volume of the bipolar microparticles, and (X) mass density of the same particles with varied RM257 concentrations. [24]

Ansel *et al.* successfully synthesized chiral polymeric microparticles by combining liquid crystal templated method and emulsion polymerization in their recent study.[63] Liquid crystal droplets (approximately 100 μm in size) were prepared by dispersing non-reactive mesogen (5CB) and reactive mesogen (RM257) into aqueous solution with containing PVA and photoinitiator. Droplets showed bipolar configuration (two boojums) due to presence of PVA (rubbed PVA shows planar anchoring). Then, droplets were exposed to UV light to polymerize the microparticles. Extraction of the non-reactive mesogen 5CB leads to formation of spindle shape with the defects at the tips. They observed that RM257 concentration should be between 5 wt. % to 20 wt. % in order to observe twisting behavior after extraction of 5CB. Mixtures of chloroform (polymeric structure can swell with) and ethanol (polymeric structure can shrink with) were prepared to tune the final shape of the microparticles. Aspect ratio of the microparticles (ua over a in Figure 2.11-A) and β (the angle between major axis of the microparticles and lines of the polymer at the equator shown in Figure 2.11-A) were defined to characterize the synthesized microparticles. They obtained Figure 2.11-B to show the effect of the fraction of ethanol on the u and β values with varied RM257 concentrations. In their analysis, increasing fraction of ethanol (x_{EtOH}) and lowering RM257 concentration resulted in higher u and β values due to higher shrinkage percentage. Finally, they showed the consistent behavior with the experimental data and proposed analytical method. However, this study did not provide any information related to the handedness of the chiral microparticles or pitch sizes of the particle. On the other hand, this study indicates that limited initial structure of the microparticles due to used method can be expanded to the chiral shapes of the particles.

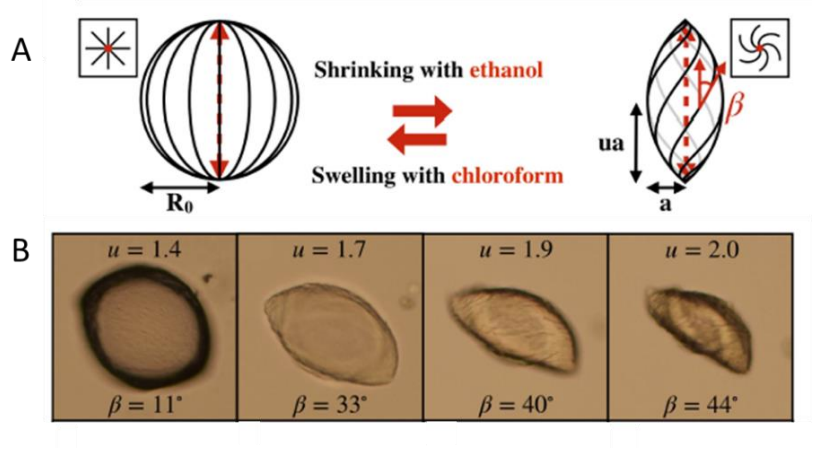

Figure 2.11 Schematic illustration of the bipolar microparticle (left side of A) and spindle shape microparticle (right side of A). (B) Images of the polymeric microparticles corresponding to fraction of ethanol = 0, 0.4, 0.6, and 0.8. [63]

Moreover, Karausta and Bukusoglu provide methods for the synthesis of liquid crystal templated polymeric porous films in order to use as an ultrafiltration membrane.[23] In their study, non-reactive mesogen 5CB and the reactive mesogen RM257 were employed to the synthesis of polymeric film. The monomer included solution was sandwiched between two functionalized surfaces where alignment of liquid crystalline material can be manipulated. Extraction of the non-reactive mesogen 5CB led to anisotropic shrinkage of polymeric films. The final shapes of the films can be seen Figure 2.12-A, B and C. RM257 concentration was varied in planar films to observe the effect of the concentration of RM257. Shrinkage percentage of the film was much higher in perpendicular direction to LC alignment compared to parallel direction to LC alignment due to polymer chain alignment. As it can be seen in Figure 2.12-D, lowering the amount of the monomer leads to higher amount of shrinkage in perpendicular direction to the LC alignment. Moreover, they showed that final to initial volume ratio is linearly dependent on RM257 concentration in Figure 2.7-E. This result is consistent with the final to initial volume ratio of the bipolar droplet [24]. The morphology of the films (geometry and size of the pores (10-40 nm)) were

successfully adjusted by liquid crystalline mesogens. Permeances of the ultrafiltration results showed high dependency on direction of the pores. Moreover, tensile test results showed that polymer films exhibit direction dependent mechanical property.

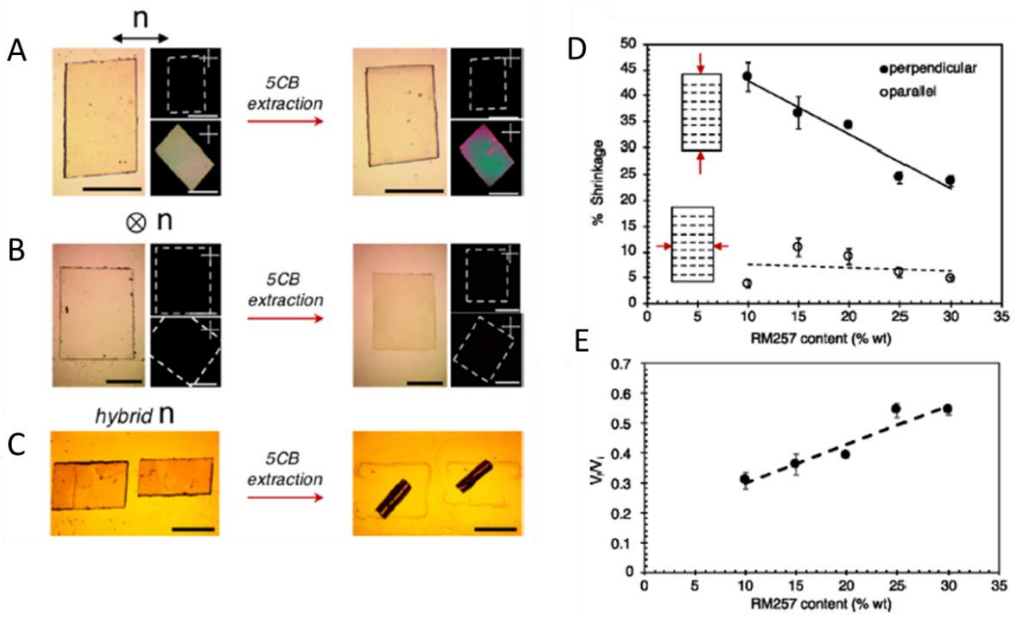

Figure 2.12 Optical images of LCE films synthesized from 20 wt.% RM257 and their extracted states. LC director is indicated with 'n'. n is planar in (A), homeotropic in (B), and hybrid in (C). (D) The result of shrinkage percentage versus RM257 concentration graph. (E) Ratio of final volume to initial volume versus RM 257 concentration graph.[23]

We showed that the introduction of the LCs as molecular templates provides additional control over the architectures of the microparticles or film structure. However, the control over the final shape of the microparticles using LC templates are currently limited to those which can be synthesized from emulsion droplets, which result in microparticles with shapes that are symmetric around their longitudinal axis. In this study, we identify and demonstrate the key parameters and principles for

precise control over the internal structuring, size and shapes of the microparticles including twisting and bending of the LC ordering maintained in the template.

CHAPTER 3

MATERIALS AND EXPERIMENTAL SECTION

3.1. Materials

Nematic liquid crystal blend E7 (mixture of 51% of 4-cyano-4'-pentylbiphenyl (5CB), 25% of 4′-heptyl-4-biphenylcarbonitrile (7CB), 16% of 4′-n-octyloxy-4-cyanobiphenyl (8OCB) and 8% of 4-cyano-4"-n-pentyl-terphenyl (5CT)), and reactive mesogen 4-(3-acryloyoxy-propyloxy)benzoic acid 2-methyl-1,4-phenylene ester (RM257) were purchased from HCCH Jiangsu Hecheng Chemical Materials Co., Ltd. (Nanjing,China). Polyvinyl alcohol (PVA), the photoinitiator 2,2 dimethoxy-2-phenylacetophenone, Dimethyloctadecyl [3-(trimethoxysilyl) propyl] ammonium chloride (DMOAP), anhydrous acetone, and toluene were purchased from Sigma-Aldrich (St. Louis, USA). Anhydrous ethanol was obtained from J.T. Baker (Phillipsburg, USA). Glass slides and cover glasses were obtained from Marienfeld GmbH (Lauda-Königshofen, Germany). The lithography masks were drawn by using AutoCad 2018 software. The lithography masks consist of circles with 260 μm and 100 μm in diameter, equilateral triangle with 100 μm in length, square with 100 μm in length, rectangular with 200 μm x 100 μm in dimensions, star shape with 100 μm in length and 36° in five edges, and heart shape with two circles with 50 μm in diameter and 68° in bottom angle (Figure 3.1).

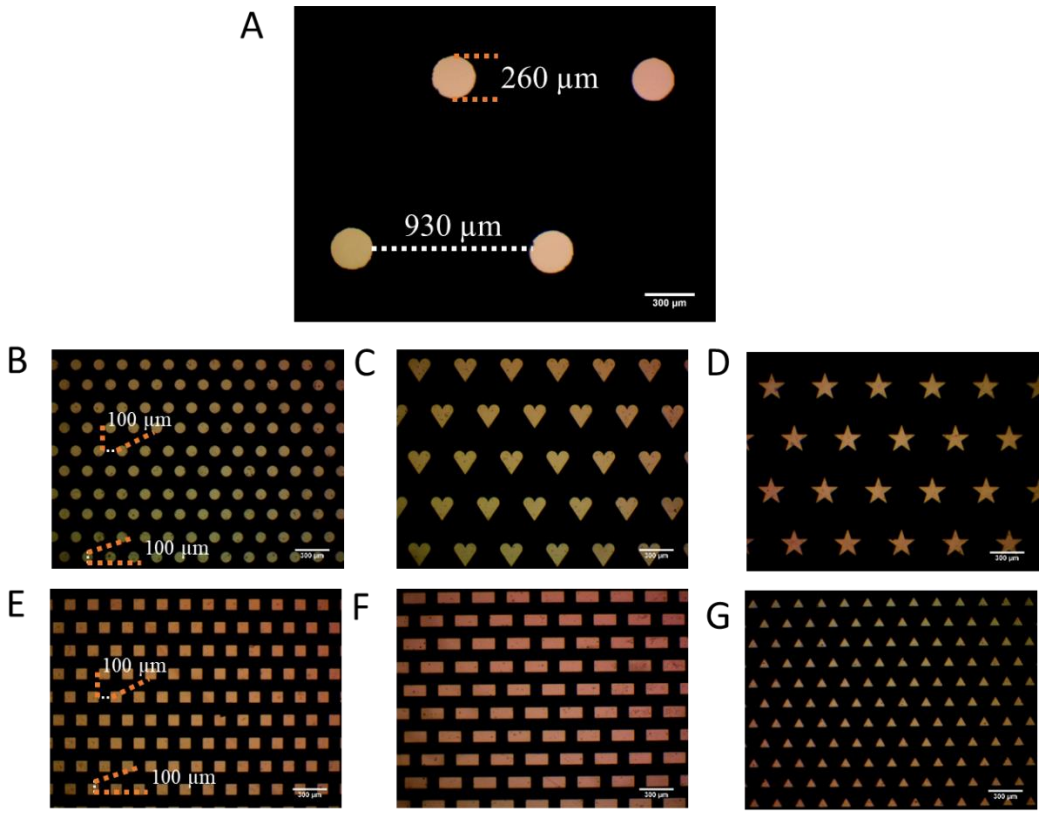

Figure 3.1 Micrograph images of the lithography masks. (A and B) Circular, (C) heart shape, (D) star shape, (E) square, (F) rectangular, (G) equiangular triangle.

3.2. Preparation of the LC-Reactive Mesogen Mixtures

The reactive LC monomer RM257 were added at 10 - 30 wt. % with the non-reactive mesogen mixture E7. The photoinitiator was then mixed at 1 wt. % based on the mass of RM257 to the mixture. Toluene, the co-solvent, was added to the LC mixture at about half of the weight of the E7 to dissolve and enable well mixing. The mixture was then mixed using a vortex mixer until a clear solution was obtained. Finally, toluene was evaporated from the solution under vacuum before use.

3.3. Preparation of the Glass Substrates

To achieve planar or homeotropic anchoring of LCs, glass slides and cover glasses were coated with PVA, DMOAP or PFDTS, respectively.

For PVA coating of the surfaces, 5 wt. % aqueous PVA solutions were prepared in deionized water. Glass surfaces were spun coated at 5000 rpm for 2 minutes. The PVA surfaces were then rubbed with a fabric to maintain uniform planar anchoring of LCs.

For DMOAP coating, glass surfaces were first activated with oxygen plasma using a Diener Electronics, Zepto Plasma Unit (Ebhausen, Germany). The plasma-etched glasses and 1 vol. % of aqueous DMOAP solution were then placed inside a staining jar and sonicated for 10 minutes to prepare a monolayer of DMOAP. Treated glasses were then rinsed with deionized water and dried under the flow of nitrogen gas.

For PFDTS coating, glass surfaces were first activated with oxygen plasma using a Diener Electronics, Zepto Plasma Unit. Then, plasma-etched glass surfaces and 75 μL of PFDTS were placed inside the desiccator and incubated overnight under vacuum. Treated glasses were then rinsed with absolute ethanol and dried. The anchoring of LCs between glass surfaces were checked using a microscope equipped with conoscopy setup before each use.

3.4. Polymerization of LC-Monomer Mixtures

The polymerizations of the LC-monomer mixtures were done between a sandwich cell prepared by placing two coated (PVA, DMOAP, or PFDTS) glass surfaces. The thicknesses of the films were maintained using polymeric Mylar spacers. The sandwich cell was then filled with LC-monomer mixture using capillary action and the mixture was polymerized using a polymer-based mask (Figure 3.1) and UV light. The mask was placed on the sandwich cell in contact with the glass cover slides. Two UV-light sources (365 nm) were used. For the uncollimated light source Spectroline (New York, USA) ENF-280 C/FE was used. For the collimated light source, ThorLabs M365LP1-C1 was used. Depending on the UV lamp sources exposure times has changed and varied 3 sec (ThorLabs (New Jersey, USA) M365LP1-C1) to 120 sec (Spectroline ENF-280 C/FE). Furthermore, depending on the mask types exposure times were varied from 1 sec to 5 sec at depending on the set power which were varied in the range 1 - 2.5 $mW.cm^{-2}$ at a distance of 3 cm from the light source. Here we note

that the exposure time of the UV light for polymerization was critical in determining the initial shapes of the microparticles. We found that shorter times (<3 sec) resulted in partial polymerization of the regions corresponding to the open mask features. On the other hand, long exposures resulted in complete polymerization of the films.

3.5. Extraction of Polymeric Particles

After polymerization, the functionalized glasses were detached and quickly rinsed with absolute ethanol inside a beaker. For the extraction of the unpolymerized part, the microparticles were centrifuged at 5000 rpm for 5 min., the supernatant was substituted with ethanol and the microparticles were redispersed in ethanol and centrifuged again. This cycle was completed for at least three times to enable complete removal of the unreacted monomers before characterization.

3.6. Optical Characterization and Brightfield (BF) and Polarized Light (PL) Microscopy

The LC alignment and measurements and characterization of the synthesized particles were performed by Olympus BX50 and BX53 microscopes equipped with 4x, 10x, 40x and 50x objectives, and crossed polarizers. The BF and PL micrographs were collected in transmission mode and reflective mode. The image analyses were done using imageJ, an open source image analysis software.

3.7. Measurement of the LC-Twist Angles

To characterize the LC twist angles, eighteen PL micrographs of the particles were taken by changing the angle of the polarizer by 10° in each step to complete 180° turn. The calculations of the angles were done by MATLAB 2014 software following the procedure to calculate the LC-twist angle found elsewhere.[64]

3.8. Toluene Vapor Experiment

Toluene reservoir was connected to exposure chamber by two valves. Baratron capacitance manometer was placed before exposure chamber to supply desired amount of toluene vapor. A pump was connected in order to remove toluene vapor.

After evacuation of the system, two valves were opened, and desired toluene vapor was delivered into the exposure chamber. Then, behavior of the sample was monitored by microscope.

CHAPTER 4

LIQUID CRYSTAL TEMPLATED POLYMERIC MICROPARTICLES SYNTHESIS COMBINED WITH PHOTOLITHOGRAPHY

4.1. Liquid Crystal Templated Microparticle Synthesis Method

The synthesis method followed in this study is shown in Figure 4.1 in four main steps. First, a mixture of a reactive mesogen and a nonreactive mesogen was prepared. Then, the mixture was filled between two functionalized surfaces that maintain a preferred anchoring of LCs (either planar or homeotropic). Next, the mixture was crosslinked locally with the use of a UV-light source (365 nm) and a photomask (Methods) for the initial shape of the particles. Finally, the cell was detached using ethanol and the microparticles were collected. For the purpose of the illustration of the method, we used a mixture of two well-known LC materials. 4-(3-acryloyloxypropyloxy) benzoic acid 2-methyl-1,4-phenylene ester (RM257) was used as the reactive mesogen and an LC mixture, E7, was used as the non-reactive mesogen template (Figure 4.1-A). Our method can provide homogenous or hybrid alignment of LCs within the microparticles such as homeotropic on one side and planar on the other side or can also provide a tunable helical twisted LC configuration within the microparticle. We show this ability to add significant complexity to the shapes of the microparticles synthesized in this study. We used rubbed polyvinyl alcohol (rubbed-PVA) and perfluorodecyltrichlorosilane (PFDTS) coated glass slides to maintain uniform planar and homeotropic anchoring, at the contacting surfaces of the sandwich cell, respectively.

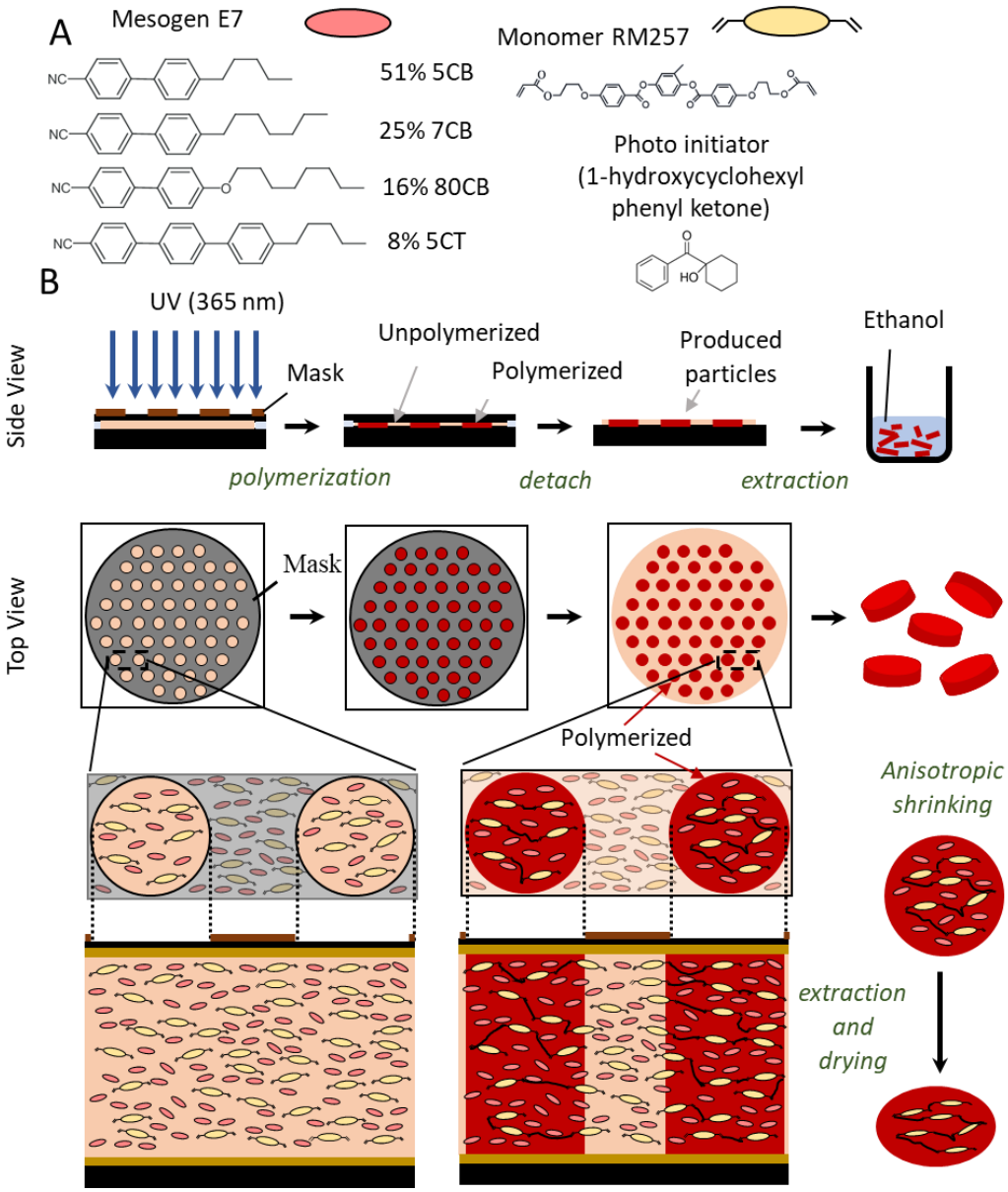

Figure 4.1 Schematic illustration of the method used for the synthesis of the microparticles. (A) the molecular structures of the reactive, nonreactive mesogens, and photo initiator used in this study, (B) The sketch of the four-step microparticle synthesis method.

Figure 4.2 shows optical micrographs of a 6 μm-thick film of 20 wt. % RM257 in E7 that was filled between two rubbed-PVA coated surfaces maintaining uniform planar

anchoring of LCs at their surfaces. The uniform planar molecular orientation within the films was maintained by rubbing the PVA coating (in a direction indicated by R) and verified from their dark appearance before polymerization under polarized light when the average alignment of the LCs was in the direction of one of the polarizers, and further supported by the appearance of a bright transmitted light when the film was rotated 45° around its optical axis. After the polymerization (using a photomask and a collimated light source) step, the orientation of the LCs within the film did not exhibit an observable change as determined from the micrographs shown in Figure 4.1-B, which is consistent with uniform planar anchoring. However, the locations of the polymerized particles can be determined using the optical micrographs from their darker appearance due to their slightly higher optical density (see inset figure and Figure A. 1.).[65]

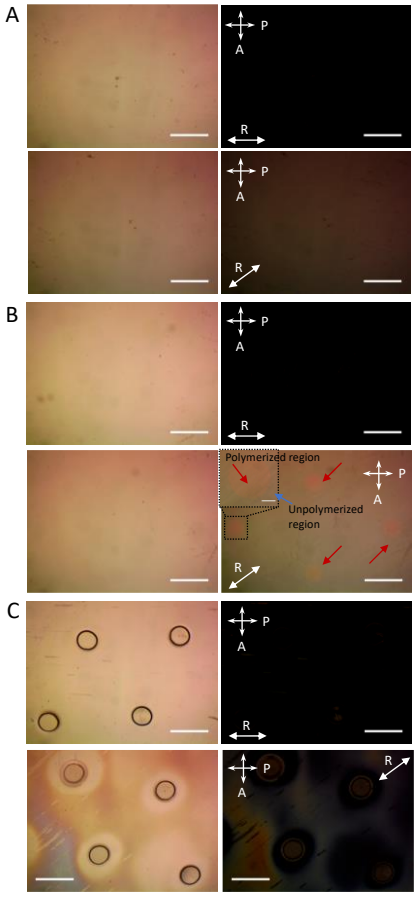

Figure 4.2 Representative optical micrographs collected during the synthesis of polymeric microparticles from a mixture of 20% by weight RM257 in E7. The top two images of each set are the brightfield and polarized light micrographs at the same orientation where the rubbing direction (indicated as R) was parallel to the polarizer. The bottom two images of each set are the brightfield and polarized light micrographs of the films when rotated 45 degrees. A 6 μm-thick film was confined between two rubbed-PVA coated glass surfaces. Micrographs shown (A) before polymerization, (B) after polymerization with UV light and a photomask (inset showing a magnified part shown in dashed lines), and (C) after detachment of the two glass surfaces after polymerization. The red arrow in (B) indicates the polymerized regions of the film. The arrows with A and P show the orientation of the two polarizers and R shows the rubbing direction of the glass slides to maintain planar anchoring. Scale bars: 500 μm, inset in B, 100 μm.

After polymerization, as an illustration, the two glass surfaces were directly detached to show the presence of the microparticles (Figure 4.2-C). As seen from the images, circular shapes and the size uniformity were maintained after polymerization. We measured the average size of the microparticles to be 256.7 ± 5.2 μm, calculated from averaging measurements from three independent synthesis each including at least 150 microparticles. This distribution shows a coefficient of variance (COV) of 2.0% indicating a monodisperse particle size distribution according to the definition of monodispersity by NIST (COV < 5%).[66]

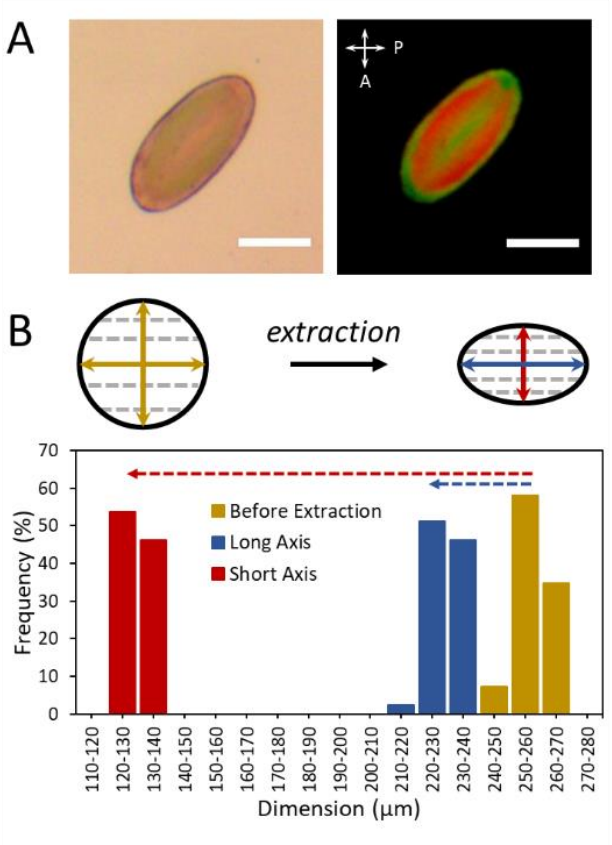

Figure 4.3 (A) A representative image of a microparticle synthesized from 20 wt.% RM257 in E7 where the nematic director was along the long axis of the microparticle. Scale bars: 100 μm. (B) The size distribution of the microparticles synthesized from a mixture of 20% RM257 in E7 before and after extraction of the unreacted mesogens, dashed line in the sketch shows the nematic director profile.

In the last step of the particle synthesis procedure, the unreacted part of the mixture was extracted using ethanol. We note that the unreacted part was dissolved in ethanol first in the usual procedure to minimize the deformation of the microparticles. Exposure to ethanol led to the sandwich cell to detach spontaneously, and slowly enough to stop polymerization and with minimal deformation of the microparticles. After extraction and drying of the microparticles, the initially circular shaped microparticles shrank and maintained elliptical shapes with flat top and bottom surfaces. The long axis of the elliptical particles was along the LC director as determined from the polarized light micrographs (Figure 4.3-A). The birefringence of the microparticles determined by their bright appearance under crossed polarizers when rotated 45º is an indicative of their aligned, complex nanostructures. The size of the microparticles were measured to be 230.0 ± 6.1 μm along the long axis and 129.0 ± 5.9 μm along the short axis after the extraction, which indicated a monodisperse size distribution with COV < 5% (Figure 4.3-B, Figure A.2.). These measurements indicated 49.7 ± 2.3% and 10.4 ± 2.4% shrinkage to occur parallel and perpendicular to the nematic director, respectively, compared to the initial sizes of the microparticles. Lastly, the alignment of the polymer chains within the microparticles was consistent with planar alignment as determined from the optical micrographs (significant extinction of light transmission when the alignment is along with the polarizer or analyzer). This also illustrates the complex, aligned nanostructure of the microparticles synthesized that were predetermined before polymerization. This complex behavior of the microparticles were not observed in samples that were synthesized at temperatures that were higher than the nematic to isotropic temperature. In other words, since microparticles were synthesized under isotropic temperature, effect of LC as a templating material were vanished. Figure 4.4 shows the images of the microparticles that were synthesized under isotropic conditions. Polarized light images were darker appearance due to isotropic conditions. Microparticles shrank in an arbitrary way and did not show complex and aligned behavior (Figure 4.4-B).

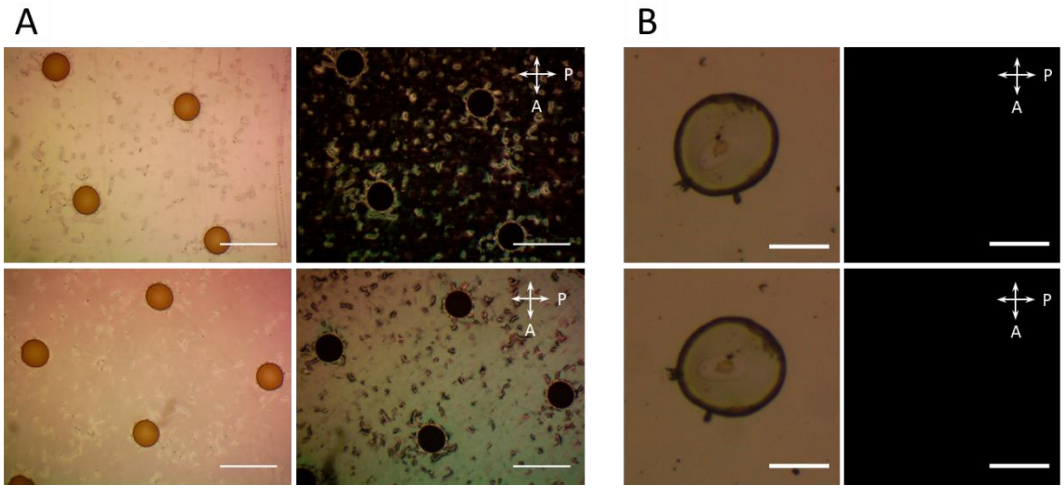

Figure 4.4 Microparticles synthesized under isotropic condition. Micrographs were collected (A) after detachment, and (B) after extraction. Images on the left panel of each figure set are brightfield (top) and 45° rotated brightfield (bottom) images whereas images on the right side of each panel are polarized light and 45° rotated polarized light images. The arrows with A and P show the orientation of the two polarizers. Scale bars in A: 500 μm, scale bars in B, 100 μm.

4.2. Effect of Reactive Mesogen Concentration and Thickness of the Film on Microparticle Shape

The shrinkage, therefore the aspect ratio of the microparticles were also influenced by the reactive mesogen content in the mixture. In order to examine the effect of the reactive mesogen, the mixture was prepared at 10 wt. %, 15 wt. %, 20 wt. %, 25 wt. %, and 30 wt. % monomer concentrations. Synthesized microparticles at given reactive mesogen concentration showed same dimensions of the circles with the photomask feature and size (260 μm). Diameter values of the circles at each reactive mesogen concentrations were given in Table 4.1.

Table 4.1 Diameter and coefficient of variable of the synthesized microparticles with 10 wt. %, 15 wt. %, 20 wt. %, 25 wt. %, and 30 wt. % RM257 concentrations after polymerization.

Monomer Concentration (%)	10	15	20	25	30
Diameter of the Circle (μm)	243.4	250.7	256.7	253.6	252.1
Standard Deviation	4.1	2.6	5.2	4.3	4.9
Coefficient of Variance (%)	1.7	1.0	2.0	1.7	1.8

Coefficient of variance values of the synthesized microparticles shows monodisperse size distribution of microparticles (Table 4.1). Monodispersity of the microparticles was achieved at varied monomer concentrations (COV<5%) and was not influenced by monomer concentrations.

Extracted microparticles (elliptic microparticles) were characterized by considering their long axis (parallel to nematic alignment) and short axis (perpendicular to nematic alignment). Dimensions of the synthesize microparticles with 10 wt. %, 15 wt. %, 20 wt. %, 25 wt. %, and 30 wt. % RM257 concentrations can be seen in Table 4.2 and extracted microparticles were illustrated in Figure 4.5-A. After extraction and shrinking, the resulting aspect ratio of the microparticles were changed from 2.42 ± 0.22 to 1.65 ± 0.10 by increasing the RM257 content from 10% to 30% by weight in E7, and they have maintained monodispersity with COV below 2%.

Table 4.2 Dimensions of the synthesized microparticles with 10 wt. %, 15 wt. %, 20 wt. %, 25 wt. %, and 30 wt. % RM257 concentrations after extraction.

Monomer Concentration (%)	10	15	20	25	30
Long Axis (μm)	201.4	220.8	230.0	226.5	225.7
Standard Deviation	3.4	7.3	6.1	7.45	7.6
Short Axis (μm)	83.6	91.3	129.0	125.1	136.9
Standard Deviation	6.5	4.3	5.9	6.6	8.7

Figure 4.5-B shows the shrinkage percentage of the microparticles along and perpendicular to the nematic director as a function of the reactive mesogen content. The shrinkage perpendicular to the nematic director was linearly dependent on the reactive mesogen content whereas it was almost independent of the reactive mesogen content along the nematic director similar to the previous studies.[23,24] This difference in the shrinkage of the microparticles along and perpendicular to the nematic director resulted in a linear concentration dependency of the aspect ratio of the microparticles maintained after the extraction of the unreacted mesogens, consistent with the past studies on the LC emulsion polymerization.[24] However, the extent of the shrinkage we observed in this study was slightly higher than that observed in past studies.[23,24] This difference was due to the very short crosslinking time (~3 sec) critical for the formation of our microparticles whereas it was 30 minutes in other studies. We found the crosslinking time to relate to the gel percent of the microparticles that we gravimetrically measured to be 75% ± 14%, which was less than 100%, the value reported for films, and microparticles synthesized from emulsions in previous studies.[23,24]

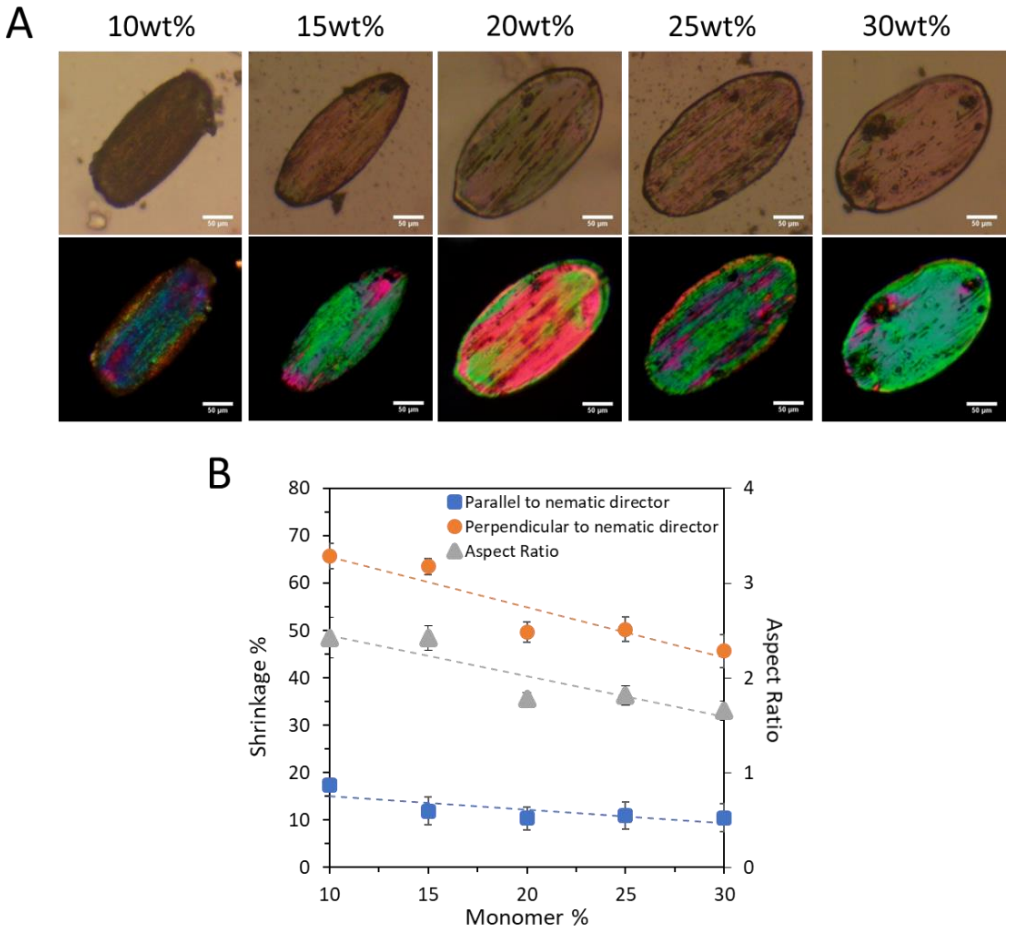

Figure 4.5 Shrinkage percentage change with respect to the monomer percentage. (A) A representative image of a microparticle synthesized from 10 wt. %, 15 wt. %, 20 wt. %, 25 wt. %, and 30 wt. % RM257 in E7 where the nematic director was along the long axis of the microparticle. (B) The plot of shrinkage percent parallel and perpendicular to the nematic director and aspect ratio of the microparticles after extraction as a function of the monomer concentration.

The shrinkage behavior of the microparticles were consistent with the shrinkages that were observed in the films that were synthesized using the same mixture.[23] This indicates the negligible effect of geometry on the shrinkage of the microparticles. In addition, we synthesized microparticles with thicknesses in the range of 1.5 μm to 160

μm from films of 20 wt.% RM257 in E7 with two uniform planar anchoring surfaces. The diameter of the synthesized microparticles can be seen in Table 4.3.

Table 4.3 Diameter and coefficient of variance of the synthesized microparticles with 1.5 μm, 6 μm, 20 μm, 40 μm, 80 μm, and 160 μm film thicknesses after polymerization.

Thickness (μm)	1.5	6	20	40	80	160
Diameter of Circle (μm)	237.6	256.7	235.9	242.5	240.0	235.6
Standard Deviation	4.7	5.2	6.7	4.3	5.0	6.0
Coefficient of Variance (%)	2.0	2.0	2.8	1.8	2.1	2.6

After extraction, microparticles shrank and formed elliptic shape microstructures. Characterization of the microparticles were performed measuring long and short axis of the microparticles (Table 4.4).

Table 4.4 Dimensions of the synthesized microparticles with 1.5 μm, 6 μm, 20 μm, 40 μm, 80 μm, and 160 μm film thicknesses after extraction.

Thickness (μm)	1.5	6	20	40	80	160
Long Axis (μm)	208.9	230.0	211.2	214.6	206.3	208.8
Standard Deviation	8.2	6.1	7.5	6.6	6.4	10.7
Short Axis (μm)	103.1	129.0	99.7	99.9	100.1	98.9
Standard Deviation	4.8	5.9	6.0	4.5	4.4	10.3

Bright field and polarized light images of the microparticles are presented in Figure 4.6.

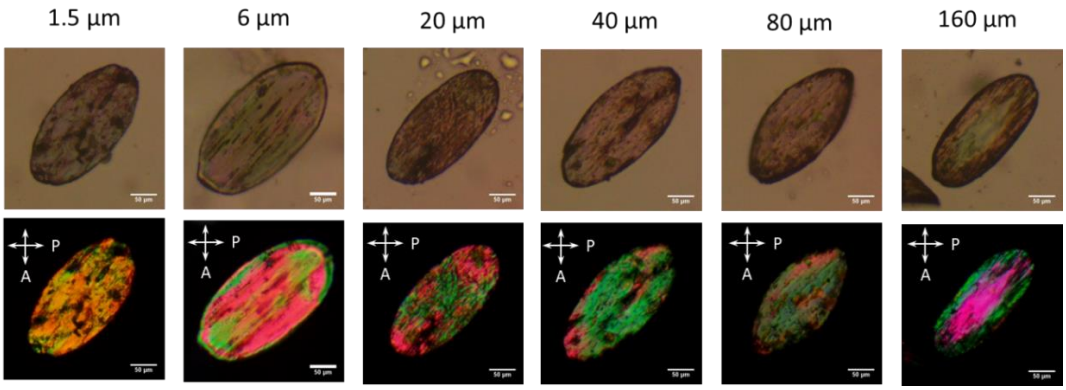

Figure 4.6 Bright field and polarized light microscope images of the microparticles were synthesized from 20 wt. % RM257 in E7 with 1.5 µm, 6 µm, 20 µm, 40 µm, 80 µm, and 160 µm film thicknesses. Thickness of the films are indicated at the top of the Figure.

We found that the shrinkage percentage or the aspect ratio of the particles maintained after the extraction was not influenced by the thickness of the microparticles (Figure 4.7). This provided an additional evidence that the shrinkage was independent of the shape of the microparticles, rather governed by the properties of the bulk material.

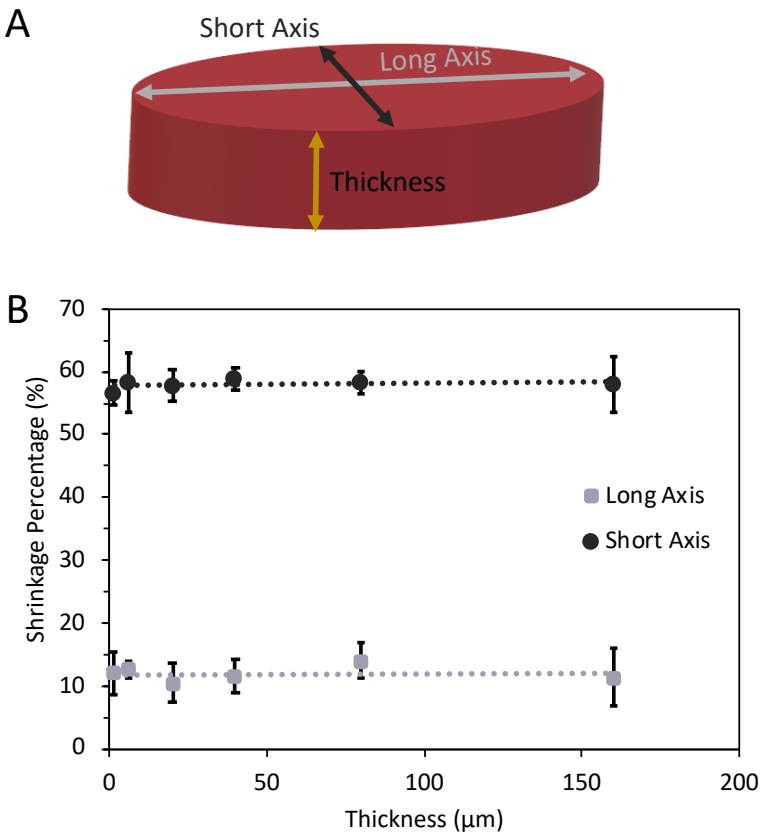

Figure 4.7 (A) Sketch showing the labeling used to define dimensions of a single microparticle. (B) Amounts of the shrinkage of the microparticles measured after extraction of the unreacted mesogens from the microparticles. The particles were synthesized from 20 wt. % RM257 in E7.

4.3. Changing Aspect Ratios of Microparticles with UV Light

Changing the shape of the UV light source provided additional control over the shapes of the microparticles. Figure 4.8 shows the three conditions in which the UV light source was a flat shaped, uncollimated source, instead of the collimated source used to synthesize microparticles shown in Figure 4.2. This provided a control over the aspect ratios of the light incident on the film. By changing the shape of the UV light-exposed region during polymerization, the initial shapes of the microparticles were changed. Shown in Figure 4.8-B are the initial aspect ratios of the microparticles that

were varied from 1.02 ± 0.04 to 1.68 ± 0.05 by changing the aspect ratios of the regions the UV light that was incident on. Since the nematic director was along the long axis of the polymeric microparticles, the particles assumed shapes with higher aspect ratios after the extraction and drying steps. The average aspect ratios of the particles were measured to vary from 1.91 ± 0.19 to 3.14 ± 0.47.

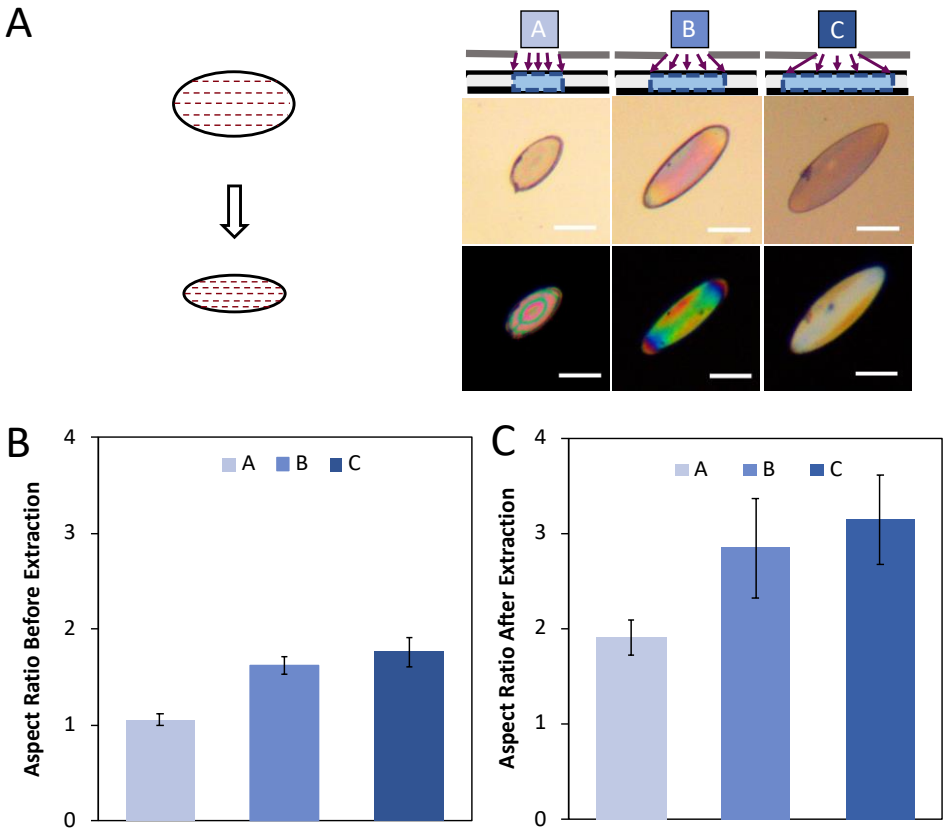

Figure 4.8 Experimental results showing the effect of the UV exposed area on the initial and final shapes and aspect ratios of the microparticles where the nematic director was along their long axis. 20 wt.% RM257 in E7 with 6 µm thickness were used in the synthesis. (A) sketch showing the UV light-exposed area (top) and corresponding brightfield (middle) and polarized light (bottom) micrographs of the microparticles synthesized. Scale bars: 100 µm. (B) The aspect ratio of the microparticles maintained after polymerization. (C) The aspect ratio of the microparticles maintained after extraction.

Consistent with these observations, it is possible to synthesize much circular microparticles by changing the nematic director. We observed the aspect ratio to decrease when the nematic director was along the short axis of the microparticles (Figure 4.9). The initial aspect ratio was consistent with Figure 4.8-B. The aspect ratio of the extracted microparticles were measured to vary from 0.51 ± 0.18 to 1.16 ± 0.04.

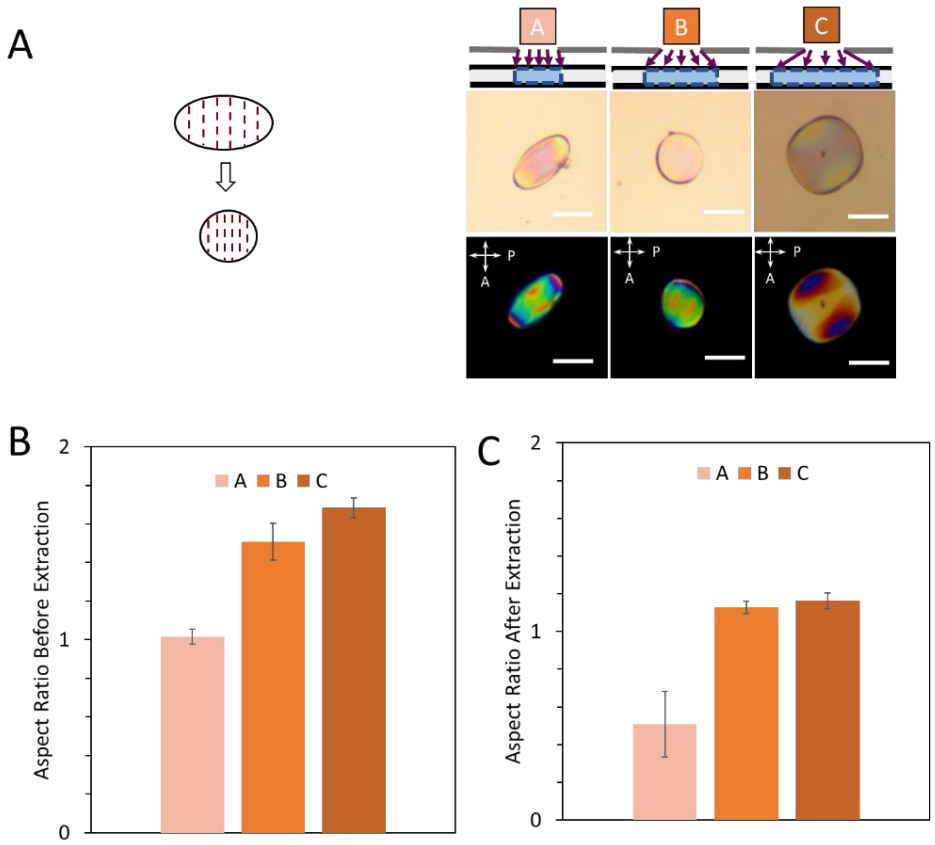

Figure 4.9 Experimental results showing the effect of the UV exposed area on the initial and final shapes and aspect ratios of the microparticles where the nematic director was along their short axis. 6 µm-thick films of 20 wt.% RM257 in E7 were used in the synthesis. (A) Sketch showing the UV light-exposed area (top) and corresponding brightfield (middle) and polarized light (bottom) micrographs of the microparticles synthesized. Scale bars: 100 µm. (B) The aspect ratio of the microparticles maintained after polymerization. (C) The aspect ratio of the microparticles maintained after extraction.

4.4. Synthesis of Three-dimensional Microstructure

Our method also provided a control over the shapes of the microparticles in the third dimension. In addition to the uniform planar anchoring parallel at the two sides of the microparticles as illustrated above, we used symmetric homeotropic anchoring and homeotropic-planar hybrid anchoring conditions and synthesized the microparticles. The homeotropic anchoring was maintained by PFDTS coating. Figure 4.10 illustrates the microparticle synthesis with homeotropic coating (for clear image see Figure A3). Dark appearance of the polarized light microscope images shows homeotropic anchoring. Conoscopic images provide additional proof for homeotropic anchoring. The microparticles with homeotropic anchoring at the two surfaces maintained a smaller but still circular shape after extraction (Figure 4.11-A). The shrinkage of these particles was found to be 54.6 ± 2.9% after the extraction of the non-reactive mesogens, which was consistent with the shrinkage amount perpendicular to the nematic director (reported above).

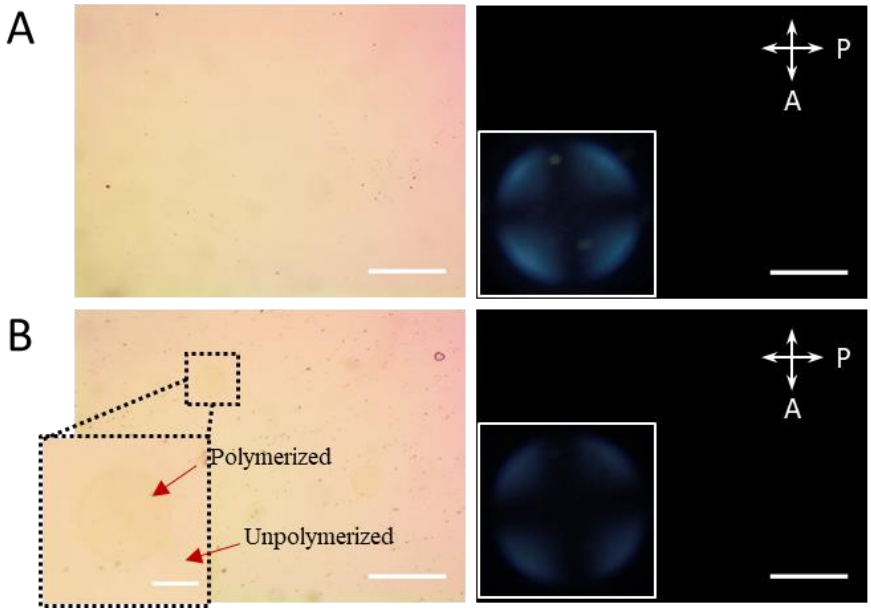

Figure 4.10 Representative optical micrographs collected from the synthesis of polymeric microparticles with homeotropic anchoring from a mixture of 20% by weight RM257 in E7. A 6 μm-thick film was confined between two PFDTS coated glass surfaces. Micrographs were collected (A) before polymerization, (B) after polymerization with UV light and a photomask (inset showing a magnified part shown in dashed lines. Images on the left panel of each figure set are brightfield (top) whereas images on the right side of each panel are polarized light images. Insets showing the conoscopic images indicative of homeotropic anchoring. Scale bars: A and B 500 μm; inset in B, 100 μm.

The microparticles synthesized from hybrid anchoring conditions maintained a curved ellipse shape with the homeotropic face at the concave side after the extraction of the non-reactive mesogens due to the shrinkage imbalance at the two sides of the microparticles (Figure 4.11-B and C). The curling of the microparticles were along or perpendicular to the long axis depending on the orientation of the LC template with respect to the long axis, which was supported by polarized light micrographs. The

shrinkages were calculated to be 51.5% ± 5.04% perpendicular to the nematic director consistent with the above measurements.

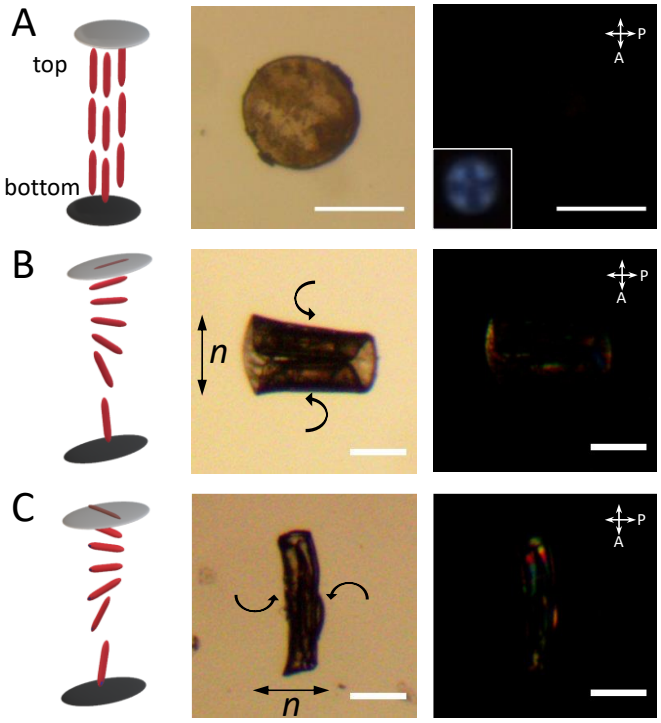

Figure 4.11 Representative sketches of the LC anchoring maintained at the confining surfaces before polymerization (left panel) and optical micrographs collected from the polymeric microparticles (brightfield, middle; polarized light, right panel) synthesized from a mixture of 20% by weight RM257 in E7 with different anchoring conditions. The film thicknesses were 6 μm and films were (A) confined between two PFDTS-coated glass surfaces mediating homeotropic alignment (inset image shows conoscopic image indicative of homeotropic anchoring), (B) confined between a PFDTS surface mediating homeotropic alignment and a rubbed PVA surface mediating uniform planar alignment along the long axis, and (C) confined between a PFDTS surface mediating homeotropic alignment and a rubbed PVA surface mediating uniform planar alignment along the short axis. n indicates the nematic director of the surface mediating planar anchoring. Scale bars: 100 μm.

4.5. Synthesis of Chiral Microparticles

Finally, when the microparticles were synthesized between two surfaces mediating uniform but unparallel planar anchoring at the top and bottom surfaces, the microparticles maintained a twisted shape after the extraction of the unreacted mesogens and drying. Within the samples prepared, we measured the LC twist angle using the methods described elsewhere[64] and found that the LC twist angle was consistent with the angle set by rubbing the contacting PVA surfaces (Figure 4.12).

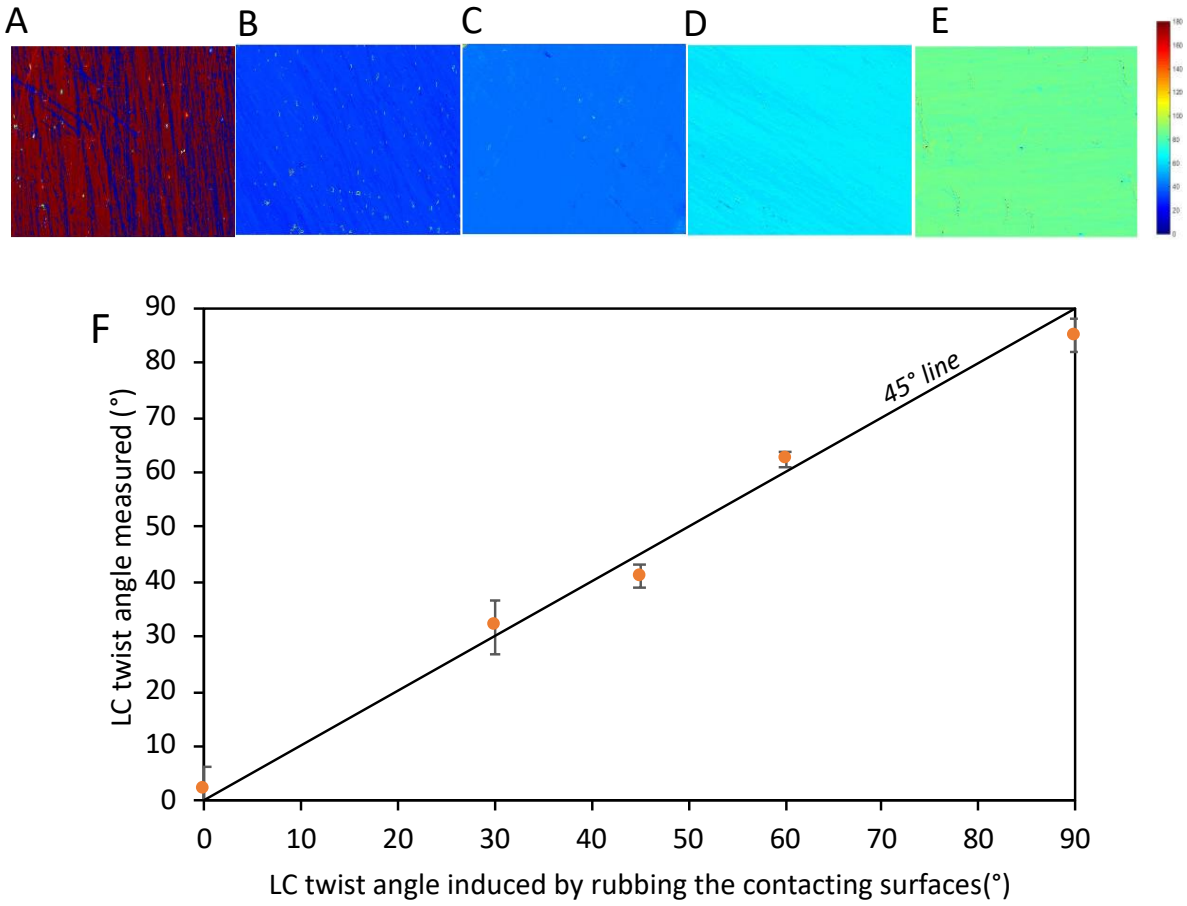

Figure 4.12 Image processing results that show LC mixture align in the direction of rubbed PVA. (A-E) The maps of the measured angles within a piece of a film is shown, the rubbing of the surfaces was done at angles of (A) 0°, (B) 30°, (C) 45°, (D) 60° and (E) 90°. (F)The plot of the measured LC-twist and rubbing angle.

Since LC mixture (20 wt.% RM257 in E7) alignment was consistent with the direction of rubbing, microparticles were synthesized from 6 μm-thick film. Synthesized microparticles are illustrated in Figure 4.13. The two surfaces of the film were rubbed at an angle with respect to each other as indicated by the sketch shown in the left panel (Figure 4.13-B). The rubbing was done such that, when combined, the uniform planar orientation at the top surface was oriented at a predetermined angle in a direction (clockwise or counterclockwise) in reference to the bottom surface, forming a twisted LC director profile through the thickness of the LC film. We found that, when the twist in the LC-template was left-handed, the microparticles maintained a right-handed twist after polymerization and extraction steps. On the other hand, when the twist of the LC-template was right-handed, the microparticles maintained a left-handed twist after polymerization and extraction steps. This was due to the shrinking asymmetry through the thickness of the film that resulted in the reversal of the handedness of the LC twist along the director which is in the chiral axis (Figure 4.13). Furthermore, the periodicity of the twist was observed to be dependent on the twist angle which was initially determined. As shown in Figure 4.13-B, the microparticles maintained shapes with shorter pitch as the angle of the LC twist was increased. When the LC-twist angle was maintained at 90° during polymerization, the microparticles maintained a symmetric curled shape.

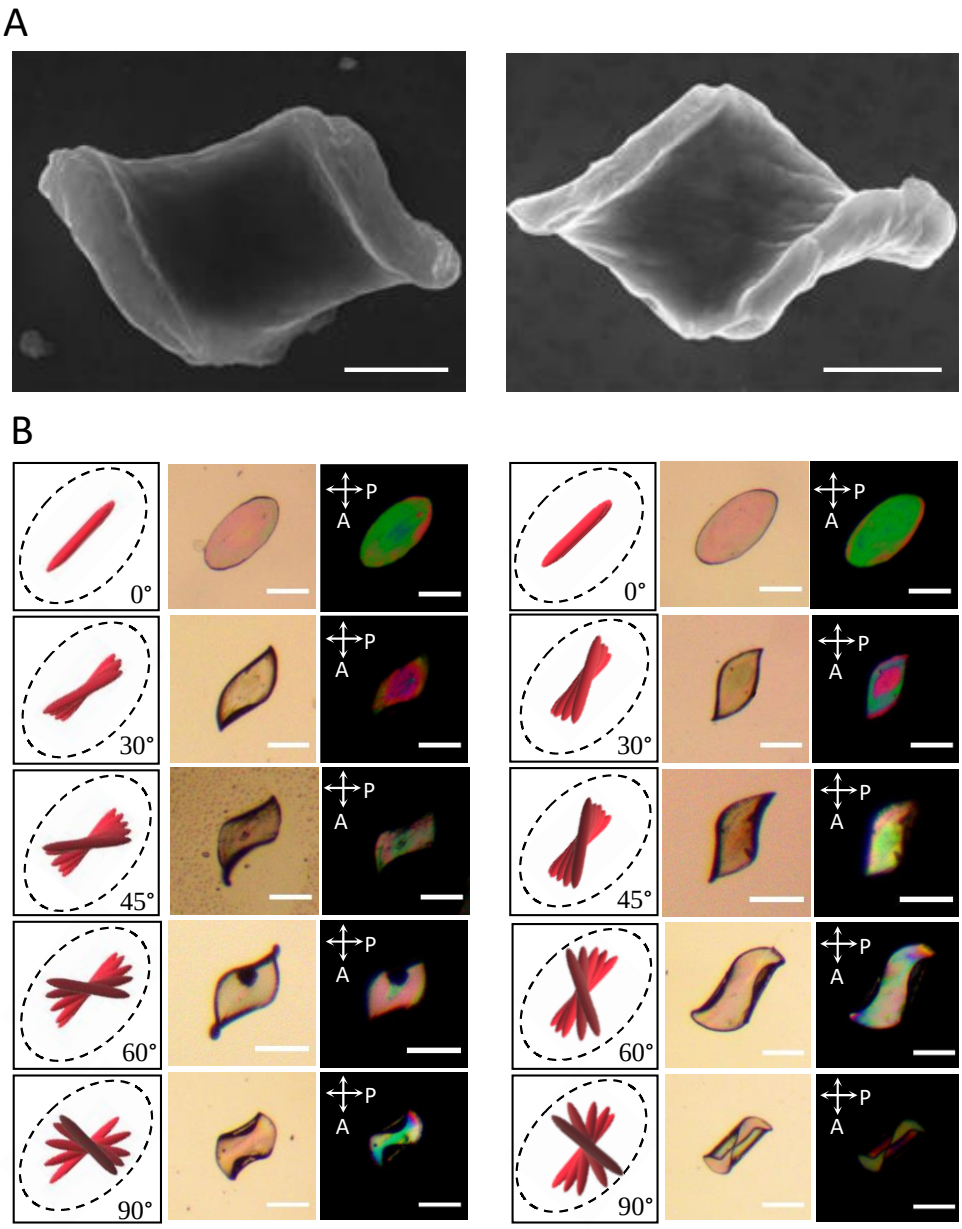

Figure 4.13 Micrographs of the microparticles synthesized between rubbed PVA glass slides mediating left-hand and right-hand twisted nematic ordering. (A) Scanning electron micrographs, scale bars: 20 µm. (B) brightfield (middle) and polarized light (right) micrographs of the microparticles synthesized between two glass slides of indicated twist angle shown in the left panel of each figure set, scale bars: 100 µm. The particles were synthesized from 20 wt.% RM257 in E7 with a film thickness of 6 µm.

Additional SEM images can be found in Figure 4.14. The samples for SEM images were prepared from a photomask that contains circular features of 100 μm in order to increase the number of microparticles, which helps in imaging with SEM. However, we were also able to collect images of microparticles synthesized from the same mask size as in Figure 4.14-B.

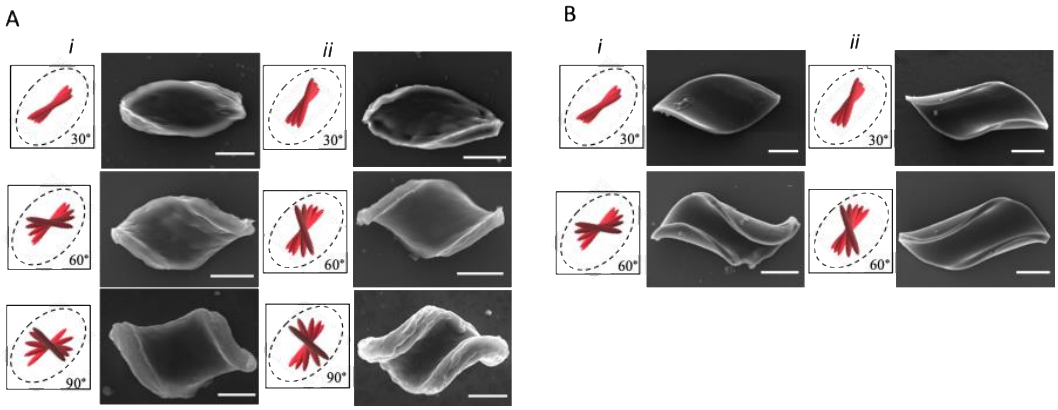

Figure 4.14 SEM images of chiral microparticles which was synthesized from a mixture of 20% by weight RM257 in E7, 6 μm spacer thickness, and adjusted LC twist angles. Circler photolithography mask with (A) 100 μm and (B) 260 μm features were used. (A-i) and (B-i) represents L-LC twist, whereas (A-ii) and (B-ii) shows R-LC twist conformation. Scale bars in A: 20 μm, Scale bars in B: 50 μm.

In addition, we have also found the chiral twisting of the microparticles is also repeatable as shown in Figure 4.15. Although the micrographs shown herein demonstrates the repeatability of the chiral twisting, we can only make a qualitative discussion based on their shapes and optical appearance. Quantitative measurements on the chiral twisting of the microparticles (such as pitch size as a function of the LC twist angle) requires comprehensive analysis on the microparticles with more elongated, regular shapes such as rectangles with high aspect ratio. Such analysis is included in the next chapter.

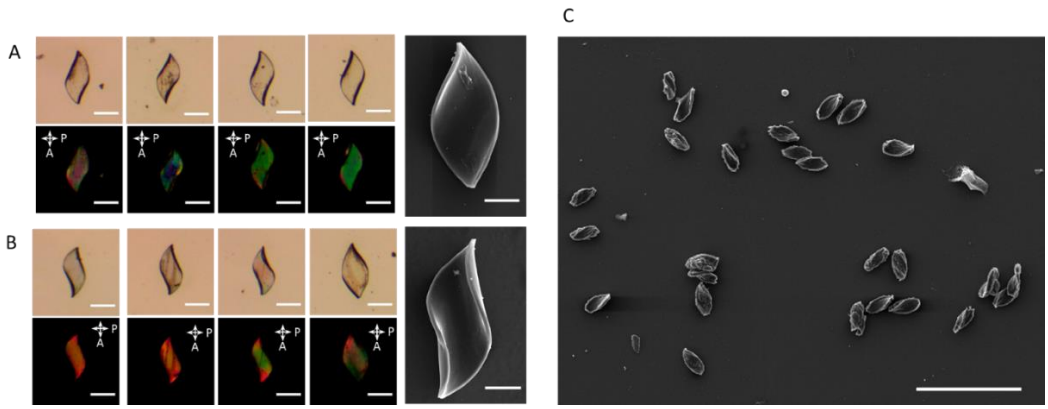

Figure 4.15 Additional micrographs of the chiral microparticles synthesized from mixtures of 20% by weight RM257 in E7, 6 μm spacer thickness, and 30° LC twist angles. Circle photolithography mask with (A and B) 260 μm and (C) 100 μm features sizes was used. (A) and (B) are the representative micrographs of the microparticles synthesized from left-handed and right-handed twist conformation, respectively. (C) SEM image of the microparticles that demonstrates the homogenous distribution of the microparticles. Scale bars in A and B: 100 μm, SEM images scale bars in A and B: 50 μm, and Scale bar in C: 200 μm.

CHAPTER 5

DESIGN PARAMETERS AND PRINCIPLES OF LIQUID CRYSTAL TEMPLATED SYNTHESIS OF POLYMERIC MICROPARTICLES VIA PHOTOLITHOGRAPHY

5.1. Synthesis Method and Design Parameters

Figure 5.1 briefly explains the procedure for the LC-templated particle synthesis procedure we followed in this study. The procedure involved two main steps. Firstly, the LC mixture was filled inside the gap between two functionalized surfaces by capillary action, the photomasks was placed, and the system was exposed to UV light (365 nm). Secondly, the glass surfaces were detached, and particles were physically removed from unreacted parts with the help of ethanol. The right column in Scheme 1 shows micrographs of sample microparticles synthesized using a mask with star shaped features. A mixture of 20 wt. % RM257 in E7 was filled between two rubbed-PVA coated glass slides (direction indicated with *R*) that mediated uniform planar anchoring (top image). Then, the mixture was locally polymerized using a photomask and UV light (middle image). Finally, unreacted part was removed from the system and particles shrank substantially perpendicular to the LC director to maintain their final shape (bottom figure). Here we note that the final shapes of the particles are critically dependent on the monomer content of the initial mixture, the thickness of the film, the LC director profile within the film and the features on the mask. Below we detailly explain how these parameters affect the shapes of the microparticles.

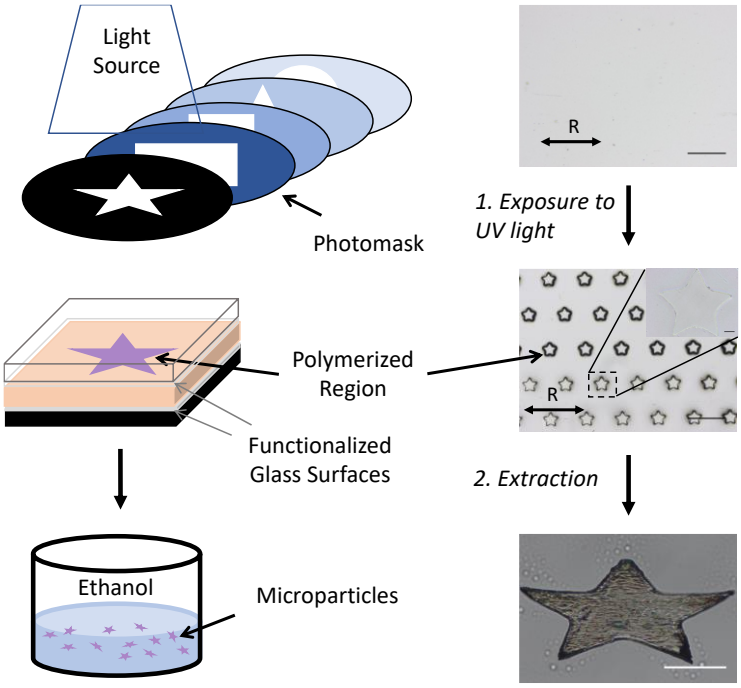

Figure 5.1 Schematic representation of the LC-templated microparticle synthesis procedure followed in the study. The left column shows the schematic representation of the procedure. The right column shows representative micrographs collected during the synthesis of star shaped microparticles following the procedure on the left. Scale bars = 300 μm for the top two micrographs, 50 μm for the inset in the middle micrograph and the bottom figure.

5.2. Effect of Photomask Feature and LC Alignment

Figure 5.2 shows the microscopy images of various microparticles synthesized following the method described. Masks with six different features (circle, triangle, square, rectangle, star and heart shape) were used to polymerize 6 μm-thick films of 20 wt. % RM257 in E7. The alignment of the LCs, which were indicated on the left of the figure, were maintained either by rubbed PVA coated surfaces for uniform planar, or DMOAP functionalized surfaces for homeotropic anchoring inside the film. After extraction of the unreacted part, the microparticles maintained their final shapes due to the anisotropic shrinkage, which we had shown to be more substantial in a

direction perpendicular to the LC director.[67] In the end, considering the symmetry of the microparticles and the anisotropy of the shrinkage, we were able to synthesize 22 different shaped microparticles using 6 different masks and 4 different uniform LC alignment within the films as shown in Figure 5.2. The corresponding polarized light micrographs of each microparticle was consistent with the alignment of the polymer chains in a direction initially maintained within the LC mixture.

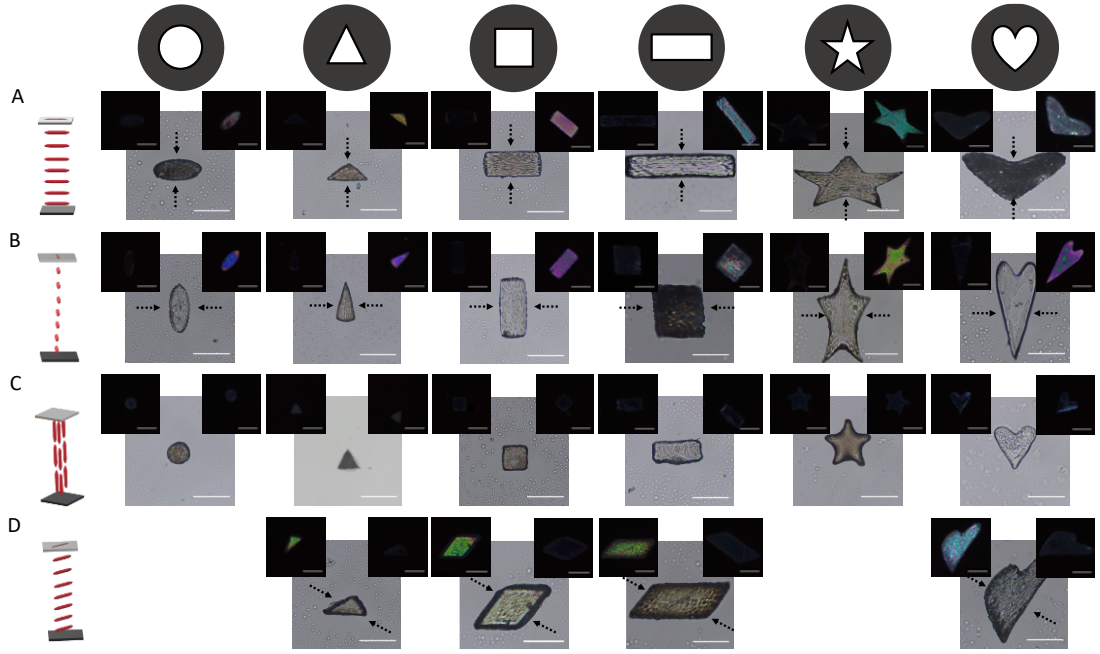

Figure 5.2 Optical micrographs of the microparticles synthesized from mixtures of 20 wt. % RM257 in E7. The top row indicates the representative features of the photomasks used in each column and the sketches on the left column indicates the LC configuration initially maintained within the film. 6 μm spacers were used to separate two functionalized surfaces. Micrographs shows the microparticles synthesized from films with an LC alignment (A) horizontal, (B) vertical, (C) in plane and (D) with 45° angle with respect to brightfield images shown. Two insets corresponding to each image were taken under polarized light. The left insets are taken at the same direction whereas the right insets were taken after the image was rotated 45° with respect to the brightfield images. Rubbed PVA surfaces were used for planar, and DMOAP functionalized surfaces were used for homeotropic anchoring. Scale bars: 50 μm.

Figure 5.3 illustrates the SEM micrographs of the particles synthesized from the same mixture. However, the heart shaped particle in Figure 5.3-A was synthesized between two DMOAP coated surfaces (for homeotropic anchoring) and the rectangular shaped particle in Figure 5.3-B was synthesized between two rubbed PVA surfaces (for uniform planar anchoring along the long axis). The SEM images show the differences in the roughness of the surfaces. The corresponding FFT patterns indicate the anisotropy of the surface roughness of the particle synthesized between rubbed PVA surface in the direction parallel to the rubbing direction of the PVA surface. In other words, surface features of the microparticles were observed to exhibit similar alignment (Figure 5.3). Thus, in addition to the shapes, control over the internal structure of the microparticles were also provided.

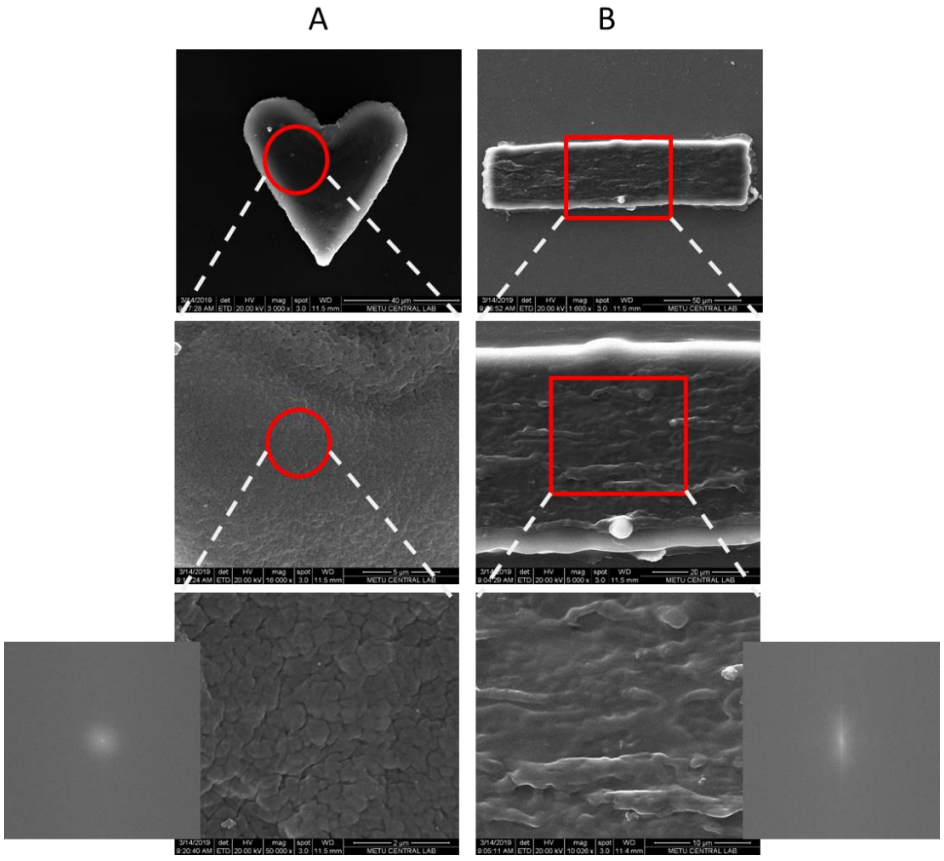

Figure 5.3 SEM images of microparticles synthesized from the mixture of 20 wt.% RM257 in E7 and 6 μm thickness. (A) The images of a heart shaped microparticle synthesized from a mixture maintained at homeotropic alignment between two DMOAP surfaces. (B) The images of a rectangular shaped microparticle synthesized from a mixture maintained at planar alignment between two rubbed PVA surfaces. The inset figures show the FFT patterns of the corresponding SEM images.

Here we note that the most important step in providing the initial shapes to the microparticles was the exposure to UV light. We have used masks with six different features, which were combinations of round and sharp-edged features, and we sought to provide a precise control over the initial shapes of such microparticles. We found the exposure time of the UV light and the thickness of the glass surfaces placed on the LC mixtures have considerable effect in determining the sizes of the microparticles and the resolution of the edges. We specifically determine UV exposure times for each

microparticle in Figure 5.2 and found that an intermediate time in the timescale of one second was required and critical to provide the initial shape of the microparticle (Table 5.1). Below this time, the locations corresponding to the features of the mask were observed to be partially polymerized, whereas, the whole LC film was observed to polymerize at longer UV exposure times. Figure 5.4 illustrates a demonstration of the selection of the UV light power and exposure times. The images were collected after polymerization of a film of 20 wt. % RM257 in E7 with the indicated setup. As shown, we have changed the thicknesses of the glass surfaces, UV power input and the UV exposure times to find the optimum procedure for sharp edged microparticles. We found that thinner glass slides, higher power input and intermediate times, for example 0.13 mm-thick glasses, 1.2 A power input and 2 seconds for triangular shaped microparticles, were required for an acceptable precision for shaping the particles. In the correct intermediate exposure times, we found that the initial sizes of the microparticles were monodisperse with coefficient of variance less than 2.7%, for example, the microparticles synthesized from rectangular shaped masks were 180.0 ± 1.2 in long axis, and 82.3 ± 1.4 in short axis μm in size.

Table 5.1 UV exposure times required to synthesize microparticle from mixtures of 20 wt. % RM257 in E7. Collimated light source energy was adjusted to 0.7A or 1.2A. Red boxes indicates the UV exposure times used in the synthesis of the corresponding microparticles.

Photomask Shape	ThorLabs M365LP1-C	
	0.7A	1.2A
Circle	2 seconds	<1 seconds
Triangular	3 seconds	2 seconds
Square	3 seconds	1 seconds
Rectangular	2 seconds	<1 seconds
Star	2 seconds	<1 seconds
Heart	2 seconds	<1 seconds

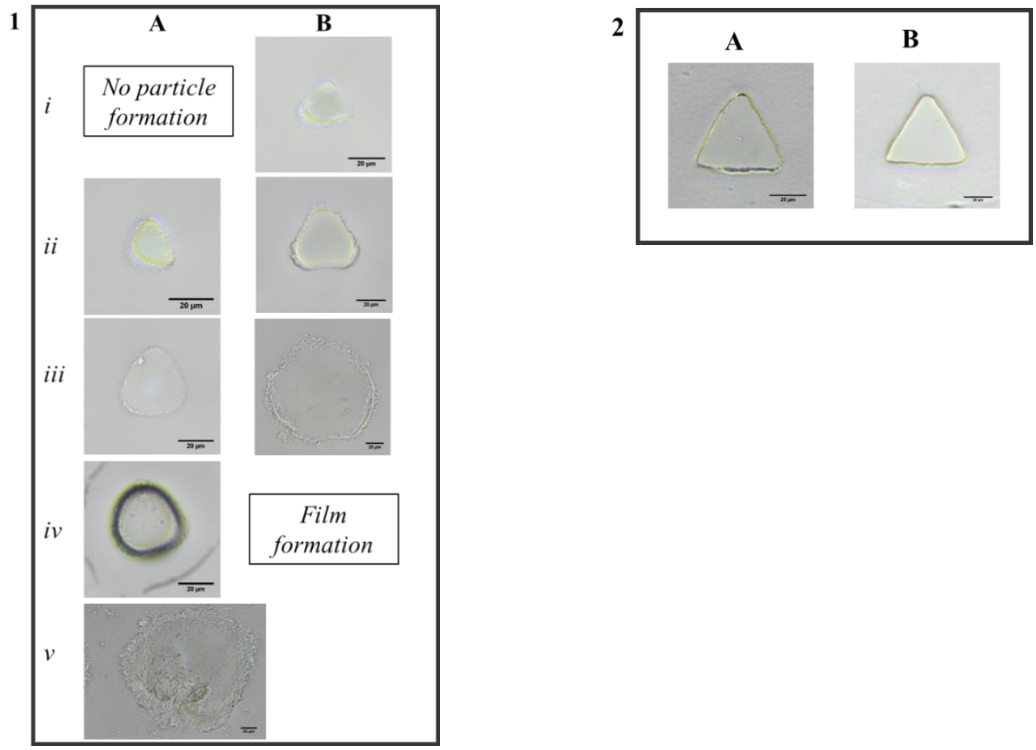

Figure 5.4 Features of the triangular shapes with varied current and UV exposure time. The images in column 1-A show the polymerized regions after exposure with current setting of 0.7A whereas the images in column 1-B show the polymerized regions after exposure with current setting of 1.2A. UV exposure times were changed from (i) 1 second, (ii) 2 seconds, (iii) 3 seconds, (iv) 4 seconds, and (v) 5 seconds. The films in column 1 were prepared between two glass surfaces with thickness of 1 mm. In the films shown in columns 2-A and 2-B were maintained between glass cover slides with 0.13 to 0.16 mm thicknesses. Microparticles were synthesized at 0.7A current in 3 seconds in 2-A, whereas in 2-B it was synthesized at 1.2A in 2 seconds.

Anisotropic shrinkage is one of the parameters to determine the final shape of the microparticle that we investigate in this study. Previously, we have shown that the shrinkage to change almost linearly from 65.6% ± 2.7% to 45.7% ± 3.5% perpendicular to the LC director when the monomer content of the mixture was changed from 10 wt. % to 30 wt. %, and almost constant at around 10.5% ± 2.4%

parallel to the nematic director.[67] We show here how predictive the shrinkage extends in determining the final shapes of the microparticles. As an illustrative example, we selected rectangular shaped microparticles to demonstrate the changes in the microparticle shapes characterized by the aspect ratio, and equilateral triangle shaped microparticles to demonstrate the changes in the microparticle shapes characterized by their top angle. For these purposes, we have synthesized rectangular shaped microparticles with molecular alignment along (*i*) the long axis and (*ii*) short axis; and equilateral triangle shaped microparticles with molecular alignment (*i*) parallel and (*ii*) perpendicular to one of the sides (Figure 5.5-A, B and D, E). We made simple calculations using the initial aspect ratio (2.0) and the shrinkages of the rectangular shaped microparticles as a function of the monomer content and the results were plotted in Figure 5.5-C (for calculation see Appendix B). As seen in the figure, the predicted values of the final aspect ratio and the experimentally observed values were quantitatively consistent with each other. For example, the experimentally observed aspect ratios of a rectangular shaped particle synthesized from 20 wt. % RM257 in E7 were 4.1 ± 0.4 and 1.1 ± 0.1 when the molecular alignments were along the long and short axis, respectively. The calculations for the same conditions gave aspect ratios of 4.1 and 1.1, respectively, consistent with the experiments. Similarly, the microparticles that were synthesized using the equilateral triangles with molecular configuration (*i*) and (*ii*) and the calculations were performed to quantify the top angle using the initial size and the shrinkage amounts as a function of the monomer content (Figure 5.5-F). When the calculations and the experimental measurements were compared, the consistency was striking as shown in Figure 5.5-F. For example, the top angle of a triangular microparticle synthesized from 20 wt. % RM257 in E7 were measured as 102° ± 5° and 37° ± 3° when the LC alignments were parallel and perpendicular to one of the sides, respectively. The calculations for the same conditions gave top angles of 97° and 34°, respectively. Furthermore, calculations of the top angles with law of cosines gave top angles of 96° ± 9° and 33° ± 3.0°, respectively. This result provides further evidence for the consistency of the result.

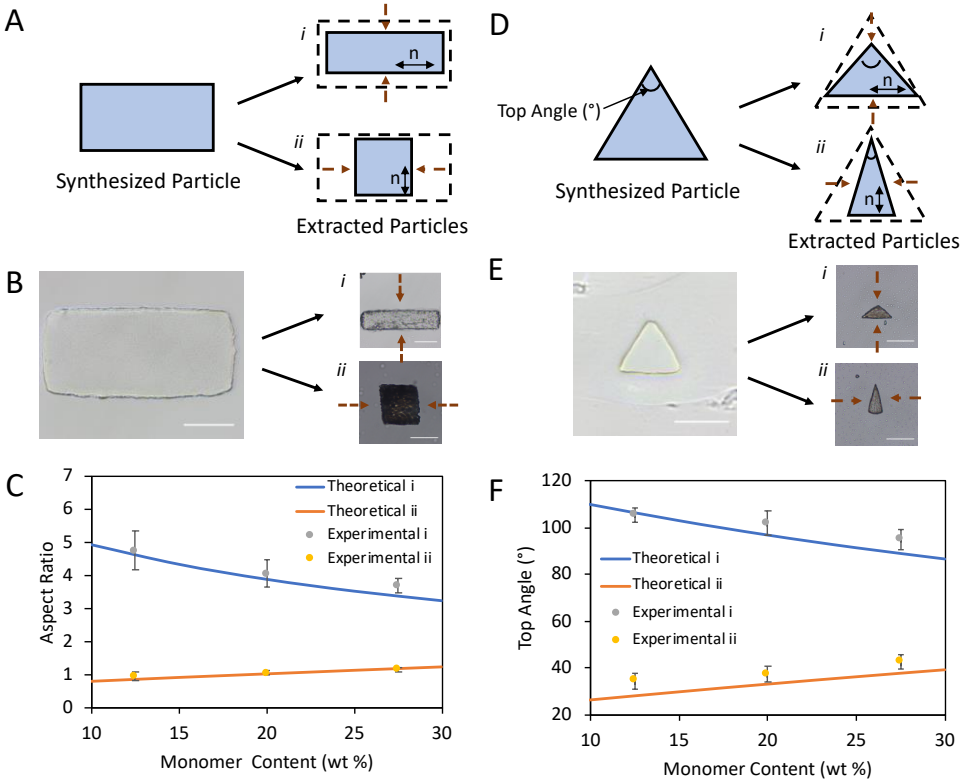

Figure 5.5 Schematic representation of (A) rectangle and (D) triangle shaped particles before and after extraction. The arrow 'n' represents the rubbing direction of the PVA functionalized surfaces. Micrograph images of rectangular (B) and triangular (E) particles. Scale bars: 50 μm. Theoretical and experimental aspect ratio of the rectangular shape particles can be found in (C). Theoretical and experimental top angle data of the triangular shape particles can be seen in (F).

5.3. Design Parameters of Bulk Chiral Twisted Polymeric Materials

We have shown a potential for a control over the chirality and the pitch size of the chiral twisted microparticles with our synthesis method. We show how precisely this could be achieved by performing measurements on the chiral twisted microparticles. For this purpose, we have synthesized rectangular shaped microparticles with LC twisting using films with known twisting of the LC director. The uniform planar LC

anchoring along the long axis was maintained on one side of the film, whereas either L- or R- twisted LC director profile with a determined angle was maintained on the opposite side of the film using rubbed-PVA coated slides. Figure 5.6-A and B show the chiral twisted rectangular microparticles synthesized from L- (left panel) and R-twisted (right panel) LC configuration with 0°, 30°, 45°, 60° and 90° twist angles. As the micrographs were compared, we arrived to two main observations. First, the microparticles synthesized from L-twisted LC configurations-maintained R-twisted shapes whereas their R-twisted counterparts resulted in microparticles with L-twisted shapes after the extraction of the unreacted mesogens. We concluded that this was due to the shrinking asymmetry through the thickness of the film that resulted in the microparticles to maintain twisted shapes with opposite handedness compared to the handedness of the LC configuration initially maintained. Second, the pitch sizes of the L-twisted shapes maintained by the microparticles were measured to be 224.6 ± 21.3 μm, 154.9 ± 18.2 μm, and 129.9 ± 14.7 μm whereas those of the R-twisted microparticles were measured to be 234.6 ± 23.2 μm, 160.9 ± 15.8 μm, and 134.5 ± 12.0 μm for the microparticles synthesized from 30°, 45°, and 60° twisted LC configurations, respectively. We reasoned that the trend of decreasing chiral pitch size upon increasing LC-twist angle could provide a relation between the LC-twist angle and the chiral pitch of the microparticles. Below we test this hypothesis by providing additional measurements of the microparticles.

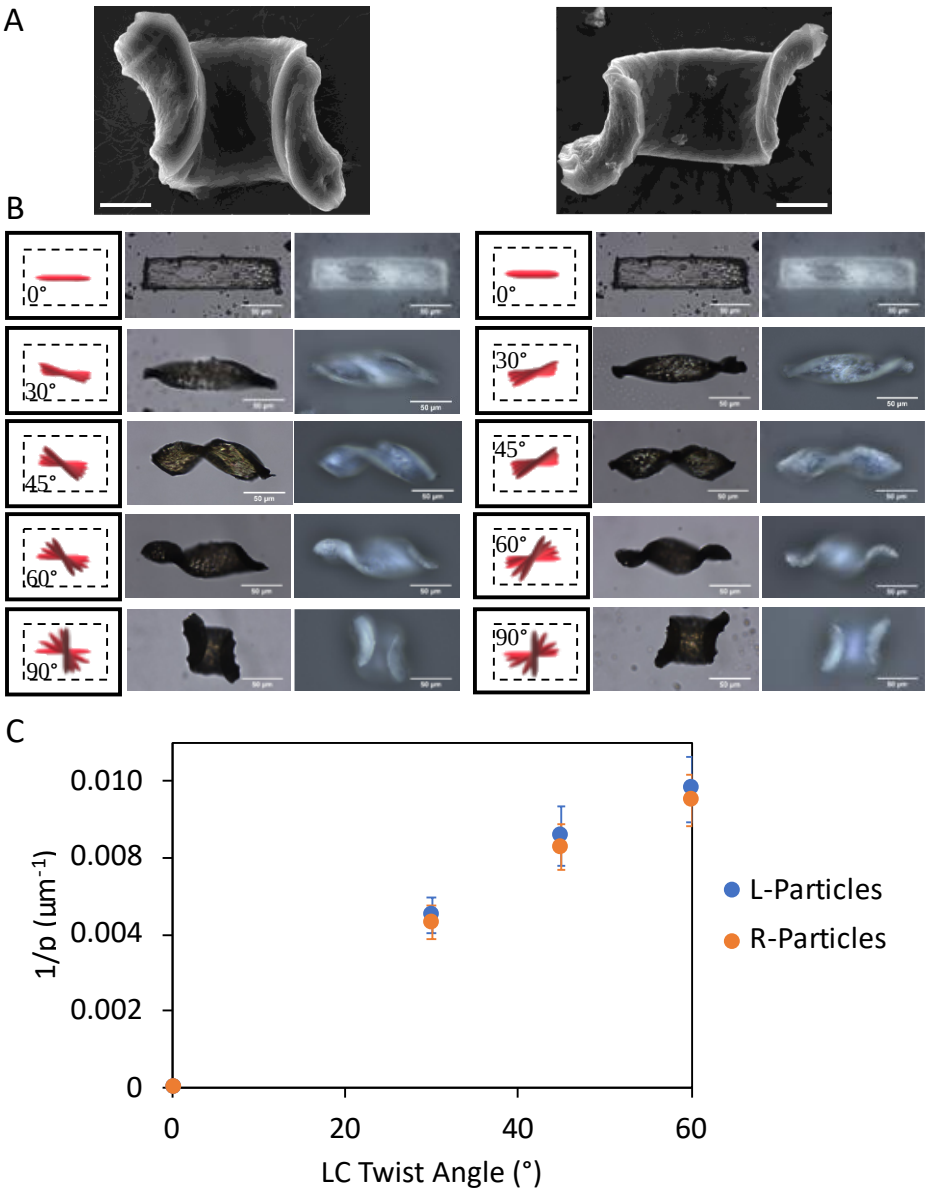

Figure 5.6 Micrographs of the microparticles synthesized between rubbed PVA glass slides mediating left-hand and right-hand twisted nematic ordering. (A) Scanning electron micrographs, scale bars: 20 μm. (B) transmission (middle) and reflection (right) mode micrographs of the microparticles synthesized between two glass slides of indicated twist angle shown in the left panel. (C) Pitch size of the chiral particles characterized with respect to angle between two PVA coated glasses. The particles were synthesized from 20 wt.% RM257 in E7 with a film thickness of 6 μm.

The microparticles were synthesized from 6 µm-thick films. This is a relatively small thickness of a film such that the LC anchoring at the two sides of the films may deviate from the rubbing direction of the surfaces. In order to check this, we made measurements of the LC-twist angles within the film and found that they were indeed the angles set by the contacting surfaces (Figure 4.12 and 5.7).

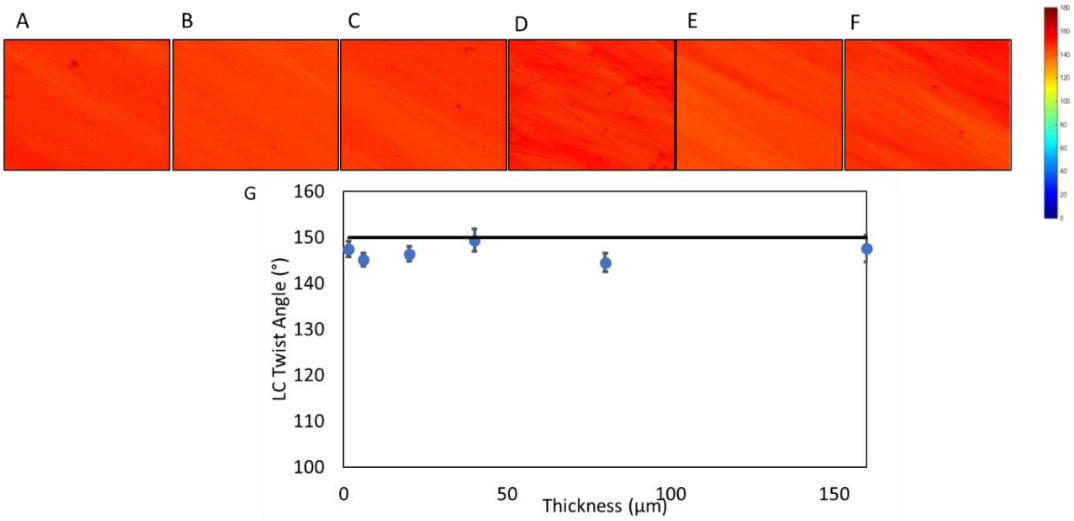

Figure 5.7 (A-F) The maps of the measured twist angles within a piece of a film with various thicknesses are shown. The thicknesses of the films were (A) 1.5 µm, (B) 6 µm, (C) 20 µm, (D) 40 µm, (E) 80 µm and (F) 160 µm, and a right-handed LC twist of 30° were maintained within the films. The plot in (G) shows the average twist angle measured with respect to thickness.

Next, we questioned whether the chiral twist in the molecular alignment within the film after polymerization were different than the twist initially set by the LC-director profile. The measurement results that are shown in Figure 5.8 revealed the LC-twist maintained within the film to be the same with the twist angle of the molecular alignment within the microparticles obtained after the extraction step. Thus, in the end, we concluded that the rubbing direction of the PVA surfaces determined the molecular director profile within the microparticles.

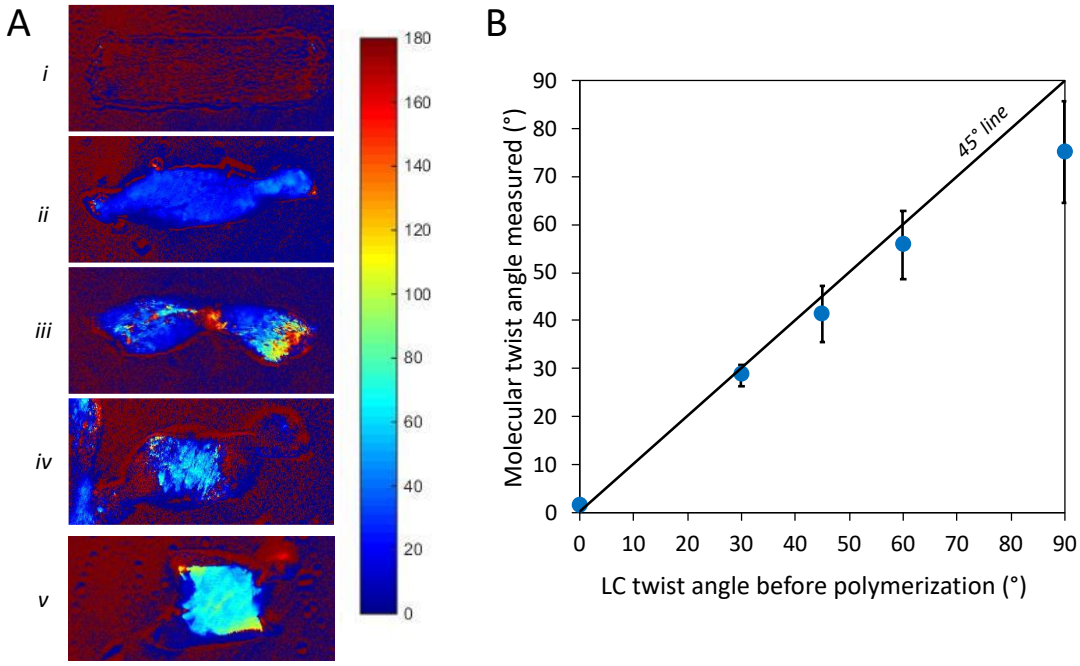

Figure 5.8 Left-hand microparticles synthesized between rubbed PVA glass slides right-hand twisted nematic ordering. (A) Configuration of the zenithal angles representing angle variation inside the particles. Twist angle of the LC adjusted as (A-i) 0°, (A-ii) 30°, (A-iii) 45°, (A-iv) 60°, and (A-v) 90°. (B) The graph of the particle zenithal angles with respect to LC twist angle.

Knowing this, when we plotted the inverse pitch size of the chiral twist of the microparticles with respect to the twist of the LC-director profile before polymerization, we found the inverse pitch size of the microparticles to be linearly dependent on the LC twist angle maintained initially (Figure 5.6-C). This is an indicative of the chiral twisting of the microparticle to be determined by the anchoring of LCs at the two sides of the film before polymerization. If this is the case, the chiral twisting of the microparticles would not be dependent on the size of the microparticles. We have tested this question with an additional set of measurements of the pitch upon changing the thickness of the microparticles. The measurements of the pitch size as a function of the thickness of the microparticles showed an independency with respect

to the thickness of the microparticles, supporting our hypothesis (Figure 5.9). Thus, we have found a relation of $1/P = 1 \times 10^{-4}\Theta$ between the pitch size (in µm) and LC twist angle (in degrees) maintained initially in the mixture.

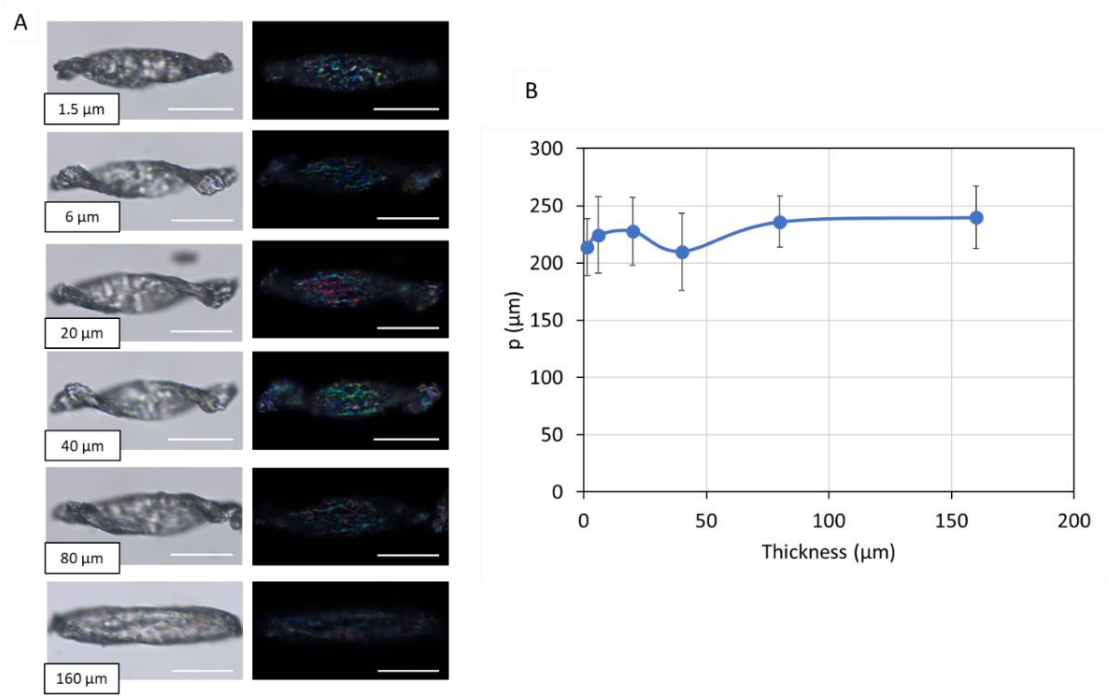

Figure 5.9 (A) Optical micrographs of particles obtained from mixtures of 20 wt. % RM257 in E7 with left handed 30° degrees twist. The thickness of the functionalized surfaces with PVA varied between 1.5 µm to 160 µm indicated at the below of each figure. Scale bars: 50 µm. (B) The graph that show the pitch of the synthesized microparticles with respect to thickness.

Knowing that the chiral twist of the microparticles could be controlled independent of the initial shape of the microparticles, it was possible to synthesize high aspect ratio chiral microparticles. This was accomplished by using a mask with rectangular features of dimensions 100 µm by 2.45 cm. The objects that were synthesized from films of LC-twist that were initially maintained at 0°, 20°, 25°, 30° and 60° are shown in Figure 5.10. As seen in the figures, the chiral twisting of the objects was dependent

on the angle of LC alignment maintained at the two surfaces of the objects, independent of the aspect ratio. However, analyzing the shapes of the objects formed with the high aspect ratio mask, we realized that there were two sets of objects; the helicoids (with Gaussian saddle-like curvature and straight central line) and spiral ribbons (with cylindrical curvature and helical central line). We observed helicoid shapes within the objects that were synthesized from an LC film with a twist of 20° (Figure 5.10-B). Above this angle, center lines of the objects were shifted from a straight line to a helical form and maintained the shape of a spiral ribbon (Figure 5.10-C-F). This observation revealed that the shape selection of helicoids to spiral ribbons would also be possible via tuning the molecular ordering profile within the polymeric materials in addition to the other methods currently available.[38,39] In order to demonstrate the precision in determining the dimensions of the ribbons, we also measured the distance of the ribbon surface to the helical central line (radius), which were observed to increase from 18.2 ± 0.8 μm to 56.4 ± 4.2 μm when the LC-twist angle was changed from 30° to 60°.

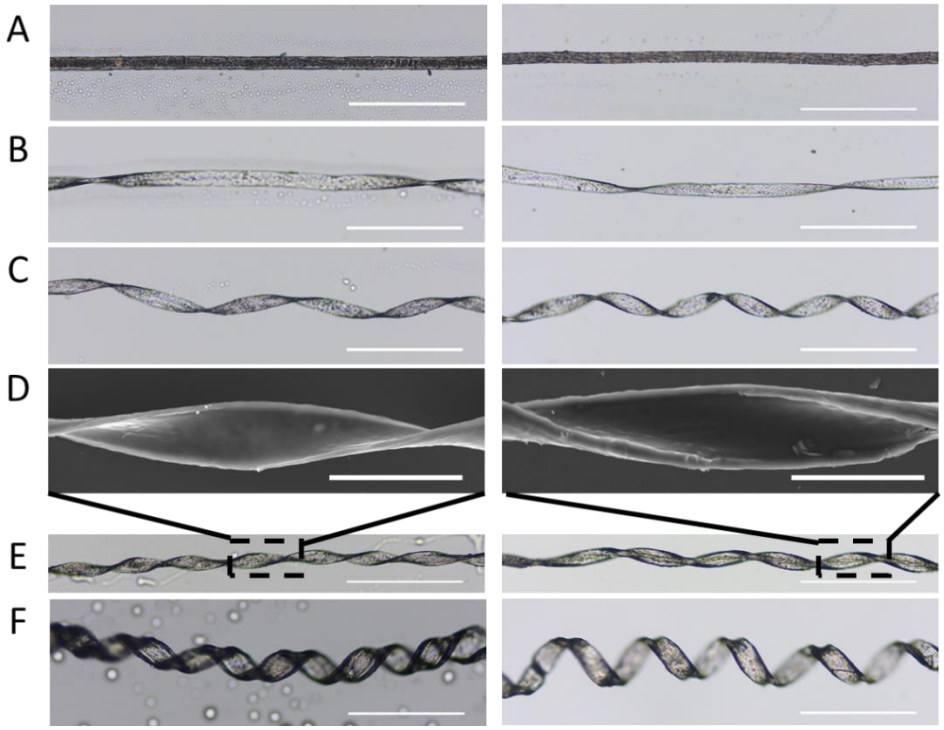

Figure 5.10 Micrographs of the spiral ribbons synthesized between rubbed PVA glass slides mediating left-hand and right-hand twisted nematic ordering. LC twist angle was adjusted (A) 0°, (B) 20°, (C) 25°, (E) 30°, and (F) 60°. Helicoid shape observed in B. Spiral ribbons can be seen in C, E, and F. Scale bars: 300 µm. (D) Scanning electron micrographs of E, scale bars: 100 µm. The chiral films were synthesized from 20 wt.% RM257 in E7 with a film thickness of 6 µm.

5.4. Design Parameters of Bent Microparticles

The last design principle, we sought to use bend distortions within the LCs to provide additional control over the shapes of the microparticles. For this purpose, we used mixtures of 20 wt.% RM257 in E7 which were confined within films of different thicknesses ranging from 1.5 µm to 320 µm. One of the surfaces in contact with the LC mixture was DMOAP that mediated homeotropic anchoring whereas the other was rubbed PVA that mediated uniform planar anchoring parallel to the long axis of the microparticles. The representative micrographs of seven different microparticles

synthesized from films of different thicknesses are shown in Figure 5.11-A. As seen, the microparticles that were synthesized from 6 μm-thick films maintained crescent shapes (Figure 5.11-B). The crescent shapes were expected because when the particle was allowed to shrink after the extraction step, the side corresponding to the homeotropic anchoring shrank more in the direction along the long axis when compared to the opposite side where the alignment was uniformly planar towards the long axis of the microparticles. Thus, the side corresponding to the homeotropic anchoring remained at the inside of the microparticles after shrinkage due to its substantial shrinkage compared to the opposite side. The radius of curvature of this crescent shape was measured to be 41 ± 11 μm at 1.5 μm thickness. If the anchoring of LCs at the two surfaces of the microparticles were homeotropic and planar as mediated by the DMOAP and rubbed PVA surfaces, respectively, one would have expected the radius of curvature of the microparticles to increase upon increasing the thickness of the microparticles because of the finite shrinkage of the two sides of the films set by the monomer content. Surprisingly however, increasing the thickness of the films, the microparticles were first maintained curled shapes similar to a closed cylindrical ring with a radius of curvature of 21 ± 2 μm when the thickness was ~20 μm. Then, upon increasing the thickness, the microparticles maintained more open shapes representing a crescent shape with a radius of curvature of 194 ± 42 μm when the thickness was 320 μm.

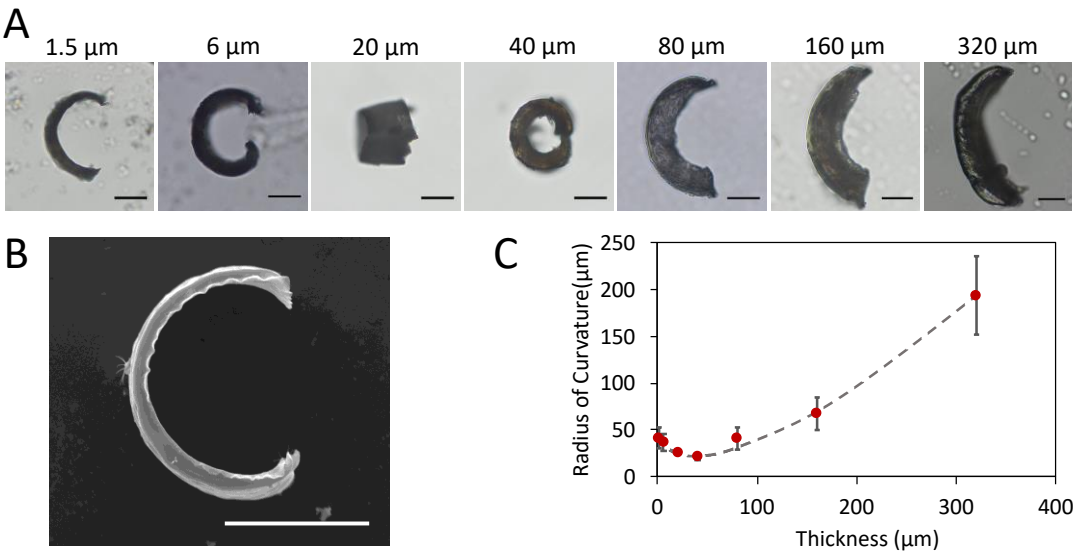

Figure 5.11 (A) Micrographs of microparticles synthesized from mixtures of 20 wt.% RM 257 in E7 between two surfaces mediating homeotropic anchoring at one side and planar anchoring at the opposite side. Thicknesses of the particles were varied from 1.5 µm to 320 µm. Scale bars: 25 µm. (B) SEM images of a microparticle synthesized from a 6 µm thick film. (C) A plot of the radius of curvature of the microparticles measured as a function of the thickness of the microparticles.

When the radius of curvature of the microparticles were plotted with respect to the thickness of the microparticles, the minimum of the radius of curvature was found to correspond to a thickness of 30 µm (Figure 5.11-C). The change of the trend of the shapes as a function of thickness above and below 30 µm was an indicative of the interplay of the surface anchoring and the elasticity of the LCs. With one constant approximation, the elastic energy stored per unit area of a film of LC with a thickness of 10 µm and homeotropic anchoring at one side and planar anchoring at the other side can be approximated to be in the order of $f_b' = K\,\pi^2 / 8d \approx 10^{-6}$ J/m^2 where K is the elastic constant (~10^{-11} J/m) and d is the thickness of the film.[45] This is indeed comparable with the typical surface anchoring energies, *W*, of the LCs (typically around 10^{-6} - 10^{-4} J/m^2). Thus, the two trends of the shapes maintained by the

microparticles with respect to changing thickness were due to the configuration of the LCs maintained within the film resulting from the interplay of the surface anchoring and the elastic energy of the LCs. In the thinner particles, the elastic effects dominated and the surface director at the two sides of the films determined the final shape of the microparticles, whereas in the thicker particles, the surface directors at the two sides of the films were determined by the contacting surfaces and the final shapes of the microparticles were determined by the thickness of the film. Overall, the interplay between the elasticity and surface anchoring provided a precise control over the curvature of the microparticles, in addition to the control over the shape via the thickness of the films.

5.5. Microparticle Size Reduction Strategies

Instead of manufacturing new photomask, we can reduce the size of the microparticles inspired by continuous flow lithography technique (CFL).[18] In CFL (mentioned in Introduction part) technique, microparticles size were reduced by employing an objective. Therefore, we employed an objective reduce the size of 100 μm photomask and it was placed between the photomask and collimated light source. Figure 5.12-A shows the representation of the used technique. As can be seen in micrograph images of Figure 5.12, microparticle size changes from 29.7 ± 3.0 μm to 70.8 ± 7.0 μm when the exposure time changes from 2 seconds to 5 seconds. Diameter of the microparticles suggested that there is a linear relation between the diameter of the microparticles and UV exposure time. Thus, we have found a relation of $D = 14.2t$ between the diameter of the microparticle (in μm) and UV exposure time (in seconds) exposed to the mixture.

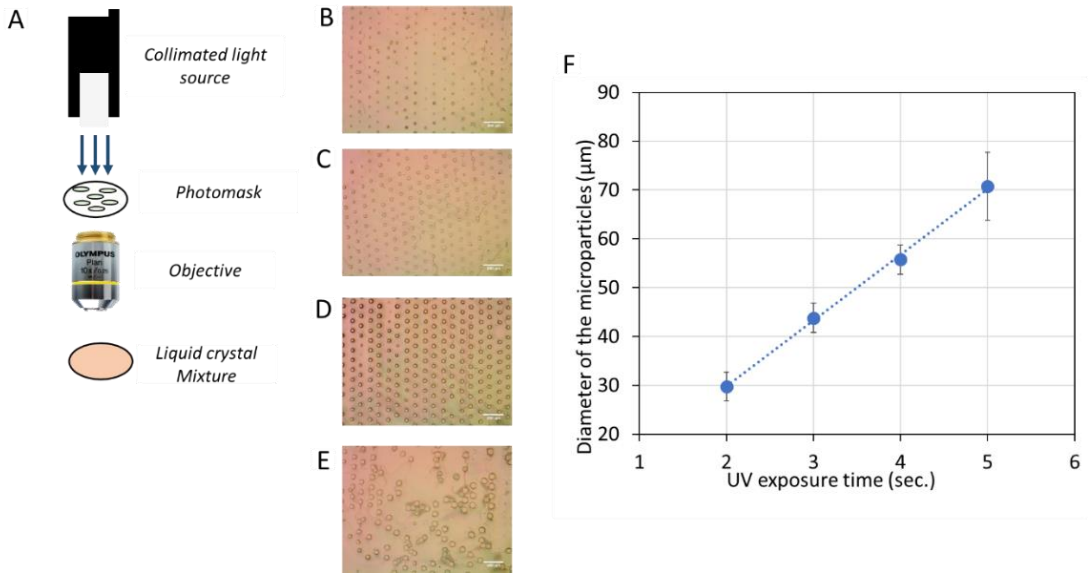

Figure 5.12 Size reduction of the microparticles which were synthesized from mixtures of 20 wt.% RM257 in E7 with 6 µm thickness. (A) Schematic representation of the experimental setup for size reduction. Micrograph of the microparticles with (B) 2 sec., (C) 3 sec., (D) 4 sec., and (E) 5 sec. exposure times. (F) A plot of the microparticle diameter as a function of UV exposure time.

However, this technique is limited to circular feature on the lithography mask with this apparatus. Particles with more complex shapes including variations in the curvatures or sharp edges would be possible with the use of a more accurate collimated light source and a setup allowing precise alignment of the objectives with more defined focal plane thicknesses. Here we note that a combination of a microscope with a UV light source and a photomask would improve this method.

CHAPTER 6

CONCLUSIONS

Overall, we have developed a new method for the synthesis of polymeric microparticles, which combines the use of photolithography with LC molecular templates that, not only provides additional control over the internal structuring and two-dimensional shape of the microparticles, but also provides control over the three-dimensional shapes. The method was a combination of LC molecular templates and photolithography. In the first step, we polymerized LC mixture (non-reactive E7 and reactive mesogen RM257) with UV light (365nm) and a photomask. Then, the unreacted part was extracted and microparticles were allowed to shrink anisotropically to maintain their final shapes. We found that our method provided precise control over the chiral twisting and bending of the microparticles that would be challenging or impossible with the synthesis of isotropic molecular counterparts. This has been accomplished by our method that provides a control over the alignment of the nematic LCs on the contacting surfaces independently. Synthesized microparticles were characterized using optical microscope for their shapes and molecular ordering.

Future studies may also be devoted to the design of microparticles using multiple types of reactive mesogens to provide more complex shapes, as well as response to the external stimuli such as light, chemicals, magnetic field, etc. [56,68,69] In the long term, such microparticles have the potential to be useful in applications ranging from emulsion stabilization, intracellular delivery, sensors, biocatalysis and photonics. In terms of the fundamental knowledge, the particles with complex nanostructures and shapes would also provide understanding of the self-assembly and interparticle interactions, including anisotropic ones, between microparticles with chiral symmetry.

6.1. Future Outlook

In this study, we have demonstrated a technique which provides control over the shapes and microstructure of the polymeric materials. Herein, we present two directions which may find interest by the literature. Below, we describe our initial observations in these two routes.

6.1.1. Microparticle Sensors

Toluene vapor exposure experiments were performed to complex microparticles which were synthesized with hybrid LC configurations. For this purpose, we used mixtures of 20 wt.% RM257 in E7 which were confined within films of different thicknesses ranging from 1.5 μm, 40 μm, and 160 μm. For the synthesis of hybrid microparticles, one of the surfaces was in contact with DMOAP for homeotropic whereas the other was rubbed PVA for planar anchoring. Simply, the microparticles in Figure 5.11 were selected as a candidate for the sensing toluene vapor. The reason for the selection of hybrid microparticle is whether relaxation of their stored energy during shrinkage upon toluene exposure would be observable or not. The top images of the Figure 6.1 show the initial state (0 ppm) of the microparticles, while the bottom images show the maximum toluene exposure (30000 ppm). As can be seen from the images, the radius of curvature of the microparticles were increased upon toluene exposure.

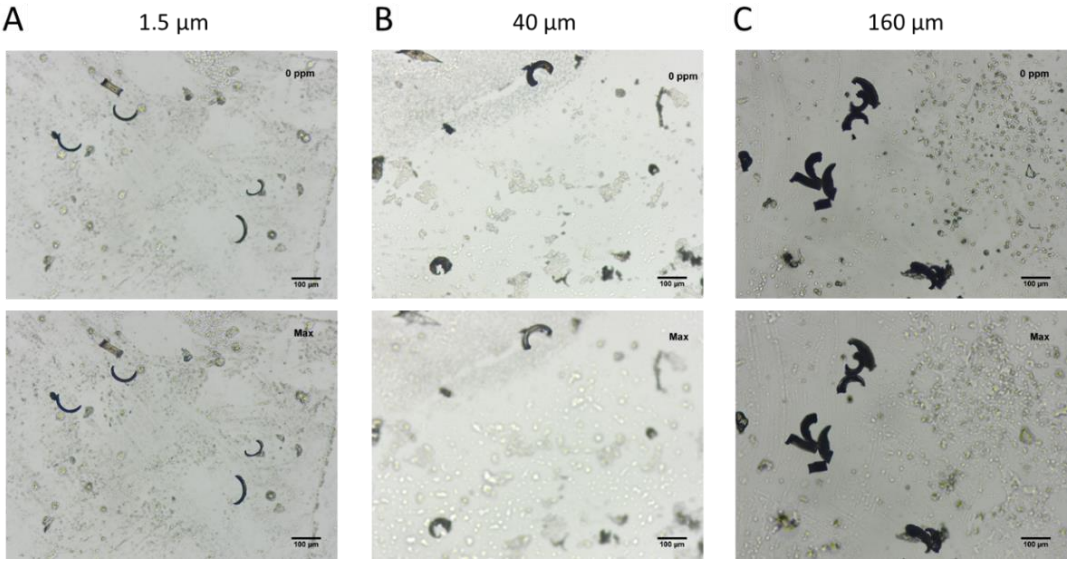

Figure 6.1 Toluene vapor exposure test was performed microparticles that were synthesized hybrid condition. The thickness of the microparticles were (A) 1.5 µm, (B) 40 µm, and (C) 160 µm. The top micrographs show initial state (0 ppm). The bottom images of the Figure represent the maximum toluene vapor limit (30000 ppm).

6.1.2. Alignment of LC-templated Microparticles in LC medium

We hypothesized that the surface of the microparticles synthesized herein may mediate non–degenerate LC anchoring. In order to test this hypothesis, LC templated microparticles were placed in nematic 5CB. Here we noted that alignment of the microparticles were dependent on two main considerations. Internal structure of the microparticles and, the alignment of the LC medium directly affects the positioning of the particles (Figure 6.2).

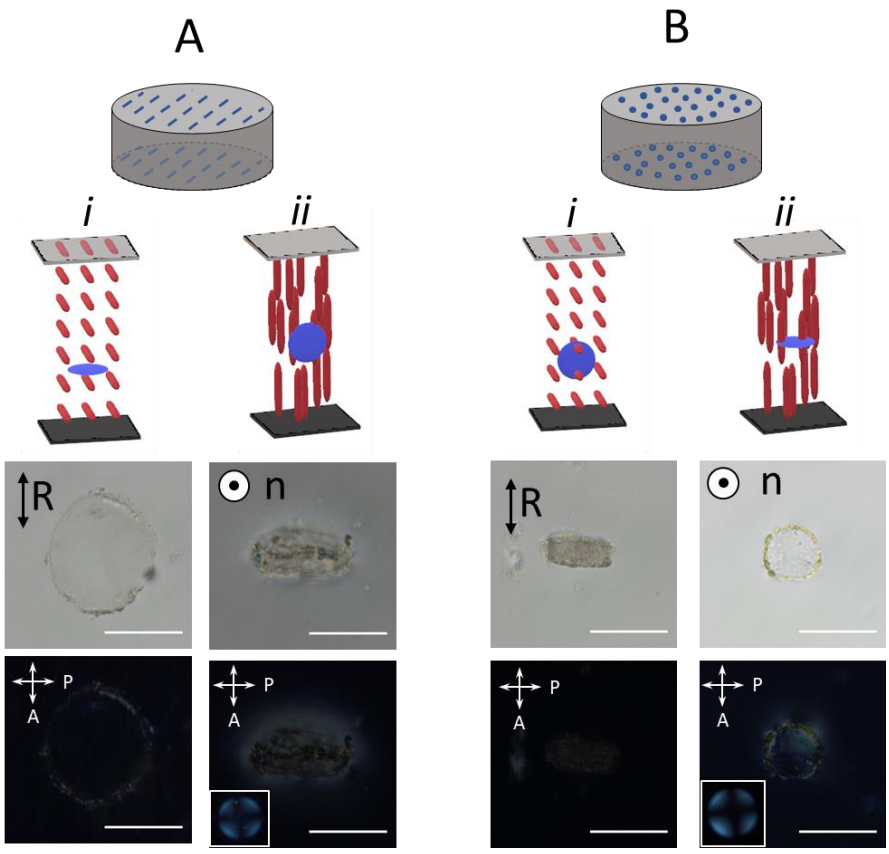

Figure 6.2 Behavior of the microparticles under LCs medium. The microparticles were synthesized mixtures of 20 wt. % RM257 in E7, 6 µm spacer thickness, and (A) two rubbed PVA surfaces or (B) two DMOAP coated surfaces. Anchoring of LC molecules were planer (A-i and B-i) or homeotropic (A-ii and B-ii). Top images show schematic representation of the system. Middle images are the brightfield micrograph images. 'n' indicates LC alignment. Bottom images are the polarized light images. Scale bars: 50 µm.

REFERENCES

(1) Slomkowski, S.; Basinska, T. Polymer Nano- and Microparticle Based Systems for Medical Diagnostics. Macromol. Symp. 2010, 295 (1), 13–22. https://doi.org/10.1002/masy.200900084.

(2) Brannon-Peppas, L. Recent Advances on the Use of Biodegradable Microparticles and Nanoparticles in Controlled Drug Delivery. Int. J. Pharm. 1995, 116, 1–9. https://doi.org/https://doi.org/10.1016/0378-5173(94)00324-X.

(3) Madivala, B.; Vandebril, S.; Fransaer, J.; Vermant, J. Exploiting Particle Shape in Solid Stabilized Emulsions. Soft Matter 2009, 5 (8), 1717–1727. https://doi.org/10.1039/b816680c.

(4) Losch, P.; Huang, W.; Goodman, E. D.; Wrasman, C. J.; Holm, A.; Riscoe, A. R.; Schwalbe, J. A.; Cargnello, M. Colloidal Nanocrystals for Heterogeneous Catalysis. Nano Today 2019, 24, 15–47. https://doi.org/10.1016/j.nantod.2018.12.002.

(5) Jindal, A. B. The Effect of Particle Shape on Cellular Interaction and Drug Delivery Applications of Micro- and Nanoparticles. Int. J. Pharm. 2017, 532 (1), 450–465. https://doi.org/10.1016/j.ijpharm.2017.09.028.

(6) Venkataraman, S.; Hedrick, J. L.; Ong, Z. Y.; Yang, C.; Ee, P. L. R.; Hammond, P. T.; Yang, Y. Y. The Effects of Polymeric Nanostructure Shape on Drug Delivery. Adv. Drug Deliv. Rev. 2011, 63 (14–15), 1228–1246. https://doi.org/10.1016/j.addr.2011.06.016.

(7) de Folter, J. W. J.; Hutter, E. M.; Castillo, S. I. R.; Klop, K. E.; Philipse, A. P.; Kegel, W. K. Particle Shape Anisotropy in Pickering Emulsions: Cubes and Peanuts. Langmuir 2014, 30 (4), 955–964. https://doi.org/10.1021/la402427q.

(8) Champion, J. A.; Katare, Y. K.; Mitragotri, S. Particle Shape: A New Design Parameter for Micro- and Nanoscale Drug Delivery Carriers. J. Control. Release 2007, 121 (1–2), 3–9. https://doi.org/10.1016/j.jconrel.2007.03.022.

(9) Dendukuri, D.; Doyle, P. S. The Synthesis and Assembly of Polymeric Microparticles Using Microfluidics. Adv. Mater. 2009, 21 (41), 4071–4086. https://doi.org/10.1002/adma.200803386.

(10) Xia, Y.; Whitesides, G. M. SOFT LITHOGRAPHY. Annu. Rev. Mater. Sci. 1998, 28 (1), 153–184. https://doi.org/10.1146/annurev.matsci.28.1.153.

(11) Jiang, S.; Chen, Q.; Tripathy, M.; Luijten, E.; Schweizer, K. S.; Granick, S. Janus Particle Synthesis and Assembly. Adv. Mater. 2010, 22 (10), 1060–1071. https://doi.org/10.1002/adma.200904094.

(12) Koch, C. C. Top-down Synthesis of Nanostructured Materials: Mechanical and Thermal Processing Methods. Rev. Adv. Mater. Sci. 2003, 5 (2), 91–99.

(13) Merkel, T. J.; Herlihy, K. P.; Nunes, J.; Orgel, R. M.; Rolland, J. P.; DeSimone, J. M. Scalable, Shape-Specific, Top-down Fabrication Methods for the Synthesis of Engineered Colloidal Particles. Langmuir 2010, 26 (16), 13086–13096. https://doi.org/10.1021/la903890h.

(14) Hernandez, C. J.; Mason, T. G. Colloidal Alphabet Soup: Monodisperse Dispersions of Shape-Designed LithoParticles. J. Phys. Chem. C 2007, 111 (12), 4477–4480. https://doi.org/10.1021/jp0672095.

(15) Lintingre, E.; Lequeux, F.; Talini, L.; Tsapis, N. Control of Particle Morphology in the Spray Drying of Colloidal Suspensions. Soft Matter 2016, 12 (36), 7435–7444. https://doi.org/10.1039/c6sm01314g.

(16) Ho, C. C.; Keller, A.; Odell, J. A.; Ottewill, R. H. Preparation of Monodisperse Ellipsoidal Polystyrene Particles. Colloid Polym. Sci. 1993, 271 (5), 469–479. https://doi.org/10.1007/BF00657391.

(17) Hwang, D. K.; Dendukuri, D.; Doyle, P. S. Microfluidic-Based Synthesis of Non-Spherical Magnetic Hydrogel Microparticles. Lab Chip 2008, 8 (10), 1640. https://doi.org/10.1039/b805176c.

(18) Dendukuri, D.; Pregibon, D. C.; Collins, J.; Hatton, T. A.; Doyle, P. S. Continuous-Flow Lithography for High-Throughput Microparticle Synthesis. Nat. Mater. 2006, 5 (5), 365–369. https://doi.org/10.1038/nmat1617.

(19) Dendukuri, D.; Tsoi, K.; Hatton, T. A.; Doyle, P. S. Controlled Synthesis of Nonspherical Microparticles Using Microfluidics. Langmuir 2005, 21 (6), 2113–2116. https://doi.org/10.1021/la047368k.

(20) Ugelstad, J.; El-Aasser, M. S.; Vanderhoff, J. W. Emulsion Polymerization : Initiation Of. J. Polym. Sci. Polym. Lett. Ed. 1973, 11 (8), 503–513.

(21) Kularatne, R. S.; Kim, H.; Boothby, J. M.; Ware, T. H. Liquid Crystal Elastomer Actuators: Synthesis, Alignment, and Applications. J. Polym. Sci. Part B Polym. Phys. 2017, 55 (5), 395–411. https://doi.org/10.1002/polb.24287.

(22) Ohm, C.; Serra, C.; Zentel, R. A Continuous Flow Synthesis of Micrometer-Sized Actuators from Liquid Crystalline Elastomers. Adv. Mater. 2009, 21 (47), 4859–4862. https://doi.org/10.1002/adma.200901522.

(23) Karausta, A.; Bukusoglu, E. Liquid Crystal-Templated Synthesis of Mesoporous Membranes with Predetermined Pore Alignment. ACS Appl. Mater. Interfaces 2018, 10 (39), 33484–33492. https://doi.org/10.1021/acsami.8b14121.

(24) Wang, X.; Bukusoglu, E.; Miller, D. S.; Bedolla Pantoja, M. A.; Xiang, J.; Lavrentovich, O. D.; Abbott, N. L. Synthesis of Optically Complex, Porous, and Anisometric Polymeric Microparticles by Templating from Liquid Crystalline Droplets. Adv. Funct. Mater. 2016, 26 (40), 7343–7351. https://doi.org/10.1002/adfm.201602262.

(25) Pekarek, K. J.; Jacob, J. S.; Mathiowitz, E. Double-Walled Polymer Microspheres for Controlled Drug Release. Nature 1994, 367 (6460), 258–260. https://doi.org/10.1038/367258a0.

(26) Cui, C.; Gan, L.; Heggen, M.; Rudi, S.; Strasser, P. Compositional Segregation in Shaped Pt Alloy Nanoparticles and Their Structural Behaviour during Electrocatalysis. Nat. Mater. 2013, 12 (8), 765–771. https://doi.org/10.1038/nmat3668.

(27) Flouraki, C.; Kaliva, M.; Papadas, I. T.; Armatas, G. S.; Vamvakaki, M. Nanoporous Polystyrene-Porphyrin Nanoparticles for Selective Gas Separation. Polym. Chem. 2016, 7 (17), 3026–3033. https://doi.org/10.1039/c6py00296j.

(28) Davis, M. E. Ordered Porous Materials for Emerging Applications. Nature. 2002, pp 813–821. https://doi.org/10.1038/nature00785.

(29) You, C. C.; Miranda, O. R.; Gider, B.; Ghosh, P. S.; Kim, I. B.; Erdogan, B.; Krovi, S. A.; Bunz, U. H. F.; Rotello, V. M. Detection and Identification of Proteins Using Nanoparticle-Fluorescent Polymer “chemical Nose” Sensors. Nat. Nanotechnol. 2007, 2 (5), 318–323. https://doi.org/10.1038/nnano.2007.99.

(30) Haines, C. S.; Li, N.; Spinks, G. M.; Aliev, A. E.; Di, J.; Baughman, R. H. New Twist on Artificial Muscles. Proc. Natl. Acad. Sci. 2018, 113 (42), 11709–11716. https://doi.org/10.1073/pnas.1802492115.

(31) Bozuyuk, U.; Yasa, O.; Yasa, I. C.; Ceylan, H.; Kizilel, S.; Sitti, M. Light-Triggered Drug Release from 3D-Printed Magnetic Chitosan Microswimmers. ACS Nano 2018, 12 (9), 9617–9625. https://doi.org/10.1021/acsnano.8b05997.

(32) Iamsaard, S.; Aßhoff, S. J.; Matt, B.; Kudernac, T.; Cornelissen, J. J. L. M.; Fletcher, S. P.; Katsonis, N. Conversion of Light into Macroscopic Helical Motion. Nat. Chem. 2014, 6 (3), 229–235. https://doi.org/10.1038/nchem.1859.

(33) Gimenez-Pinto, V.; Ye, F.; Mbanga, B.; Selinger, J. V.; Selinger, R. L. B. Modeling Out-of-Plane Actuation in Thin-Film Nematic Polymer Networks: From

Chiral Ribbons to Auto-Origami Boxes via Twist and Topology. Sci. Rep. 2017, 7 (February), 45370. https://doi.org/10.1038/srep45370.

(34) Champion, J. A.; Katare, Y. K.; Mitragotri, S. Making Polymeric Micro- and Nanoparticles of Complex Shapes. Proc. Natl. Acad. Sci. 2007, 104 (29), 11901–11904. https://doi.org/10.1073/pnas.0705326104.

(35) Helgeson, M. E.; Chapin, S. C.; Doyle, P. S. Hydrogel Microparticles from Lithographic Processes: Novel Materials for Fundamental and Applied Colloid Science. Curr. Opin. Colloid Interface Sci. 2011, 16 (2), 106–117. https://doi.org/10.1016/j.cocis.2011.01.005.

(36) Nie, Z.; Li, W.; Seo, M.; Xu, S.; Kumacheva, E. Janus and Ternary Particles Generated by Microfluidic Synthesis: Design, Synthesis, and Self-Assembly. J. Am. Chem. Soc. 2006, 128 (29), 9408–9412. https://doi.org/10.1021/ja060882n.

(37) Zou, W.; Yan, Y.; Fang, J.; Yang, Y.; Liang, J.; Deng, K.; Yao, J.; Wei, Z. Biomimetic Superhelical Conducting Microfibers with Homochirality for Enantioselective Sensing. J. Am. Chem. Soc. 2014, 136 (2), 578–581. https://doi.org/10.1021/ja409796b.

(38) Pashuck, E. T.; Stupp, S. I. Direct Observation of Morphological Tranformation from Twisted Ribbons into Helical Ribbons. J. Am. Chem. Soc. 2010, 132 (26), 8819–8821. https://doi.org/10.1021/ja100613w.

(39) Gimenez-Pinto, V.; Ye, F.; Selinger, J. V.; Takigawa, T.; Urayama, K.; Selinger, R. L. B.; Sawa, Y. Shape Selection of Twist-Nematic-Elastomer Ribbons. Proc. Natl. Acad. Sci. 2011, 108 (16), 6364–6368. https://doi.org/10.1073/pnas.1017658108.

(40) Liu, G. F.; Zhang, D.; Feng, C. L. Control of Three-Dimensional Cell Adhesion by the Chirality of Nanofibers in Hydrogels. Angew. Chemie - Int. Ed. 2014, 53 (30), 7789–7793. https://doi.org/10.1002/anie.201403249.

(41) Liu, J.; Liu, J.; Chu, L.; Zhang, Y.; Xu, H.; Kong, D.; Yang, Z.; Yang, C.; Ding, D. Self-Assembling Peptide of d-Amino Acids Boosts Selectivity and Antitumor Efficacy of 10-Hydroxycamptothecin. ACS Appl. Mater. Interfaces 2014, 6 (8), 5558–5565. https://doi.org/10.1021/am406007g.

(42) Hu, A.; Yee, G. T.; Lin, W. Magnetically Recoverable Chiral Catalysts Immobilized on Magnetite Nanoparticles for Asymmetric Hydrogenation of Aromatic Ketones. J. Am. Chem. Soc. 2005, 127 (36), 12486–12487. https://doi.org/10.1021/ja053881o.

(43) Chen, X.; Zhang, S.; Dikin, D. A.; Ding, W.; Ruoff, R. S.; Pan, L.; Nakayama, Y. Mechanics of a Carbon Nanocoil. Nano Lett. 2003, 3 (9), 1299–1304. https://doi.org/10.1021/nl034367o.

(44) Bukusoglu, E.; Bedolla Pantoja, M.; Mushenheim, P. C.; Wang, X.; Abbott, N. L. Design of Responsive and Active (Soft) Materials Using Liquid Crystals. Annu. Rev. Chem. Biomol. Eng. 2016, 7 (1), 163–196. https://doi.org/10.1146/annurev-chembioeng-061114-123323.

(45) Lockwood, N. A.; Gupta, J. K.; Abbott, N. L. Self-Assembly of Amphiphiles, Polymers and Proteins at Interfaces between Thermotropic Liquid Crystals and Aqueous Phases. Surf. Sci. Rep. 2008, 63 (6), 255–293. https://doi.org/10.1016/j.surfrep.2008.02.002.

(46) F. C. Frank. On the Theory of Liquid Crystals. Discuss. Faraday Soc. 1958, 25 (I), 19–28.

(47) C. W. Oseen. The Theory of Liquid Crystals. Trans. Faraday Soc. 1932, 29 (l), 883–899.

(48) Petsch, S.; Rix, R.; Khatri, B.; Schuhladen, S.; Müller, P.; Zentel, R.; Zappe, H. Smart Artificial Muscle Actuators: Liquid Crystal Elastomers with Integrated Temperature Feedback. Sensors Actuators, A Phys. 2015, 231, 44–51. https://doi.org/10.1016/j.sna.2014.10.014.

(49) Li, Y.; Pruitt, C.; Rios, O.; Wei, L.; Rock, M.; Keum, J. K.; Mcdonald, A. G.; Kessler, M. R. Controlled Shape Memory Behavior of a Smectic Main-Chain Liquid Crystalline Elastomer. Macromolecules 2015, 48 (9), 2864–2874. https://doi.org/10.1021/acs.macromol.5b00519.

(50) Fleischmann, E. K.; Liang, H. L.; Kapernaum, N.; Giesselmann, F.; Lagerwall, J.; Zentel, R. One-Piece Micropumps from Liquid Crystalline Core-Shell Particles. Nat. Commun. 2012, 3, 1178. https://doi.org/10.1038/ncomms2193.

(51) Buguin, A.; Li, M. H.; Silberzan, P.; Ladoux, B.; Keller, P. Micro-Actuators: When Artificial Muscles Made of Nematic Liquid Crystal Elastomers Meet Soft Lithography. J. Am. Chem. Soc. 2006, 128 (4), 1088–1089. https://doi.org/10.1021/ja0575070.

(52) Bera, T.; Freeman, E. J.; McDonough, J. A.; Clements, R. J.; Aladlaan, A.; Miller, D. W.; Malcuit, C.; Hegmann, T.; Hegmann, E. Liquid Crystal Elastomer Microspheres as Three-Dimensional Cell Scaffolds Supporting the Attachment and Proliferation of Myoblasts. ACS Appl. Mater. Interfaces 2015, 7 (26), 14528–14535. https://doi.org/10.1021/acsami.5b04208.

(53) Vennes, M.; Zentel, R. Liquid-Crystalline Colloidal Particles. Macromol. Chem. Phys. 2004, 205 (17), 2303–2311. https://doi.org/10.1002/macp.200400296.

(54) Kotikian, A.; Truby, R. L.; Boley, J. W.; White, T. J.; Lewis, J. A. 3D Printing of Liquid Crystal Elastomeric Actuators with Spatially Programed Nematic Order. Adv. Mater. 2018, 30 (10), 1–6. https://doi.org/10.1002/adma.201706164.

(55) Ambulo, C. P.; Burroughs, J. J.; Boothby, J. M.; Kim, H.; Shankar, M. R.; Ware, T. H. Four-Dimensional Printing of Liquid Crystal Elastomers. ACS Appl. Mater. Interfaces 2017, 9 (42), 37332–37339. https://doi.org/10.1021/acsami.7b11851.

(56) Oosten, C. L. Van; Bastiaansen, C. W. M.; Broer, D. J. Actuators Modularly Driven by Light. Nat. Mater. 2009, 8 (8), 677–682. https://doi.org/10.1038/nmat2487.

(57) Yang, Z.; Huck, W. T. S.; Clarke, S. M.; Tajbakhsh, A. L. I. R.; Terentjev, E. M.; Centre, T. N.; Avenue, J. J. T.; Cb, C. Shape-Memory Nanoparticles from Inherently Non-Spherical Polymer Colloids. 2005, 4 (June). https://doi.org/10.1038/nmat1389.

(58) Yang, H.; Buguin, A.; Taulemesse, J.-M.; Kaneko, K.; Méry, S.; Bergeret, A.; Keller, P. Micron-Sized Main-Chain Liquid Crystalline Elastomer Actuators with Ultralarge Amplitude Contractions. J. Am. Chem. Soc. 2009, 131 (41), 15000–15004. https://doi.org/10.1021/ja905363f.

(59) Mondiot, F.; Wang, X.; Pablo, J. J. de; Abbott, N. L. Liquid Crystal-Based Emulsions for Synthesis of Spherical and Non- Spherical Particles with Chemical Patches. J. Am. Chem. Soc. 2013, 135 (27), 9972–9975. https://doi.org/10.1021/ja4022182.

(60) Lee, K. M.; Bunning, T. J.; White, T. J. Autonomous, Hands-Free Shape Memory in Glassy, Liquid Crystalline Polymer Networks. Adv. Mater. 2012, 24 (21), 2839–2843. https://doi.org/10.1002/adma.201200374.

(61) Wang, X.; Bukusoglu, E.; Abbott, N. L. A Practical Guide to the Preparation of Liquid Crystal-Templated Microparticles. Chemistry of Materials. 2017, pp 53–61. https://doi.org/10.1021/acs.chemmater.6b02668.

(62) Wang, X.; Zhou, Y.; Kim, Y.; Miller, D. S.; Zhang, R.; Martinez-Gonzalez, J. A.; Bukusoglu, E.; Zhang, B.; Brown, T. M.; Pablo, J. J. de; et al. Patterned Surface Anchoring of Nematic Droplets at Miscible Liquid–Liquid Interfaces. Soft Matter 2017, 13, 5714–5723. https://doi.org/10.1039/c7sm00975e.

(63) Ansell, H. S.; Kim, D. S.; Kamien, R. D.; Katifori, E.; Lopez-Leon, T. Threading the Spindle: A Geometric Study of Chiral Liquid Crystal Polymer Microparticles. 2019, 1, 1–5.

(64) Miller, D. S.; Carlton, R. J.; Mushenheim, P. C.; Abbott, N. L. Introduction to Optical Methods for Characterizing Liquid Crystals at Interfaces. Langmuir 2013, 29 (10), 3154–3169. https://doi.org/10.1021/la304679f.

(65) Liu, D.; Broer, D. J. Liquid Crystal Polymer Networks: Preparation, Properties, and Applications of Films with Patterned Molecular Alignment. Langmuir 2014, 30 (45), 13499–13509.

(66) Jillavenkatesa, A.; Dapkunas, S. J.; Lum, L.-S. H. NIST Recommended Practice Guide: Particle Size Characterization; U.S. Government Printing Office: Washington, DC, USA, 2001.

(67) Akdeniz, B.; Bukusoglu, E. Liquid Crystal Templates Combined with Photolithography Enable Synthesis of Chiral Twisted Polymeric Microparticles. Macromol. Rapid Commun. 2019, 1900160, 1900160. https://doi.org/10.1002/marc.201900160.

(68) Yao, Y.; Waters, J. T.; Shneidman, A. V.; Cui, J.; Wang, X.; Mandsberg, N. K.; Li, S.; Balazs, A. C.; Aizenberg, J. Multiresponsive Polymeric Microstructures with Encoded Predetermined and Self-Regulated Deformability. Proc. Natl. Acad. Sci. 2018. https://doi.org/10.1073/pnas.1811823115.

(69) White, T. J.; Broer, D. J. Programmable and Adaptive Mechanics with Liquid Crystal Polymer Networks and Elastomers. Nat. Mater. 2015, 14 (11), 1087–1098. https://doi.org/10.1038/nmat4433.

APPENDICES

A. Representative Micrograph Images

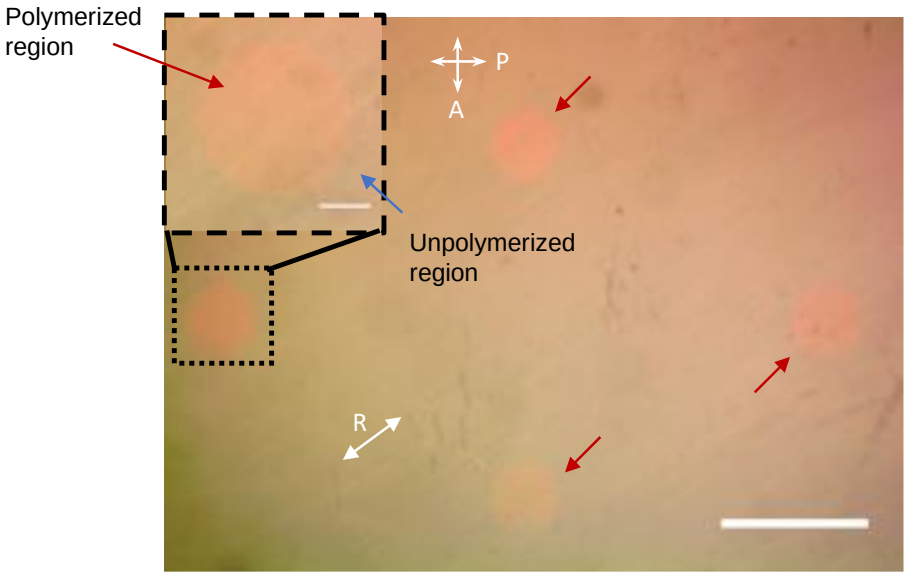

Figure A. 1. Representative brightfield micrograph image after polymerization with UV light (inset showing a magnified part shown in dashed lines). The red arrows indicate the polymerized regions, whereas the blue arrow indicate the unpolymerized regions of the film. The figure is same as Figure 1B with the adjusted as +30% brightness. Scale bar: 500 μm, inset, 100 μm.

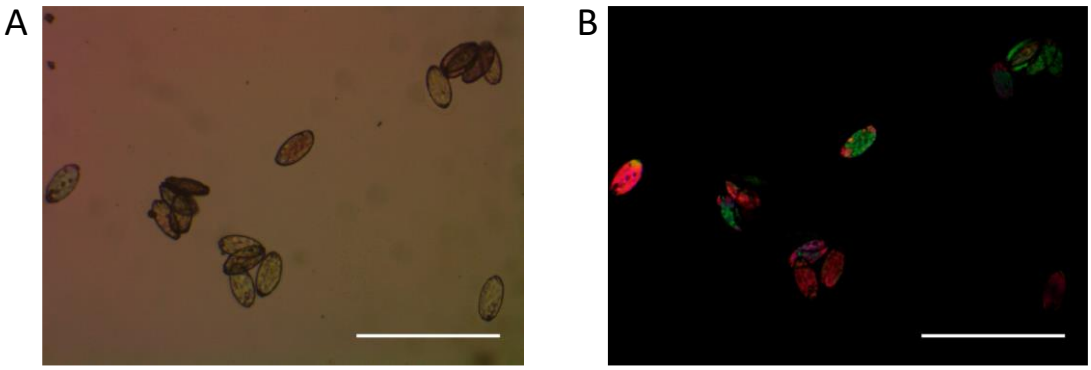

Figure A. 2. Representative (A) brightfield and (B) polarized light micrographs of the microparticles synthesized from a mixture of 20% by weight RM257 in E7 with uniform planar anchoring. The photomask circular features used in the synthesis was 100 μm. Scale bars: 300 μm.

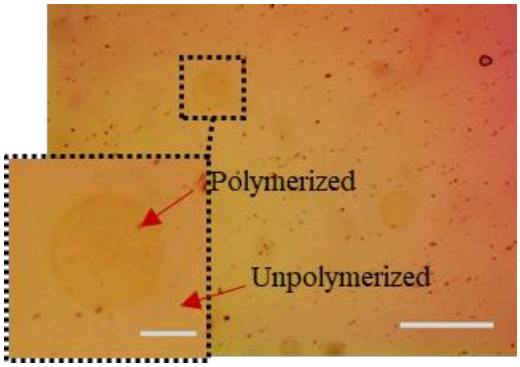

Figure A. 3. Representative brightfield micrograph image after polymerization with UV light (inset showing a magnified part shown in dashed lines). The red arrows indicate the polymerized regions, whereas the blue arrow indicate the unpolymerized regions of the film. The figure is same as Figure 1B with the adjusted as +30% brightness. Scale bar: 500 μm, inset, 100 μm.

B. Theoretical Aspect Ratio and Top Angle Calculation of Rectangular and Triangle Shaped Microparticles

Best equations for the shrinkage percentage (φ) and monomer percentage (x) were determined by using Figure 4.5 as $\varphi_1 = -0.2922 \cdot x + 18.046$ and $\varphi_2 = -1.0644 \cdot x + 76.271$ along parallel to nematic director and perpendicular to nematic director, respectively.

For rectangular shaped microparticles;

The schematic representation of rectangular shaped microparticles are given in Figure B. 1.

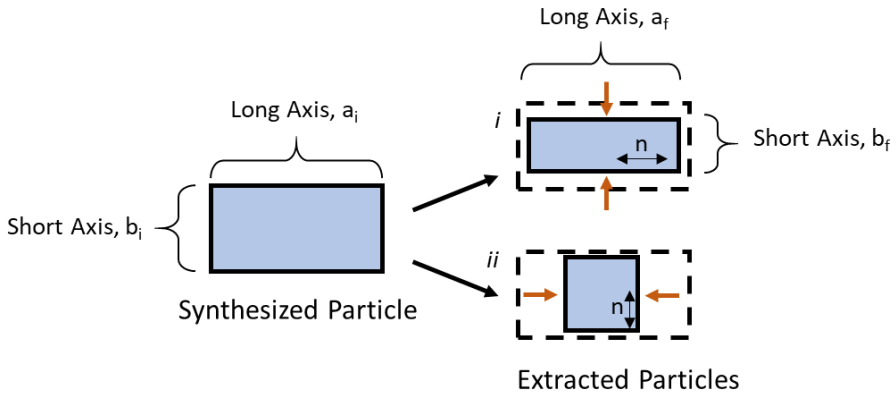

Figure B. 1. Schematic representation of rectangular shaped microparticles. Rubbing direction (indicated as n) is (*i*) parallel to long axis, or (*ii*) short axis. The equation for each case can be seen below.

For i;

$$a_f = \frac{(100-\varphi_1)}{100} \cdot a_i \qquad \text{Equation B.1}$$

$$b_f = \frac{(100-\varphi_2)}{100} \cdot b_i \qquad \text{Equation B.2}$$

For ii;

$$a_f = \frac{(100-\varphi_2)}{100} \cdot a_i$$ Equation B.3

$$b_f = \frac{(100-\varphi_1)}{100} \cdot b_i$$ Equation B.4

For triangular shaped microparticles;

The schematic representation of triangular shaped microparticles are given in Figure B. 2.

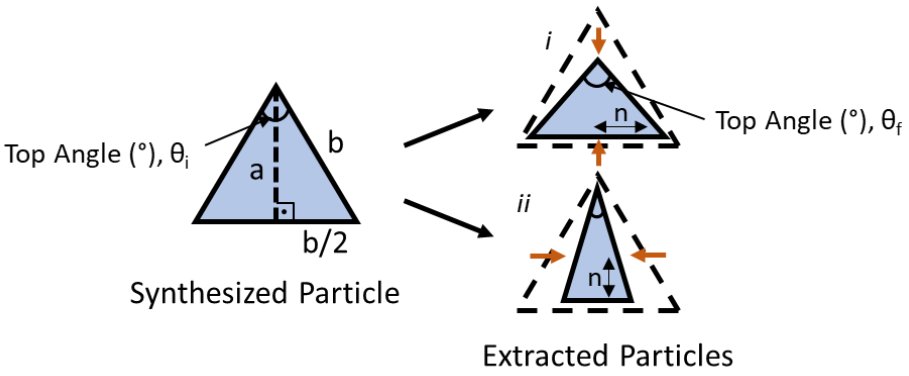

Figure B. 2. Schematic representation of triangular shaped microparticles. Rubbing direction (indicated as n) is (*i*) parallel to b, or (*ii*) a.

The equation for each case can be seen below.

For i;

$$\theta_f = 2 \cdot tan^{-1}\left\{\frac{\left[\frac{b\cdot(100-\varphi_1)}{100}\right]}{2\cdot\left[\frac{a\cdot(100-\varphi_2)}{100}\right]}\right\}$$ Equation B.5

For ii;

$$\theta_f = 2 \cdot tan^{-1}\left\{\frac{\left[\frac{b\cdot(100-\varphi_2)}{100}\right]}{2\cdot\left[\frac{a\cdot(100-\varphi_1)}{100}\right]}\right\}$$ Equation B.6